9950-398

AESD-TME-3043

A STUDY ON THE ELECTROLYSIS OF SULFUR DIOXIDE AND WATER FOR THE SULFUR CYCLE HYDROGEN PRODUCTION PROCESS

final report prepared for

THE JET PROPULSION LABORATORY
Contract No. 955380

by

Westinghouse Electric Corporation
Advanced Energy Systems Division
Box 10864
Pittsburgh, Pennsylvania 15236

July, 1980

"This work was performed for the Jet Propulsion Laboratory, California Institute of Technology sponsored by the National Aeronautics and Space Administration under Contract NAS-7-100."

LEGAL NOTICE

ABSTRACT

A series of tests was performed with experimental electrolysis cells that used various platinum catalyzed carbon electrodes. Major improvements in cell performance were attained as indicated by measured cell voltages. When operated at 200 mA/cm^2 current density using 50 w/o acid at 50°C and 1 atm, a reference cell required 1.22 volts and degraded rapidly. After several improvements had been incorporated into electrodes and the test cell configuration, a later cell required only 0.77 volts under identical operating conditions. This cell exhibited stable operation with no measurable performance degradation. At a lower current density, 100 mA/cm^2, the cell required only 0.63 volts.

A one-week endurance test was conducted with an intermediate cell which was operated at a 100 mA/cm^2 for 173 hours. This cell produced a stable voltage of 0.675 volts with no degradation after the first 80 hours.

Experimental efforts also included kinetic studies on metal electrodes, measurements of temperature effects on electrode kinetics, investigations of electrocatalytic activities of metal electrodes over a wide range of acid concentrations, cyclic voltametric studies and evaluation of alternate catalysts.

From diffusivity experiments, several materials were identified that have diffusion coefficients substantially lower than the reference material, microporous rubber. A cation exchange membrane material, P-4010, exhibited an excellent diffusion coefficient, more than two orders of magnitude lower than that of rubber. Also, measurements of ionic resistivity were made on eight materials. Microporous rubber had the lowest resistivity, approximately 2 ohm-cm while the other materials ranged from 8 to 21 ohm-cm.

SUMMARY

Westinghouse is developing the Sulfur Cycle, a hybrid thermochemical/electrochemical process for generation of hydrogen from water. During 1979, research and development work on the electrolytic aspects of the process were sponsored by the Jet Propulsion Laboratory via interagency transfer from the Department of Energy. The objectives of this work were to increase the understanding of the electrochemistry of depolarized anodes in sulfurous/sulfuric acid solutions and to provide a foundation for the long term development of efficient, long life and inexpensive electrolyzer systems. The scope of work was comprised of four technical tasks: electrode fabrication development, evaluation of electrode kinetics, investigation of separator materials and laboratory model operations. A summary of progress under each of these tasks is given herein.

DEVELOPMENT OF ELECTRODE FABRICATION TECHNIQUES

To provide tangible evidence of progress in the development of electrodes, a series of tests was performed with experimental single cells that used various platinum catalyzed carbon electrodes. Over a period of seven months, major improvements in cell performance were attained as indicated by measured cell voltages. When operated at 200 mA/cm^2 current density using 50 w/o acid at 50°C and 1 atm, a reference cell (designated OC-1) which used briquetted carbon electrodes, required 1.22 volts and degraded at a rate of 16 mV/hr. After several improvements had been incorporated into electrodes and test cell configuration, one of the cells (designated LC-12) required only 0.77 volts under identical operating conditions. This cell exhibited stable operation with no measurable performance degradation. At a lower current density, 100 mA/cm^2, LC-12 required only 0.63 volts.

Some of the improvements incorporated into LC-12 included:

- the use of commercially available porous carbon substrates
- a reduction in platinum catalyst loading in the anode from 10 to 7 mg/cm^2
- the incorporation of a carbon cloth layer as part of the anode structure catalyzed with 2 mg/cm^2 of fine platinum particles deposited on carbon "black pearls"
- an improved cell configuration that incorporated a cylindrical geometry with attendant O-ring sealing.

A one-week endurance test was conducted with one of the intermediate cells (designated LC-8). This cell had all of the features of LC-12 except for the fine particle platinum on the carbon cloth. Instead, LC-8 used a platinum catalyzed carbon powder with a Teflon binder on the cloth. Operated at a 100 mA/cm^2 current density for 173 hours continuously, Cell LC-8 demonstrated a stable voltage of 675 mV with no degradation after the first 80 hours. During the first 80 hours, the cell voltage had increased from 644 mV to 675 mV because of a slight performance degradation at the anode.

In addition to platinum catalyzed electrodes, a novel process was developed for using palladium oxide as a catlayst on the anode. Carbon cloth anodes were prepared with the PdO catalyst and tested in an experimental cell. At 200 mA/cm^2 current density, this cell (designated LC-10) required 0.89 volts. The achievable performance with PdO catalyzed anodes, however, should be substantially better than obtained from Cell LC-10 because of low overpotentials measured during related kinetic studies.

Chemical compositions of a tested Pt-catalyzed carbon plate cathode and a tested PdO-catalyzed carbon cloth anode were characterized using ESCA techniques. After an electrolysis experiment, sulfide ions were found to be present on the tested electrodes. However, no elemental sulfur or SO_2-containing species were observed.

A detailed technical discussion of the cell performance results, electrode fabrication experience, associated chemical analyses and microphotos is contained in Section 2.2.

EVALUATION OF ELECTRODE KINETICS AND CATALYSIS

Experimental efforts in this area included kinetic studies on metal electrodes, measurements of temperature effects on electrode kinetics, investigations of electrolcatlaytic activities of metal electrodes over a wide range of acid concentrations, cyclic voltametric studies and evaluation of alternate catalysts.

From tests in 50 w/o sulfuric acid at 25°C, a preoxidized palladium electrode exhibited limiting current densities more than an order of magnitude greater than a similar electrode composed of platinum. A silver electrode was also evaluated and was intermediate between palladium and platinum. However, silver was found to be not chemically stable in strong acids. These experiments provided verification of the potential attractiveness of palladium catalyzed electrodes as an alternative to platinum. The measured activation energy for sulfur dioxide oxidation on the palladium electrode was ~25 kcal/mole.

Temperature effect measurements conducted at 1 atm showed significant improvements in exchange current densities and reductions in anode overpotentials as the temperature increased from 25°C to 90°C. This trend was observed for both preanodized platinum and palladium electrodes.

Measurements of electrode potential over a range of acid concentrations from 20 to 70 w/o have shown that the linear region of the Tafel plot is nearly replicated from 20 to 50 w/o acid. At 60 and 70 w/o acid, substantial increases in electrode potential were measured, but the Tafel slope did not change significantly.

A number of cyclic voltametric measurements were made using platinum, palladium, iridium, rhodium and ruthenium electrodes. In the anodic sweep, the SO_2 oxidation reaction commenced at potentials where the growth of chemisorbed oxygen-containing layer was initiated. No reduction peak was detected on the cathodic

sweep, indicating that this reaction is highly irreversible. On most metal electrodes, the chemical transformation of the chemisorbed species to metal oxides creates passivated surface layers which strongly inhibit the SO_2 oxidation reaction.

Several potentially attractive catalysts, oxides and mixed oxides, were evaluated from measurements that resulted in plots of current density versus electrode potential. Measurements with palladium oxide on a carbon substrate indicated superior performance compared to carbon or platinum black on carbon. Oxides of iridium and ruthenium on titanium substrates exhibited unacceptable performance while palladium oxide on a titanium/titanium oxide substrate was comparable in performance to platinum black on a titanium substrate. Section 2.1 discusses the significance of the kinetic and catalysis experiments in some detail along with theoretical considerations.

INVESTIGATION OF SEPARATOR MATERIALS

While cell tests have used a commercially available microporous rubber membrane that has proved to be adequate for experimental/developmental cells, it is desirable to find a gas separator that has improved qualities compared to rubber. For this reason, experiments were made on two key separator figures of merit: (1) diffusivity for sulfur dioxide-containing species, and (2) ionic resistivity. Both of the quantities should be as low as possible.

From the diffusivity experiments, several materials were identified that have diffusion coefficients substantially lower than microporous rubber. One of these materials, P-4010, a cation exchange membrane material, has an excellent diffusion coefficient, more than two orders of magnitude lower than that of microporous rubber diaphragm.

Measurements of diffusion coefficients as functions of temperature were made with three materials, microporous rubber, P-4010 and Nafion-120. As expected, the diffusion coefficients increased slightly with temperature.

Measurements of ionic resistivity; i.e., the resistivity to hydrodrium ions, were made in sulfur dioxide saturated solutions and in sulfur dioxide free solutions via an interruptor technique. Eight materials were tested in 50 w/o and at 23°C. Microporous rubber had the lowest resistivity, approximately 2 ohm-cm. The other materials ranged from 8 to 21 ohm-cm. While P-4010 had the lowest diffusion coefficient for sulfur dioxide, it also had the highest resistivity among those tested. Since the thickness of P-4010 membranes is small in cell tests, it should offer an ionic resistance comparable to microporous rubber.

LABORATORY MODEL OPERATIONS

The closed cycle Laboratory Model of the Sulfur Cycle that had been built by Westinghouse in 1978 was used periodically during the year to support the electrolyzer work. The Model also was operated, including the high temperature subsystems, for demonstration purposes to visitors and dignitaries.

Early in the year, the Model's electrolyzer subsystem was used to evaluate a small cell with platinum screen electrodes while the electrolyzer test facility was being refurbished. Later, the Model was used to evaluate the performance of an experimental bipolar packed bed multicell that had been devised and built at the Westinghouse Research and Development Center.

TABLE OF CONTENTS

TABLE OF CONTENTS (Continued)

LIST OF TABLES

LIST OF FIGURES

LIST OF FIGURES (Continued)

LIST OF FIGURES (Continued)

LIST OF FIGURES (Continued)

ACKNOWLEDGMENTS

The authors would like to express their appreciation to R. W. Buckman, Jr. and G. H. Farbman for their constant interest and encouragement. Special thanks are due to E. R. Garcia, D. R. Zamba and H. F. Ebner who performed the experimental work. The authors also wish to thank Dr. R. Shalvoy of Institute for Mining and Minerals Research, University of Kentucky and Dr. A. S. Manocha of Westinghouse Research and Development Center for conducting ESCA studies on tested electrodes and electrode materials. Valuable analytical data from K. Guardipee and H. Silva of Westinghouse Research and Development Center are greatly appreciated. The authors also are grateful to L. R. Eisenstatt and G. O. Yatsko for conducting SEM/EDA studies and for technical assistance, respectively. Finally, sincere acknowledgments are due to B. J. Chiappetta and E K. Walter who did an excellent job in typing drafts and the final version of this report.

W. T. P. Lu, Principal Investigator

R. L. Ammon, Manager
Materials Science

G. H. Parker, Manager
Hydrogen Production Programs

1.0 INTRODUCTION

Westinghouse Electric Corporation is currently developing the Sulfur Cycle, a hybrid thermochemical-electrochemical process for the production of hydrogen and oxygen from water. The development work has been cofunded by the Conservation (STOR) and Solar Divisions of the Department of Energy; the work funded by STOR on research and development of the electrolytic subsystem was contracted via interagency-transfer through the Jet Propulsion Laboratory during 1979. Technical work under the JPL contract was completed during February 1980 and this document represents the final report for that contract.

The Sulfur Cycle, in its most general form, consists of two chemical reactions – one for producing hydrogen and the other for oxygen. The production of oxygen occurs via the thermal reduction of sulfur trioxide obtained from sulfuric acid.

$$H_2SO_4 \rightarrow H_2O + SO_3 \rightarrow H_2O + SO_2 + 1/2\ O_2 \qquad (1)$$

The process is completed by using the sulfur dioxide from the thermal reduction step to depolarize the anode of an electrolyzer. The overall reaction occurring electrochemically is:

$$2\ H_2O + SO_2 \rightarrow H_2 + H_2SO_4 \qquad (2)$$

The net result of Reactions 1 and 2 is the decomposition of water into hydrogen and oxygen and the sulfur oxides are involved as recycling intermediates.

Although electrical power is required in the electrolyzer, much smaller quantities than those necessary in conventional water electrolysis are needed. The energy needs of the process are thermal energy, for the acid vaporization and sulfur trioxide reduction steps, and electrical energy for the electrolysis

and auxiliary power (e.g., pumps, circulators, etc.). The temperature levels desired for the thermal inputs are compatible with the capability of solar collectors. The electrical power can be provided by a solar-electric plant, by fuel cells fed with a portion of the hydrogen and oxygen produced in the process, or by power from a remote generating plant.

Work under JPL contract has represented a continuation of research and development performed by Westinghouse during 1978 under Contract No. EG-77-C-02-4378 for the Department of Energy. Development activities in the sulfur dioxide depolarized electrolysis technology were mainly in four different areas: (1) Evaluation of Electrode Kinetics and Electrode Catalysis, (2) Development of Electrode Fabrication Techniques, (3) Investigation of Separator Materials and (4) Laboratory Model Operations. The objectives of the work reported herein were to increase the understanding of the electrochemistry of depolarized anode electrolysis in sulfuric/sulfurous acid solutions and provide a foundation for the long-term development of efficient, long-life and inexpensive electrolyzer systems. This work constitutes a portion of the overall development of the Sulfur Cycle. A complementary program on the thermochemical aspects of the process is funded separately by DOE/Solar Energy under Contract No. ET-78-C-02-4705.

2.0 TECHNICAL DISCUSSION

2.1 EVALUATION OF ELECTRODE KINETICS AND ELECTRODE CATALYSIS

The results of process study have revealed[1] that, the cell voltage of an SO_2-depolarized electrolyzer plays a significant role in determining the overall energy efficiency of the sulfur-based hybrid cycle. Mathematically, the overall cell voltage (E_{cell}) of the electrolyzer may be represented by an equation of the form:

$$E_{cell} = E_r + \eta_a + \left|\eta_c\right| + IR \qquad (1)$$

where η_a is the anode overpotential, η_c the cathode overpotential and IR the ohmic loss in the electrolyte, metallic components and metal-metal contacts. Furthermore, the voltage efficiency (ε) of the electrolyzer is normally defined as:

$$\varepsilon = \frac{E_r}{E_{cell}} \qquad (2)$$

By use of platinum-catalyzed carbon electrodes, the SO_2-depolarized electrolyzer exhibits a voltage of ∿650 mV at 100 mA/cm^2 while it operates at 50°C and atmospheric pressure[2]. This includes ∿250 mV in the anodic overpotential, ∿40 mV in the cathodic overpotential and ∿60 mV in the ohmic loss. It is obvious that the anodic overpotential arising from the irreversibility of the SO_2 oxidation reaction on the platinum catalyst is the major source of the efficiency loss in the electrolyzer.

A comprehensive knowledge of the mechanism of the SO_2 oxidation reaction is needed to improve the voltage efficiency of the cell. This reaction has been intensively studied in dilute sulfuric acid solutions on platinum[3-8], gold[5,9] and graphite[10]. Quantitative information regarding the anodic oxidation of SO_2 in concentrated acid solutions or on metals other than platinum

and gold are sparce. As has been pointed out[1,11,12], however, high concentration of sulfuric acid in the electrolyzer is of crucial importance to maximize the energy efficiency of the Sulfur Cycle Hydrogen Production Process.

The objective of the present work is to understand the electrochemistry of electrolysis in the SO_2-saturated sulfuric acids. A number of candidate materials which are chemically stable under the operating conditions, were evaluated for electrochemical oxidation of sulfur dioxide. Effects of temperature and acid concentration on the electrode kinetic parameters were investigated. Cyclic voltammetric studies were conducted on metal electrodes to determine the influence of oxygen-containing films on the reaction kinetics. Attempts were also made to find alternate catalysts of low cost and promising activities to substitute for platinum in the electrochemical oxidation of sulfur dioxide in acidic media.

2.1.1 Kinetic Studies on Metal Electrodes

From the results of polarographic studies, Rosenthal and Veseloskii[3] concluded that dissolved sulfur dioxide is oxidized by the oxygen-containing species adsorbed electrochemically on the electrode surface. More precisely, the anodic oxidation of sulfur dioxide takes place via a purely chemical oxidation step between the dissolved sulfur dioxide and the oxygen-containing film at the anode. Thus, the reaction mechanism proposed for SO_2 oxidation may be expressed as follows[3]:

$$Pt + H_2O \rightarrow PtO_{ads} + 2\,H^+ + 2\,e^- \qquad (3)$$

$$PtO_{ads} + SO_2 + H_2O \rightarrow Pt + H_2SO_4 \qquad (4)$$

Based primarily on the charging characteristics of platinized Pt-foil electrodes in a 1.0 N H_2SO_4 solution saturated with SO_2, Bogdanovskii and Shlygin[4] have noted that the SO_2 oxidation reaction commences at 0.45 V versus RHE (reversible hydrogen electrode). At this potential, the surfaces of platinum electrodes are normally free of oxygen-containing films[13,14]. Therefore, they have disagreed with the "oxide mechanism" proposed by Rosenthal and Veseloskii[3],

and have suggested that this reaction occurs by a direct transfer of electrons from the adsorbed SO_2 molecules to the platinum anode. This electron-radical mechanism should involve the following steps:

$$SO_2 \rightarrow (SO_2)_{ads} \tag{5}$$

$$(SO_2)_{ads} \rightarrow SO_2^+ + e^- \tag{6}$$

$$SO_2^+ + 2\ H_2O \rightarrow HSO_3 + H_3O^+ \tag{7}$$

$$HSO_3 \rightarrow HSO_3^+ + e^- \tag{8}$$

$$HSO_3^+ + 2\ H_2O \rightarrow H_2SO_4 + H_3O^+ \tag{9}$$

More recently, Appleby and Pichon[7] have reported that the kinetics of the SO_2 oxidation reaction is independent of pH in dilute sulfuric acid solutions ranging from 0.01 N to 1.0 N. These workers proposed that the electrochemical oxidation of sulfur dioxide proceeds via the formation of dithionic acid, $H_2S_2O_6$, that is,

$$SO_2 + H_2O \rightarrow H_2SO_3^+ + e^- \tag{10}$$

$$2\ H_2SO_3^+ \rightarrow H_2S_2O_6 + 2\ H^+ \tag{11}$$

This reaction is finally completed by a disproportional step as follows:

$$H_2S_2O_6 \rightarrow SO_2 + H_2SO_4 \tag{12}$$

Owing to the use of an SO_2-depolarized electrolyzer in the Sulfur Cycle Hydrogen Production Process, the electrochemical oxidation of sulfur dioxide in concentrated sulfuric acids is of potential industrial importance[15,16]. Unfortunately, the reaction mechanisms discussed previously are only suitable for SO_2 oxidation in dilute sulfuric acid solutions. For the anodic oxidation of SO_2 in concentrated acid solutions (higher than 40 w/o), Appleby and Pichon[7] first proposed a reaction scheme which is quite similar to the "oxide

mechanism" by Rosenthal and Veselovskii[3]. The modified reaction paths involve three steps, that is

$$M + H_2O \rightarrow MOH + H^+ + e^- \quad (13)$$

$$MOH \rightarrow MO_{ads} + H^+ + e^- \quad (14)$$

$$SO_2 + H_2O + MO_{ads} \rightarrow H_2SO_4 + M \quad (15)$$

where M represents an active site for SO_2 oxidation.

Taking these various theories into account, experimental kinetic studies of the SO_2 oxidation reaction were carried out on a number of candidate materials including Pt, Pd, Ag, Rh, Au, Ru, Re and Ir.* In the preparation of test electrodes, a wire or rod of candidate materials was electrically connected to a platinum wire by spot welding. Each electrode was sealed in a shrinkable Teflon tubing such that a surface area of approximately 1 cm^2 was exposed to the electrolyte. Prior to each experiment, a test electrode was degreased using acetone and then pretreated cathodically at 10 mA/cm^2 in SO_2-free sulfuric acid solution for at least 10 minutes.

The measuring solutions (50 w/o H_2SO_4) were prepared from Fisher analyzed reagent grade sulfuric acid and distilled water. With a view to minimizing impurities, each measuring solution was further purified by pre-electrolysis at a current density of about 2 mA/cm^2 on a Pt-gauze cathode for at least 24 hours, followed by bubbling a highly pure nitrogen gas to eliminate traces of oxygen and hydrogen dissolved in the solution.

Electrochemical studies were conducted in a three-compartment cell as shown in Figure 1. The working electrode was placed so close (about 0.5 mm) to the Luggin capillary that the ohmic loss (i.e., IR drop) between the test and the

*The work on Rh, Au, Ru, Re and Ir electrodes was completed before the date of this contract, February 22, 1979.

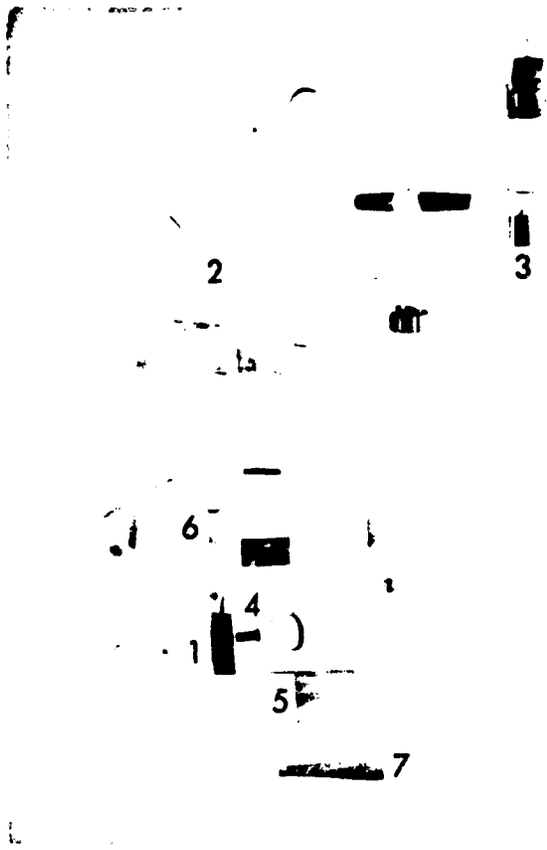

1. Working Electrode
2. Counter Electrode
3. Reference Electrode (Reversible Hydrogen Electrode)
4. Luggin Capillary
5. Frit Filter
6. Hydrogen Compartment
7. SO_2 Gas Inlet

Figure 1. Three Compartment Cell for Kinetic Studies.

reference electrode was negligible. A platinum spiral, positioned in a Teflon compartment separated by a Nafion membrane from the glass vessel, served as a counter electrode. The reference electrode used was a reversible hydrogen electrode (RHE) with sulfuric acid of the same concentration as the measuring solution. The electrochemical measurements were made at 25°C using a PAR Model 371 potentiostat. During each run the electrolyte within the main compartment (i.e., the glass vessel) was deaerated with SO_2 and magnetically stirred. It should be noted that the potentials quoted in this report are referred to the reversible hydrogen electrode (RHE).

Figure 2 shows the Tafel plots for SO_2 oxidation on a Pd electrode, determined by use of the steady state potentiostatic method. Starting at 0.4 V, the polarization potential of the freshly prepared electrode was increased in steps. In the direction of increasing potential, there was a little difficulty in achieving steady currents within a short period of time. Consequently, the quasi-stable current at each potential was recorded after five minutes of equilibration. At the highest polarization potential, 1.0 V, the Pd electrode was potentiostated for 30 minutes. The preanodization process resulted in the formation of stable surface films on the electrode, and thus steady currents were generally observed in the direction of decreasing potential.

As seen from Figure 2, well-defined Tafel regions of at least two decades long appear on both the freshly prepared and the preanodized Pd electrodes. As has been reported[17,18], palladium oxide, PdO, is formed on a bare palladium electrode at potentials above 0.79 V by a reaction as follows:

$$Pd + H_2O \rightarrow PdO + 2\ H^+ + 2\ e^- \qquad (16)$$

Thus, an oxide film is apparently present on the freshly prepared Pd electrode at potentials higher than 0.79 V and on the preanodized Pd electrode. In the potential range of 0.76-0.88 V, the freshly prepared electrode exhibits a linear Tafel region. This electrode also shows the same Tafel slope as the preanodized electrode (being ~54 mV/decade). Furthermore, the latter has higher electrocatalytic activities than the former at potentials ranging from 0.61 V to 0.85 V. It is thus concluded that the formation of PdO film on the Pd

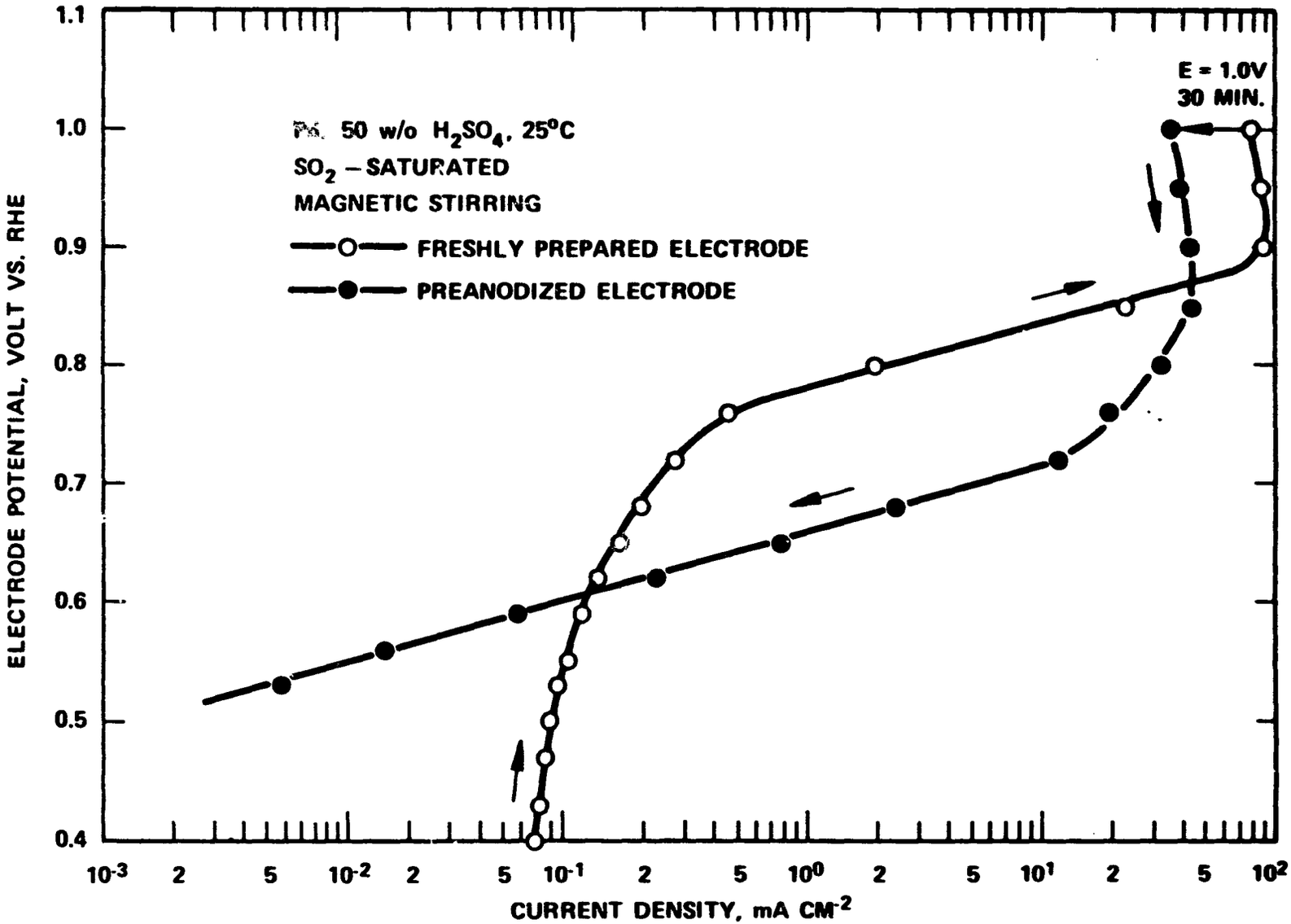

Figure 2. Tafel Plots for SO_2 Oxidation on Palladium Electrode in SO_2-Saturated Sulfuric Acid Solutions (50 w/o, 25°C).

electrode does not inhibit the electrochemical oxidation of SO_2. More precisely, PdO is a "right type of oxide" which expedites the SO_2 oxidation reaction.

Figure 3 gives Tafel plots for SO_2 oxidation on preanodized Pd, Ag and Pt electrodes. Three separate measurements were performed on each electrode. It was found that, prior to each experiment, tne preanodization of a test electrode resulted in rather reproducible data. In fact, the potential-current density relationships shown in Figure 3 represent the average values of thee individual studies on each electrode. Kinetic parameters for the anodic oxidation of SO_2 on these electrodes are summarized in Table 1.

The performance characteristics of Pt electrodes are considered as a baseline for comparison. The limiting current densities on Pd and Ag electrodes are higher than on Pt electrodes by a factor of about 30 and 4, respectively. At the temperature of study, 25°C, the observed Tafel slopes on Pd and Pt electrodes (being ∿54 and ∿67 mV/decade, respectively) are very close to RT/F, where R is the gas constant, T the absolute temperature and F the Faraday constant. Referring to the modified reaction mechanism discussed previously, a Tafel slope of RT/F strongly supports the hypothesis that the formation of adsorbed oxygen-containing species on an active site M is rate determining in the SO_2 oxidation reaction:

$$MOH \rightarrow MO_{ads} + H^+ + e^- \qquad (14)$$

A slightly lower Tafel slope (∿4T/5F) is observed on the Ag electrode. For SO_2 at 1 atm. and 25°C, the exchange current densities, obtained by extrapolating the linear Tafel region to the calculated reversible potential for SO_2 oxidation in 50 w/o H_2SO_4 solution (being approximately 0.29 V) are 1.5×10^{-10}, 2.5×10^{-9} and 1.9×10^{-10} A/cm^2 on Pd, Ag and Pt electrodes, respectively. According to Appleby and Pichon[7], the exchange current density for SO_2 oxidation on a smooth Pt electrode is $\sim 10^{-11}$ A/cm^2 in 44 w/o H_2SO_4 solution at 50°C. Furthermore, Pd and Ag electrodes exhibit lower anodic overpotentials than Pt electrode at various current densities. At 1 mA/cm^2, for example, the polarization potentials on Pd and Ag electrodes are about 120 and 225 mV, respectively, less than on Pt electrode (see Table 1).

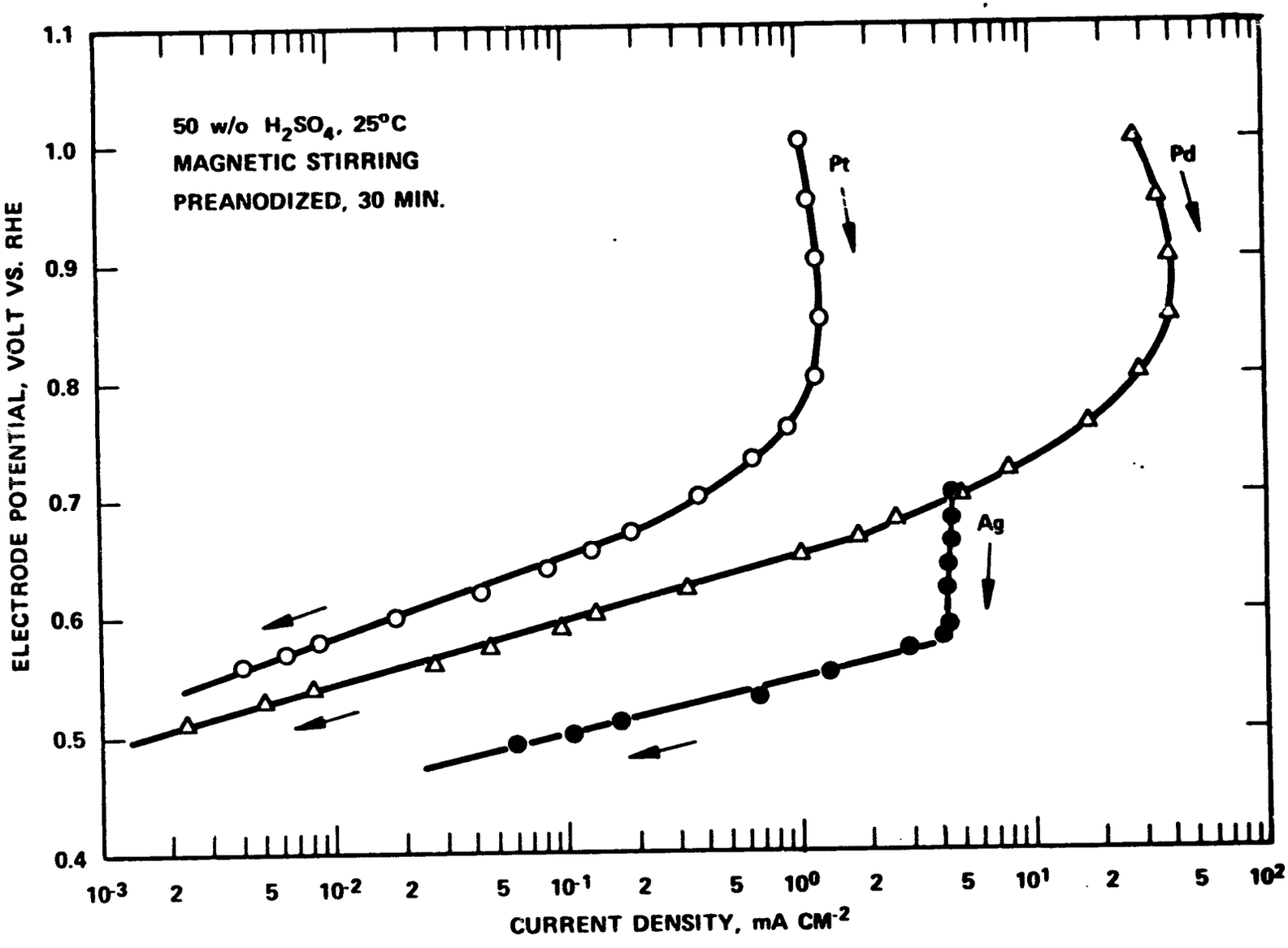

Figure 3. Tafel Plots for SO_2 Oxidation on Preanodized Platinum, Palladium and Silver Electrodes in SO_2-Saturated Sulfuric Acid Solutions (50 w/o, 25°C).

TABLE 1

ELECTRODE KINETIC PARAMETERS FOR SO_2 OXIDATION ON PLATINUM, PALLADIUM AND SILVER

(50 w/o H_2SO_4 Solutions at 25°C)

Electrode	Tafel Slope (mV/Decade)	Transfer* Coefficient	Exchange Current Density (A/cm^2)	Limiting Current Density (A/cm^2)	Polarization Potential at 1 mA/cm^2 (V)
Pt	67	0.88	1.9×10^{-10}	1.2×10^{-3}	0.77
Pd	54	1.09	1.5×10^{-10}	4.0×10^{-2}	0.65
Ag	47	1.25	2.5×10^{-9}	4.5×10^{-3}	0.545

*Transfer Coefficient = 2.303 RT/bF where b is the Tafel Slope.

It has been pointed out[19] that, on a preanodized Ag electrode, the surface films (presumably composed of silver oxide and/or silver sulfate) dissolve very slowly in sulfuric acid. Therefore, Ag is not suitable for use as an electrocatalyst in acid media. On the other hand, a preanodized Pd electrode which is covered by an oxide film, is superior to the Pt electrode in the anodic oxidation of SO_2.

2.1.2 Temperature Effects on Electrode Kinetics

Under atmospheric conditions, the reversible potential (E_r) for the anodic oxidation of sulfur dioxide is strongly dependent on the acid concentration and temperature. The reversible electrode potential may be represented by an equation of the form:

$$E_r = E_r^\circ + 2.303\ (RT/2F)\ \log\ (4m^3\gamma^3/a_{H_2O}) \qquad (17)$$

where E_r° is the standard reversible potential, R the gas constant, T the absolute temperature, F the Faraday constant, m the molality of sulfuric acid solution, γ the mean activity coefficient of the electrolyte and a_{H_2O}, the activity of water in the solution. As has been pointed out[7], quantitative information regarding the variations of γ and a_{H_2O} with temperature and acid concentration is insufficient. However, changes in the reversible electrode potential with temperature are given by

$$\left(\frac{\partial E_r}{\partial T}\right)_p = \frac{\Delta S}{2F} \qquad (18)$$

where ΔS represents the entropy change for the reaction:

$$SO_2(g) + 2\ H_2O(\ell) \rightarrow H_2SO_4(aq) + H_2(g) \qquad (19)$$

In the temperature range of 25-90°C, ΔS is approximately independent of temperature. Thus, the dependence of the reversible electrode potential for SO_2 oxidation may be expressed as:

$$E_r = E_{r,\,298} + \frac{\Delta S}{2F}(T - 298) \qquad (20)$$

where $E_{r,\,298}$ is the reversible electrode potential at 25°C. It is noted that, at standard state, the entropy change for the reaction (19) is -24.01 cal/k/mole. On the basis of this ΔS value, the values of E_r at different temperatures can be calculated. Figure 4 shows the variation of the reversible electrode potentials for SO_2 oxidation with temperature in 50 w/o sulfuric acid solution.

Increasing temperature should accelerate the reaction rate on the electrode surface. The kinetics of the SO_2 oxidation reaction, however, are strongly dependent on the concentration of SO_2-containing species dissolved in the electrolyte. As has been pointed out[20-22], the solubility of SO_2 in sulfuric acid solutions decreases significantly with increasing temperature at atmospheric pressure. In sulfuric acids of concentration ranging from 50 to 80 w/o, it was proved[7] that SO_2 solubility (at 1 atm.) reduces from 1 M at 20°C to 0.1 M at 95°C. Therefore, the dependence of electrode kinetic parameters on temperature is a complex set of phenomena, particularly in the limiting current regions where diffusion of reactants from the bulk to the electrode surface is the rate-controlling step. The studies of temperature effect on electrode kinetic parameters for SO_2 oxidation were conducted on smooth Pd and Pt electrodes and on a platinized Pt electrode using 50 w/o sulfuric acid solutions. Electrochemical measurements were made at four different temperatures, that is 25, 50, 70 and 90°C, by a steady state potentiostatic method. Prior to each experiment, test electrodes were preanodized at 1.0 V for 30 minutes. Current-potential relationships were determined in the direction of high currents to low currents.

Figure 5 shows Tafel plots for SO_2 oxidation on the preanodized Pd electrode at various temperatures. Distinct linear Tafel regions of approximately three decades long are observed for the full range of temperature. As illustrated in Table 2, transfer coefficients at temperatures of study are all close to unity (i.e., Tafel slope being close to RT/F). These results indicate that the reaction mechanism of SO_2 oxidation is independent of temperature ranging from 25 to 90°C. There is very little or no improvement in the limiting

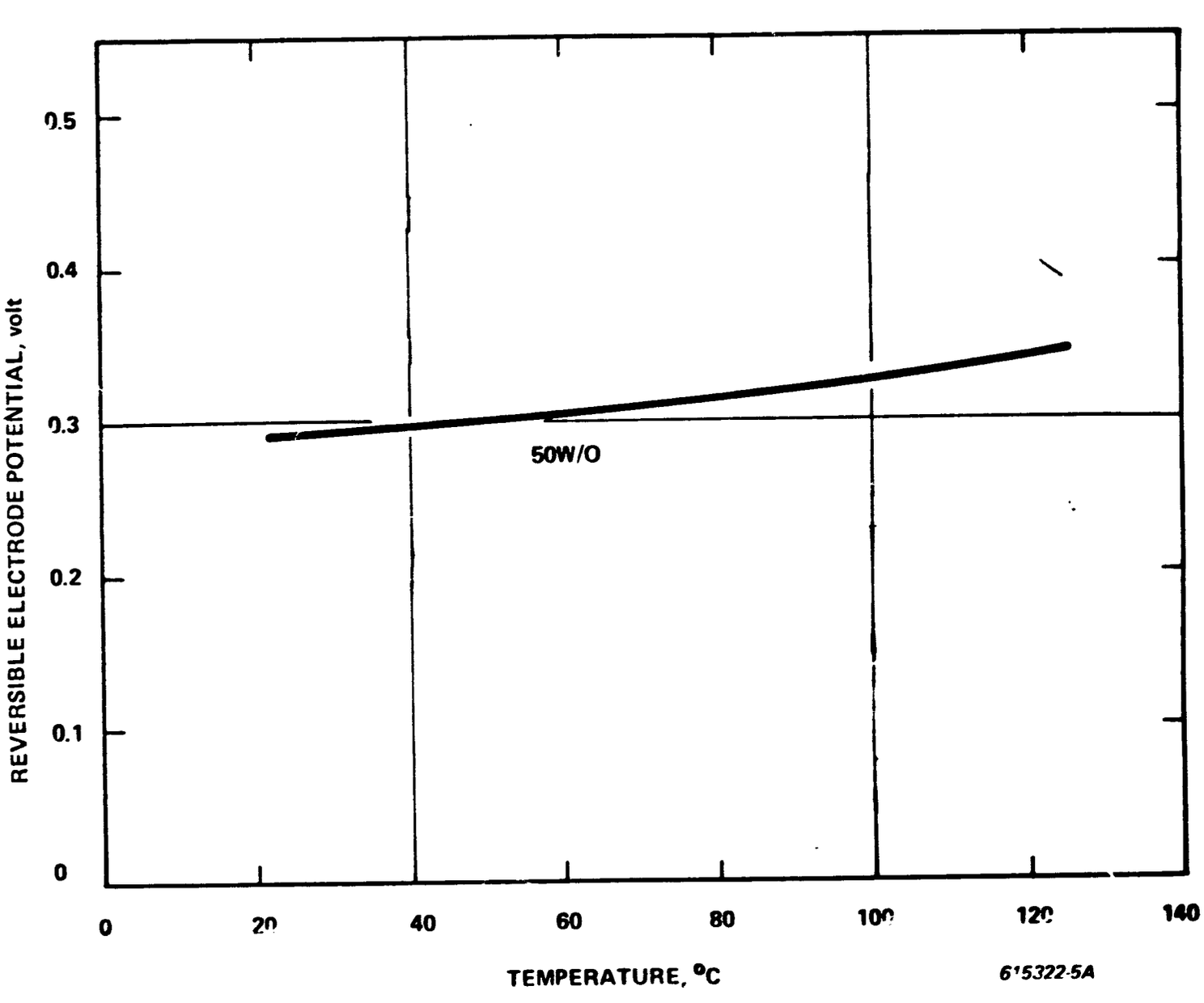

Figure 4. Variation of the Reversible Cell Potential of an SO_2-Depolarized Electrolyzer with Temperature.

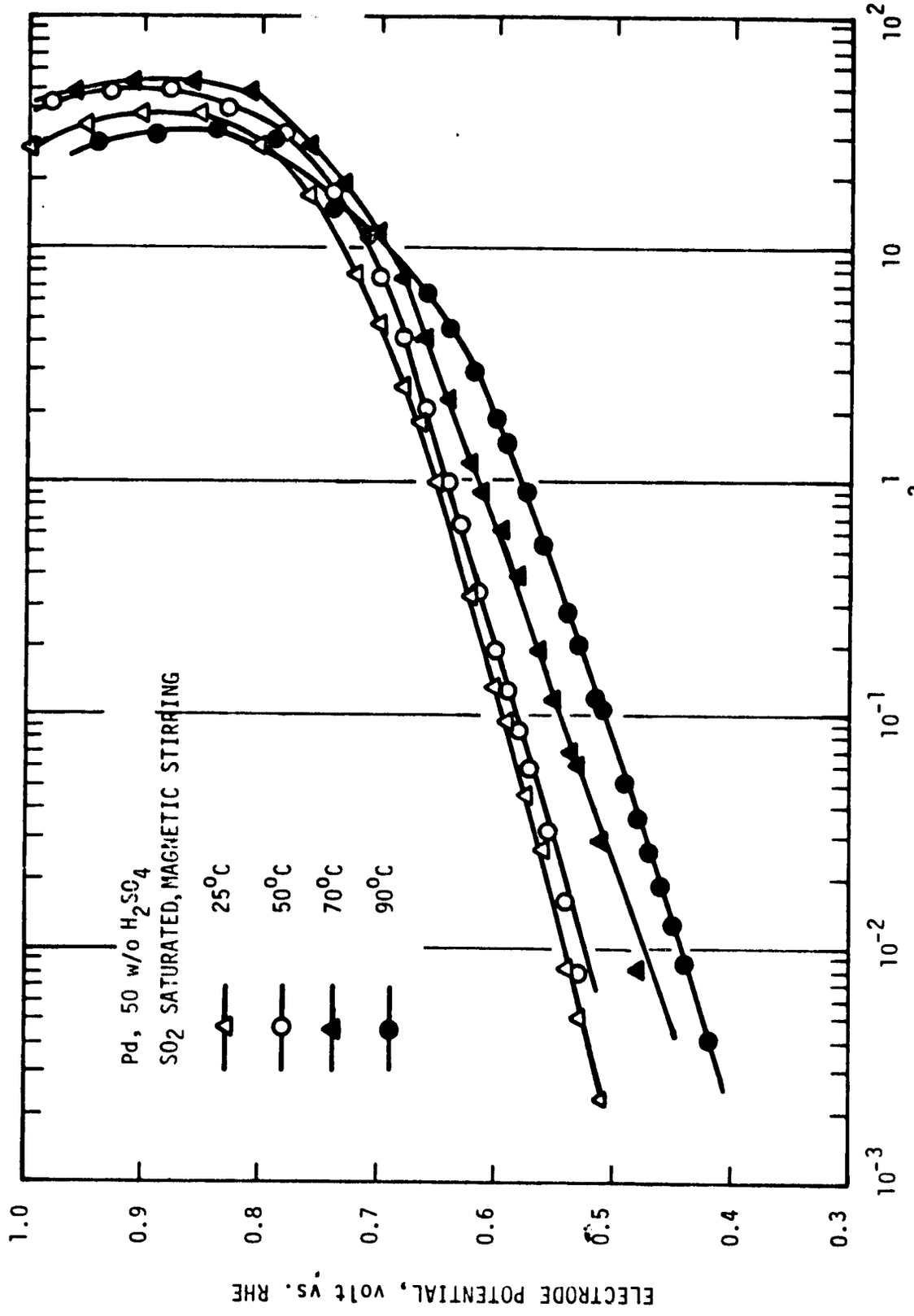

Figure 5. Tafel Plots for SO_2 Oxidation on Preanodized Palladium Electrode at Temperatures of 25, 50, 70 and 90°C.

TABLE 2

ELECTRODE KINETIC PARAMETERS FOR SO_2 OXIDATION ON PREANODIZED PALLADIUM ELECTRODES IN 50 W/O H_2SO_4 SOLUTIONS

Temperature (°C)	Tafel Slope (mV/Decade)	Transfer* Coefficient	Exchange Current Density (A/cm^2)	Limiting Current Density (A/cm^2)	Overpotential at 1 mA/cm^2 (mV)
25	54	1.09	1.5×10^{-10}	4.0×10^{-2}	360
50	59	1.09	5.0×10^{-9}	4.9×10^{-2}	340
70	72	0.92	5.0×10^{-8}	5.4×10^{-2}	310
90	70	1.03	1.9×10^{-7}	3.3×10^{-2}	260

*Transfer Coefficient = 2.303 RT/bF where b is the Tafel Slope.

current density arising from the temperature increase. This is essentially due to the significant reduction of SO_2 solubility in the electrolyte, caused by increasing temperature[7,20-22]. In the linear Tafel region, however, polarization potentials on the Pd electrode decrease while exchange current densities increase distinctly with the temperature increase. As shown in Figure 5, an improvement of about 100 mV in the anode overpotential at 1 mA/cm^2 is achieved by increasing the test temperature from 25 to 90°C.

Since there is no change in the reaction mechanism in the temperature range of 25-90°C, the Arrhenius activation energy for the anodic oxidation of SO_2, $\Delta H_o^{\ddagger}$, under the reversible condition can be calculated by an equation of the form:

$$\Delta H_o^{\ddagger} = -2.303\ R\ \partial \log i_o / \partial (1/T) \qquad (21)$$

where i_o represents the exchange current density. Figure 6 shows the log i_o versus reciprocal temperature plot, in which i_o values are obtained from Table 2. On the smooth Pd electrode, the activation energy for SO_2 oxidation determined from this plot, is as high as ∿25 Kcal/mole. In 50 w/o KOH solution, the activation energy for oxygen evolution on nickel is ∿18 Kcal/mole[23]. Apparently the anodic oxidation of SO_2 is a highly irreversible process, requiring a higher overpotential than the oxygen evolution reaction.

The dependence of electrode kinetic parameters on temperature for the anodic oxidation of SO_2 on a smooth Pt electrode is shown in Figure 7 as well as Table 3. Each temperature increase produces an obvious enhancement in the experimental exchange current densities and limiting current densities. For the electrochemical oxidation of SO_2 on the smooth Pt electrode, only small shifts in the polarization potential are observed at temperatures above 50°C. Nevertheless, significant improvements in the overpotential result from increasing temperature (see Table 3). At 1 mA/cm^2, for instance, the temperature increase from 25 to 90°C yields a reduction of ∿160 mV in the overpotential. The observed Tafel slops (being close to RT/F) are approximately constant at temperatures of study, indicating that the reaction mechanism on the smooth Pt electrode is also independent of temperature.

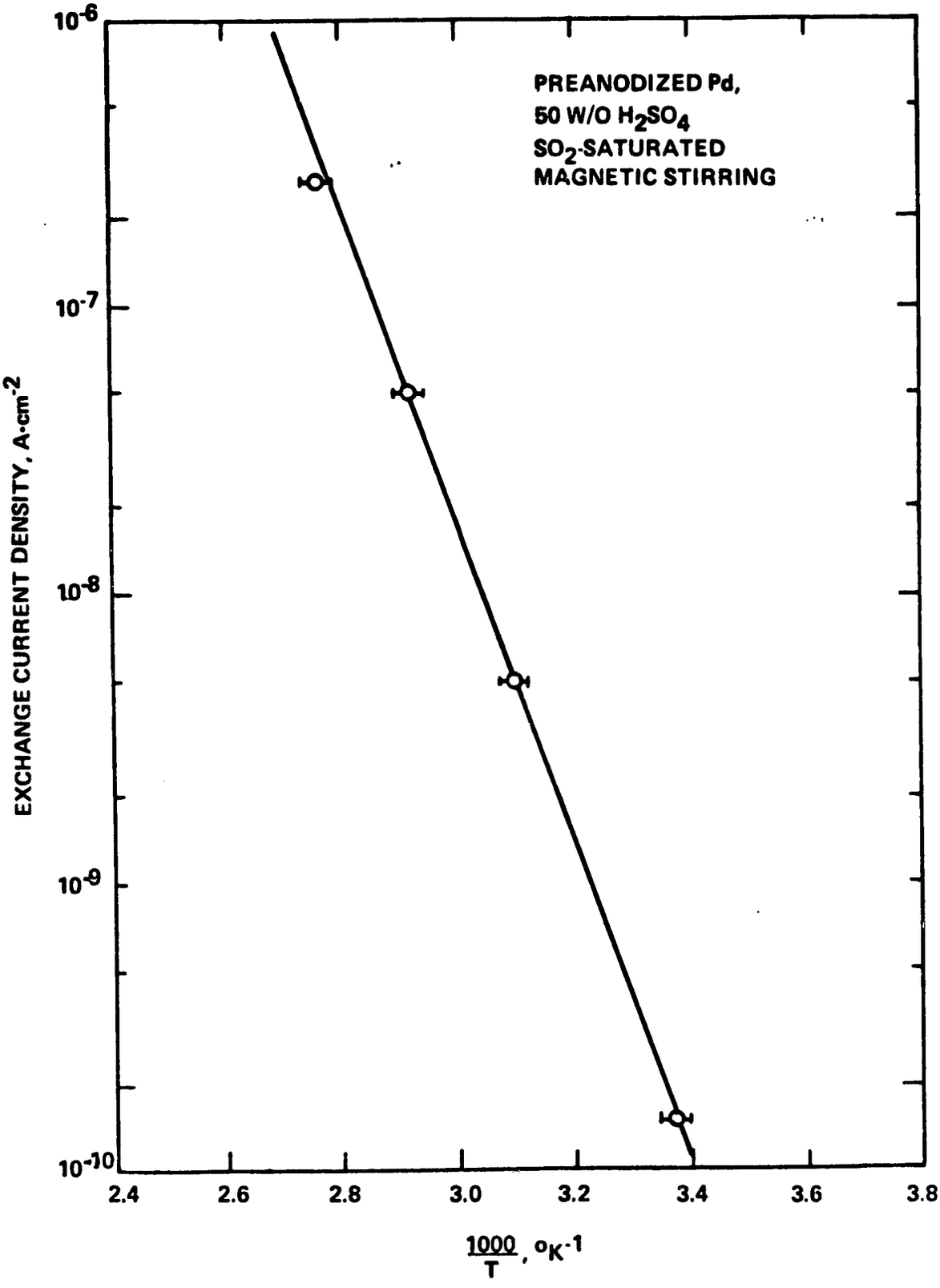

Figure 6. Arrhenius Plot for SO_2 Oxidation on a Smooth Palladium Electrode in 50 w/o Sulfuric Acid Solutions at Atmospheric Pressure.

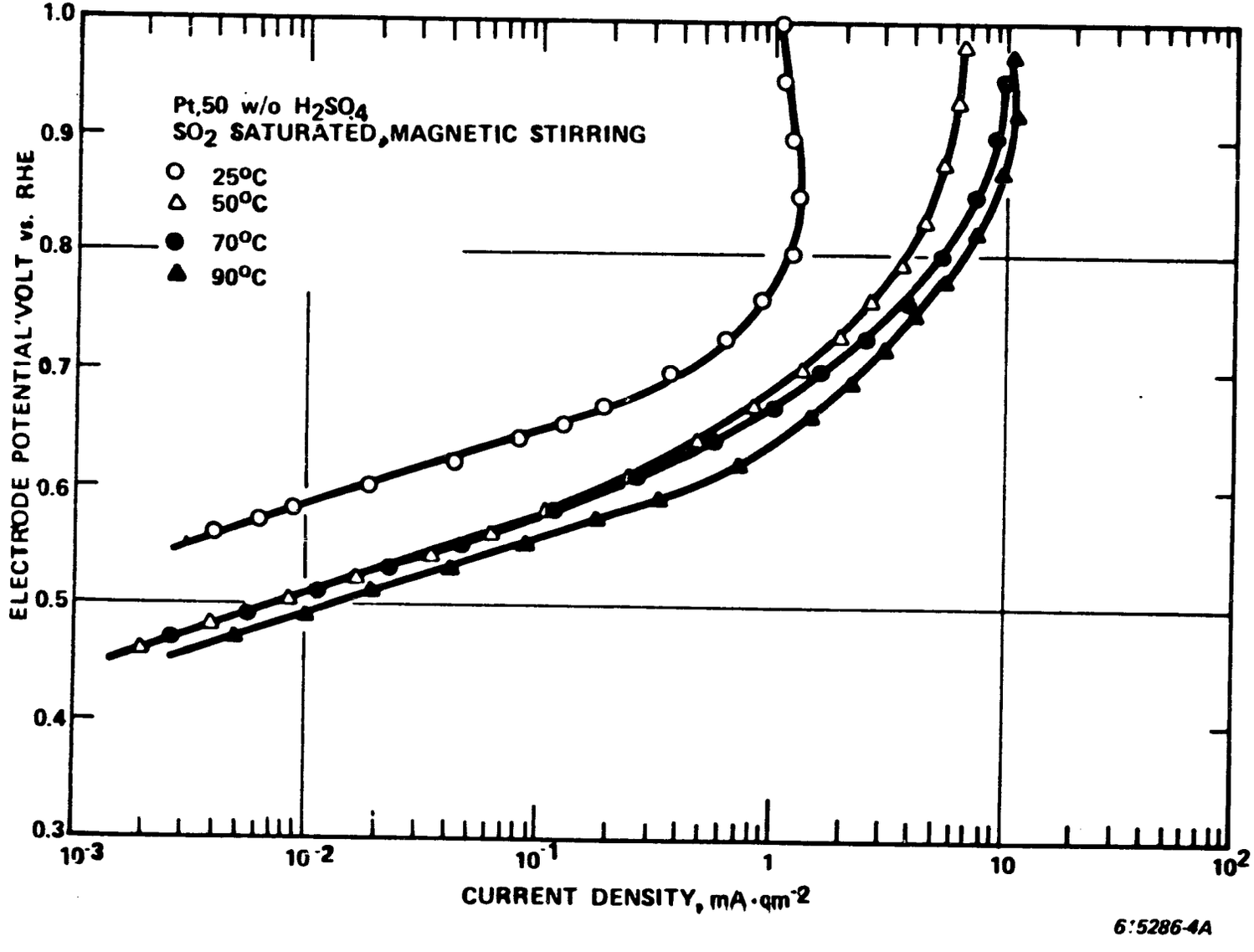

Figure 7. Tafel Plots for SO_2 Oxidation on Preanodized Platinum Electrode at Temperatures of 25, 50, 70 and 90°C.

TABLE 3

ELECTRODE KINETIC PARAMETERS FOR SO_2 OXIDATION ON PREANODIZED PLATINUM ELECTRODES IN 50 W/O H_2SO_4 SOLUTIONS

Temperature (°C)	Tafel Slope (mV/Decade)	Transfer* Coefficient	Exchange Current Density (A/cm^2)	Limiting Current Density (A/cm^2)	Overpotential at 1 mA/cm^2 (mV)
25	67	0.88	1.9×10^{-10}	1.2×10^{-3}	480
50	68	1.06	4.3×10^{-9}	6.6×10^{-3}	380
70	68	1.00	6.2×10^{-9}	9.8×10^{-3}	360
90	67	0.93	2.9×10^{-8}	1.1×10^{-2}	320

*Transfer Coefficient = 2.303 RT/bF where b is the Tafel Slope.

Figure 8 illustrates the current-potential relationships for SO_2 oxidation on a platinized Pt electrode at various temperatures. The test electrode was prepared by electrodepositing a layer of Pt black on a platinum foil ($\sim$2 cm^2). During the experiment, this electrode was fully immersed in the electrolyte. At each temperature, the limiting current density on the platinized Pt electrode is much higher than on the smooth Pt electrode (see Figure 7). For the anodic oxidation of SO_2 on the platinized electrode, the Tafel slope increases distinctly while the limiting current density decreases slightly with increasing temperature. On an electrocatalyst, the limiting current density is dependent on the transfer rate and the availability of reactants (i.e., SO_2-containing species). With the platinized Pt electrode, the limiting current densities are rather high (being above 60 mA/cm^2 at temperatures of study), and thus the consumption rate of SO_2 is significant. Therefore, the kinetics of the SO_2 oxidation reaction in the limiting density region is predominated by the solubility of SO_2 in the electrolyte, which decreases with increasing temperature.

It is concluded that, under atmospheric pressure, the temperature increase results in significant improvements in the exchange current density and anodic overpotential for SO_2 oxidation. On the smooth Pd and Pt electrodes, however, the reaction mechanism is approximately independent of temperature ranging from 25 to 90°C. Since the solubility of SO_2 in the electrolyte decreases significantly with increasing temperature, the effect of temperature on the limiting current density for SO_2 oxidation turns out rather complicated. At elevated pressures (above 5 atmospheres)[7,24], the temperature increase may cause more profound influence on the electrode kinetics of the SO_2 oxidation reaction.

2.1.3 Effects of Acid Concentration of Electrode Kinetics

As described previously, the dependence of the reversible electrode potential (E_r) for the anodic oxidation of SO_2 on the acid concentration is given by

$$E_r = E_r^\circ + 2.303(RT/2F) \log (4\, m^3 \gamma^3 / a_{H_2O}^2) \qquad (17)$$

At 25°C, the activities of water (a_{H_2O}) in aqueous sulfuric acids have been compliled in the work by Robertson and Dunford[25]. The mean activity coefficients for sulfuric acids of various concentrations may be obtained from

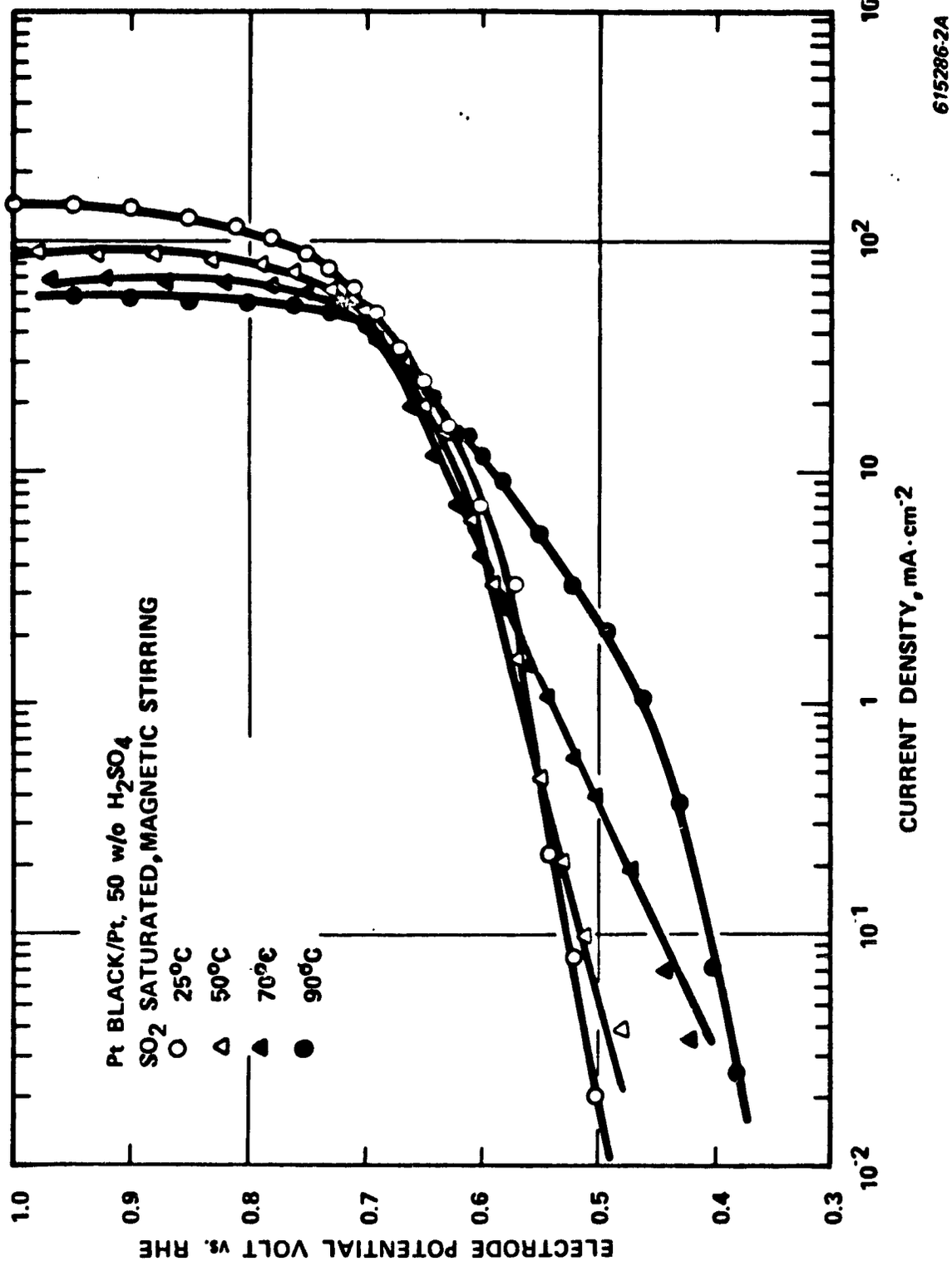

Figure 8. Tafel Plots for SO_2 Oxidation on a Platinized Platinum Electrode at Temperatures of 25, 50, 70 and 90°C.

"International Critical Tables."[26] On the basis of Equation (17), the dependence of the reversible electrode potential on acid concentration is shown in Figure 9. This curve is in good agreement with that calculated by Struck and coworkers[23].

Effects of acid concentration on electrode kinetic parameters were conducted on a smooth Pd electrode at 25°C. Tafel plots for SO_2 oxidation in sulfuric acids of concentration 20, 30, 40, 50, 60, and 70 w/o were determined using a steady state potentiostatic method. Experimental results shown in Figure 10 represent the averaged values of three individual experiments. The electrode kinetic parameters in various sulfuric acids are summarized in Table 4.

The preanodized Pd electrode exhibits a Tafel slope of approximately RT/F in sulfuric acids of concentration ranging 20-50 w/o. In more concentrated solutions (i.e., 60 and 70 w/o), a slightly low Tafel slope 4 RT/5 F is observed. The exchange current densities are obtained by extrapolating the linear Tafel regions to the reversible potentials for the anodic oxidation of SO_2. As shown in Figure 9, the calculated reversible potentials increase with the acid concentration. Consequently, the experimental exchange current densities on the Pd electrode increase also with increasing concentration. In sulfuric acids ranging from 40 to 70 w/o, however, the increase of acid concentration results in a significant decrease in the limiting current density and a distinct enhancement in the polarization potential. The influence of acid concentration on these kinetic parameters are hardly detectable in less concentrated solutions.

Conclusively, the SO_2 oxidation reaction exhibits rather high polarization potentials in sulfuric acids of concentration above 60 w/o, essentially due to low activities of water in the electrolyte[7,25]. As far as the overall energy efficiency of the sulfur-based cycle is concerned, the operation of an SO_2-depolarized electrolyzer using sulfuric acids of concentrations higher than 60 w/o may not be economical.

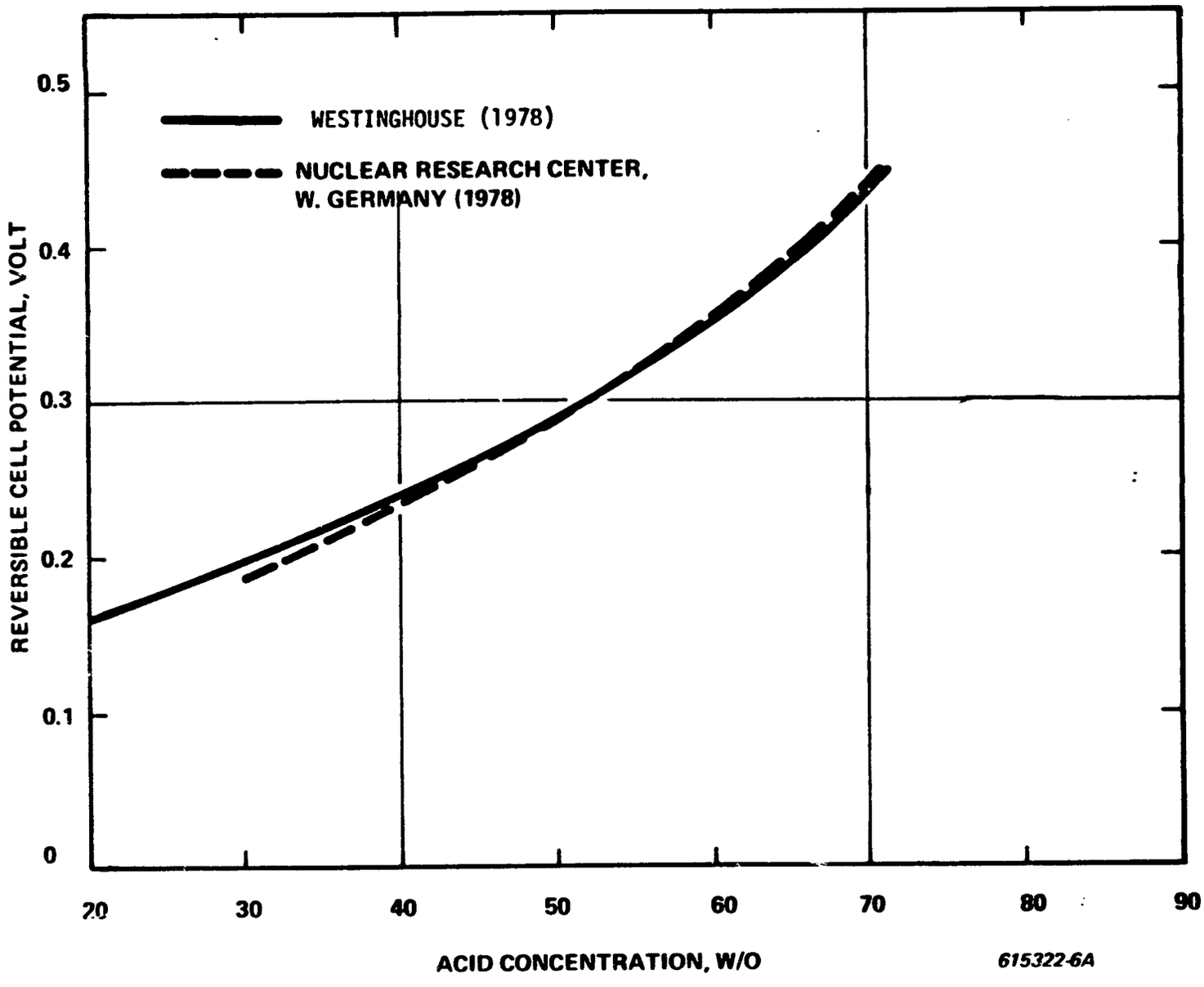

Figure 9. Dependence of the Reversible Cell Potential of an SO_2-Depolarized Electrolyzer on Acid Concentration at 25°C.

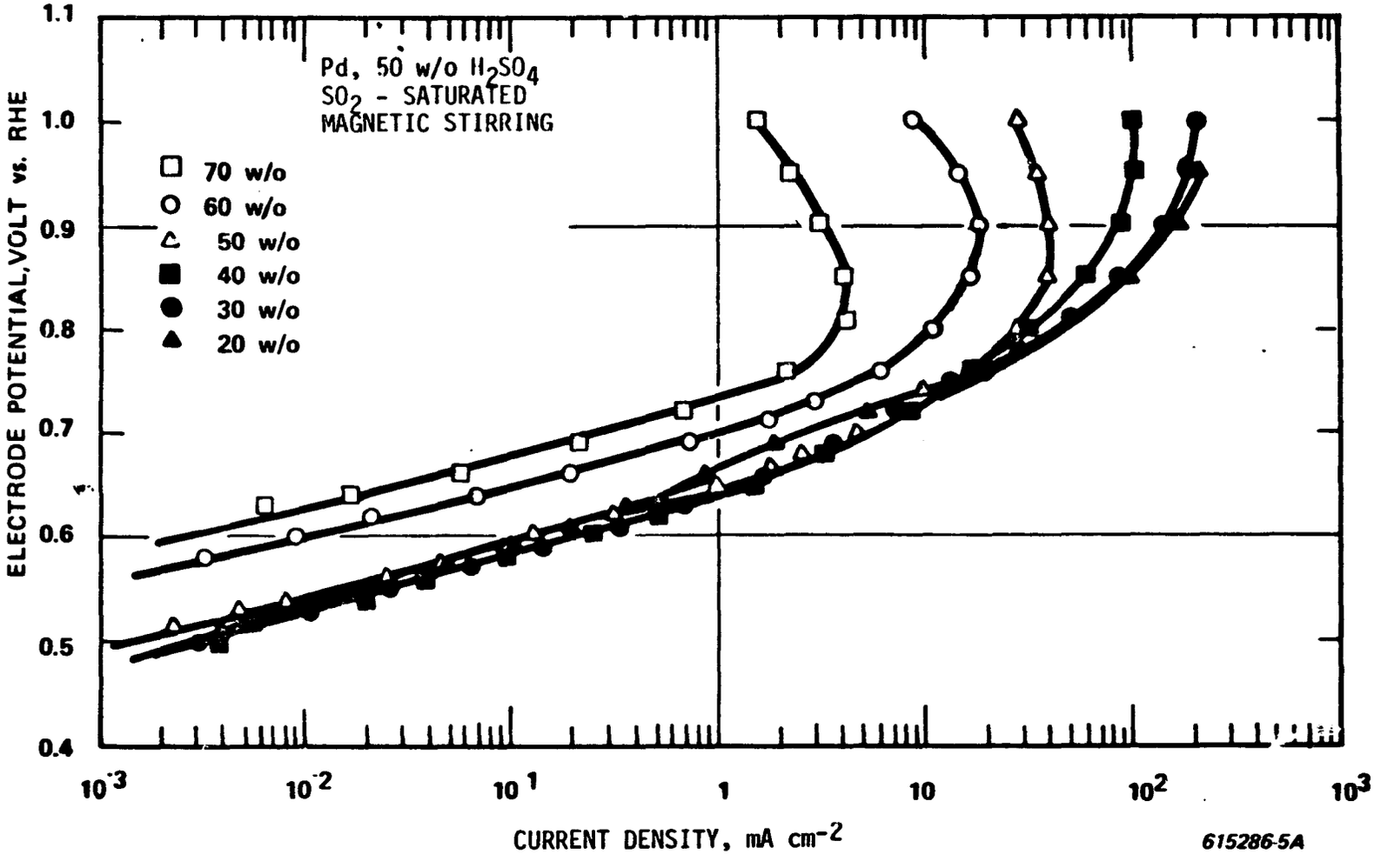

Figure 10. Tafel Plots for SO_2 Oxidation on a Preanodized Palladium Electrode in Sulfuric Acids of Concentration 20, 30, 40, 50, 60 and 70 w/o at 25°C.

TABLE 4

ELECTRODE KINETIC PARAMETERS FOR SO_2 OXIDATION ON PREANODIZED PALLADIUM ELECTRODES IN SULFURIC ACIDS OF VARIOUS CONCENTRATIONS

Concentration (w/o)	Tafel Slope (mV/Decade)	Transfer* Coefficient	Exchange Current Density (A/cm^2)	Limiting Current Density (A/cm^2)
20	60	0.99	6.4×10^{-12}	2.2×10^{-1}
30	55	1.07	9.0×10^{-12}	2.0×10^{-1}
40	55	1.07	5.8×10^{-11}	1.0×10^{-1}
50	54	1.09	1.5×10^{-10}	4.0×10^{-2}
60	49	1.20	1.0×10^{-10}	1.8×10^{-2}
70	49	1.20	1.1×10^{-9}	4.4×10^{-3}

*Transfer Coefficient = 2.303 RT/bF where b is the Tafel Slope.

2.1.4 Cyclic Voltametric Studies

The voltametric method has been extensively used to investigate the reaction mechanism of SO_2 oxidation on platinum[5-8,27] and gold[5,9]. The previous studies were, however, carried out only in dilute acid media. According to the work by Seo and Sawyer[5,27], an activated electrode surface can be achieved by cycling the potential of a platinum or gold electrode between -0.15 V and 1.50 V versus SCE (saturated calomel electrode) directly in an SO_2-containing electrolyte. In the cathodic sweep, the SO_2-containing species in the solution is electroreduced in the potential region for hydrogen evolution[5,27]. As a result, the reduction reaction may lead to the formation of adsorbed sulfur and H_2S on the electrode surface[9,27-29]. With a view to eliminating the adsorbed impurities, this study was conducted at potentials above 0.30 V versus RHE, where hydrogen evolution does not occur.

The voltametric studies were carried out on Pt, Pd, Ir, Rh and Ru electrodes in a three-compartment glass cell as shown in Figure 11. A cylindrical platinum gauze, placed in a compartment separated by frit glass from the main vessel, served as the counter electrode. A reversible hydrogen reference electrode was connected to the vessel by a Luggin capillary. The test electrodes and measuring solutions were prepared as described in Section 2.1.1. The electrochemical measurements were conducted in 50 w/o H_2SO_4 solution at 25°C using a PAR Model 173 potentiostat coupled with a PAR Model 175 Programmer. The cyclic voltammograms were recorded by use of an X-Y recorder at various scan rates ranging from 1 mV/sec to 1 V/sec. Each test electrode was degreased by immersion in acetone, was then thoroughly rinsed with distilled water and was cathodically pretreated (at $\sim$1 mA/cm^2) in an SO_2-free H_2SO_4 solution. Prior to each experiment, the pretreated electrode was potentiostated at + 0.3 V in the measuring solution for 5 minutes. By applying a linear potential sweep of 100 mV/sec, the first ten traces of continuous cyclic i-V curves were recorded.

Figure 12 shows the first traces of cyclic i-V curves on a freshly prepared Pt electrode in both SO_2-free and SO_2-saturated H_2SO_4 solutions. It should be noted that the current density scales for the two voltametric curves are significantly different. In the SO_2-free electrolyte, the formation of

1. Working Electrode
2. Counter Electrode
3. Reference Electrode (Reversible Hydrogen Electrode)
4. Luggin Capillary
5. Frit Glass
6. Hydrogen Compartment
7. Main Compartment
8. SO_2 Gas Inlet

Figure 11. Three Compartment Glass Cell for Voltametric Studies.

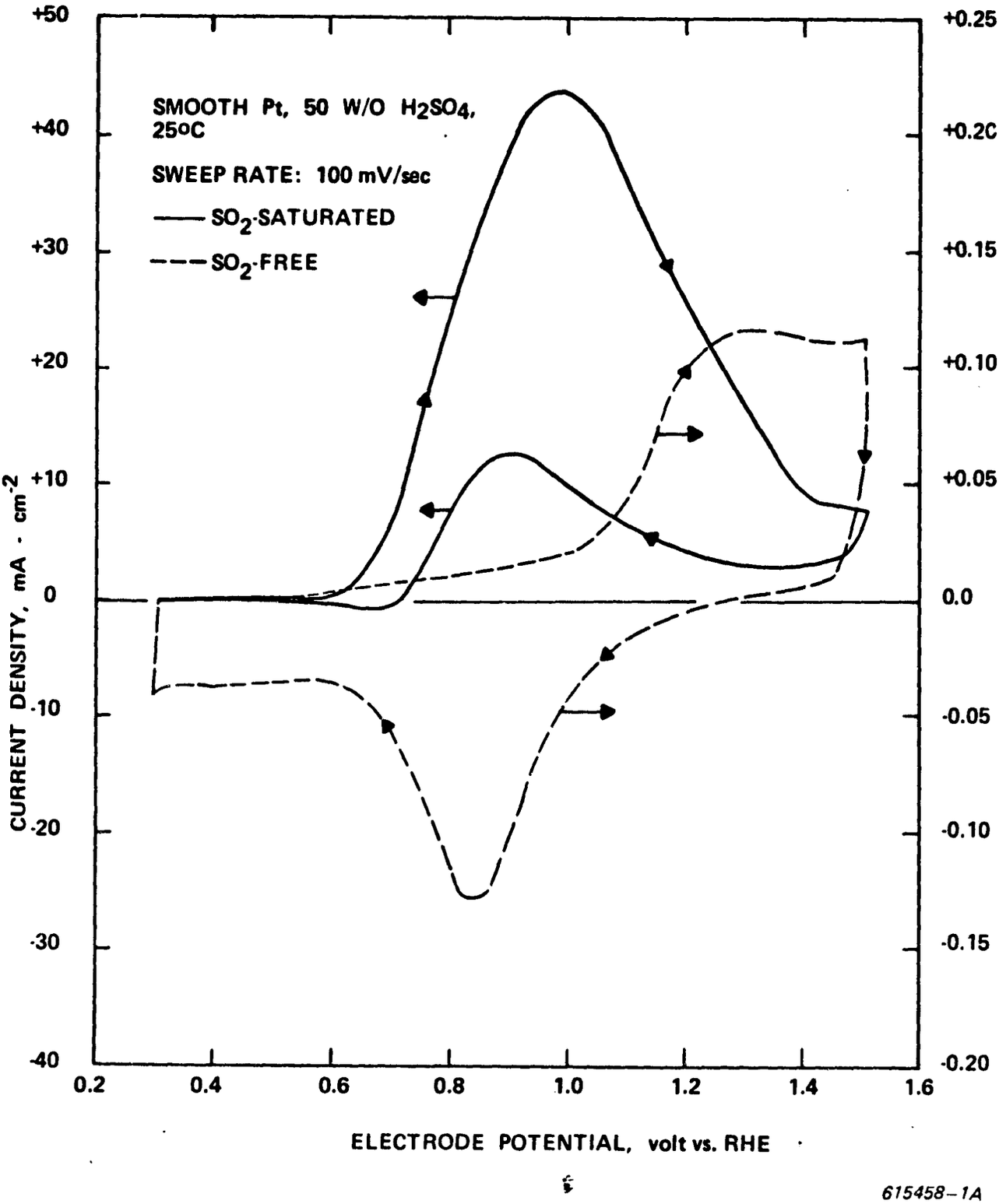

Figure 12. Cyclic Voltammograms on a Smooth Platinum Electrode at 100 mV/sec in Both SO_2-Free and SO_2-Saturated Acid Solutions at 25°C.

chemisorbed oxygen-containing layer on the bare electrode surface commences at an anodic potential of ∿0.55 V (see Figure 12). Ellipsometric studies[14] indicated that, starting at a potential ∿0.95 V, the chemisorbed oxygen-containing layer on a Pt anode is converted to platinum oxide (PtO), by the "place exchange mechanism"[30]. The anodic and cathodic peaks observed at 1.30 and 0.83 V, respectively, are thus attributed to the formation and reduction of PtO film.

In the SO_2-saturated acid solution, the anodic and cathodic peaks corresponding to the formation and reduction of oxide film are entirely obscured by the relatively high currents for the SO_2 oxidation reaction. As shown in Figure 12, this reaction commences at approximately the same potential as the formation of chemisorbed oxygen-containing layer (being ∿0.55 V). In the anodic i-V curve, the observed current density decreases significantly with a further rising potential after reaching the peak maximum at ∿0.98 V. Similar results have been reported for the electrooxidation of ethylene[31] and ethylene glycol[32]. This phenomenon is essentially due to "passivation" of the Pt anode. As discussed previously, the conversion of chemisorbed oxygen-containing layer to PtO film takes place at potentials above 0.95 V[14]. It is obvious that the passivated layer which strongly inhibits the SO_2 oxidation reaction on a Pt anode, is substantially composed of PtO.

In the cathodic i-V curve, no detectable reduction peak is observed, indicating that the SO_2 oxidation reaction is entirely irreversible. As seen from Figure 12, the electroreduction of PtO film in the cathodic sweep starts at ∿1.25 V. The complete reduction of oxide film occurs at potentials below 0.6 V. Nevertheless, on the partially reduced Pt electrode, an anodic peak for SO_2 oxidation appears at ∿0.90 V. This observation indicates that the electrocatalytic activity of an oxide-covered Pt anode for the electrooxidation of SO_2 is rejuvenated by the electroreduction of PtO film.

The first traces of cyclic i-V curves on a freshly prepared Pd electrode are demonstrated in Figure 13. In the SO_2-free electrolyte, two anodic peaks are detected at 1.03 and 1.14 V. It has been found experimentally[17] that, on a bare Pd anode, palladium oxide, PdO, is formed at potentials above 0.79 V by the following reaction:

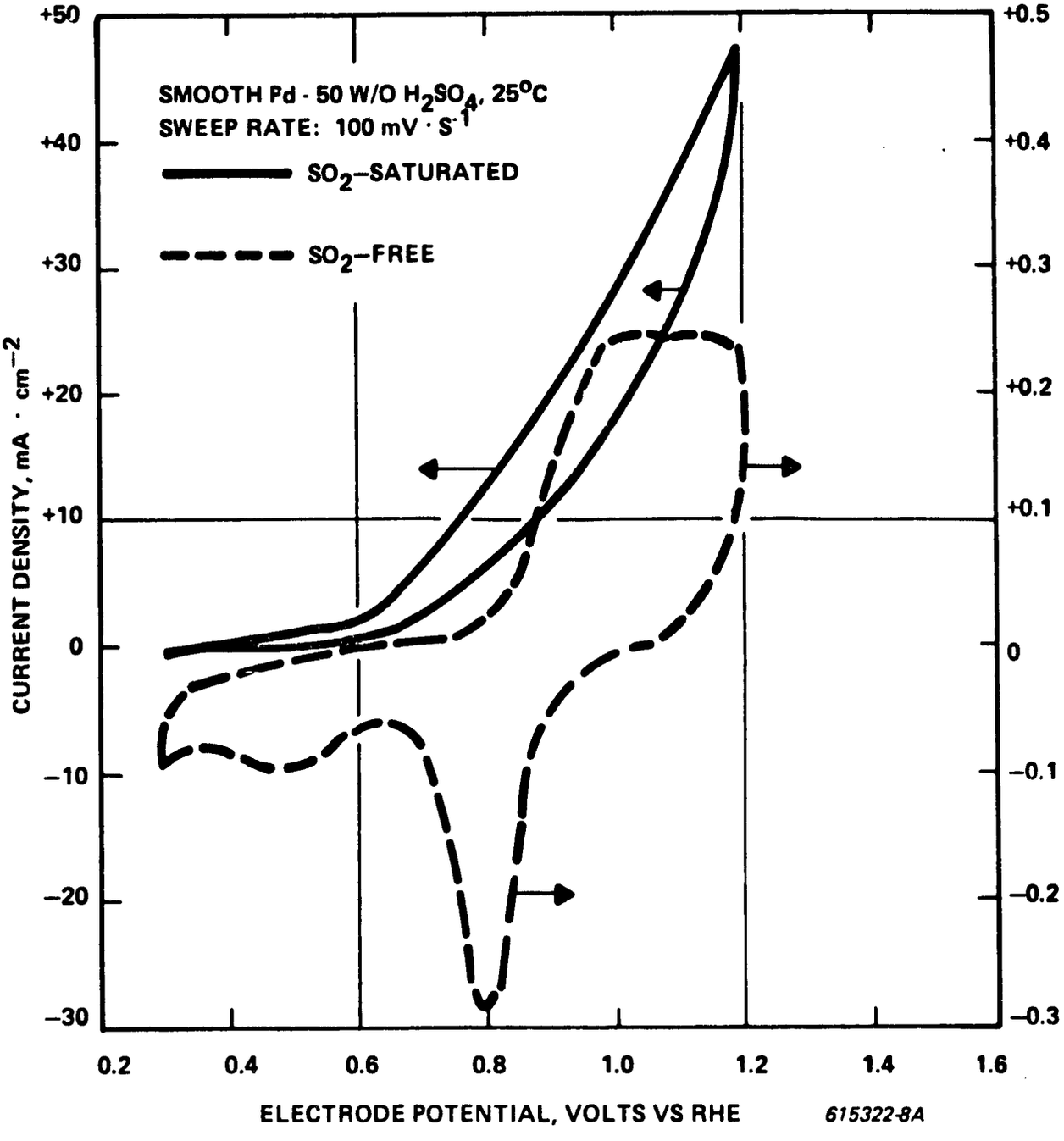

Figure 13. Cyclic Voltammograms on a Smooth Palladium Electrode at 100 mV/sec in Both SO_2-Free and SO_2-Saturated Acid Solutions at 25°C.

$$Pd + H_2O \rightarrow PdO + 2H^+ + 2e^- \qquad (16)$$

According to the work by Goldberg and Hepler[33], the standard potential for the formation of hydrated palladium oxide, $Pd(OH)_2$, is ∿0.896 V. Therefore, in the anodic sweep up to 1.2 V, the chemical transformation of chemisorbed oxygen-containing layer to palladium oxide films should take place.

In the SO_2-saturated electrolyte, the cyclic voltammogram on the Pd electrode is somewhat different from that on the Pt electrode. On a bare Pd anode, the SO_2 oxidation reaction also commences at a potential where the growth of chemisorbed oxygen-containing layer is initiated (being ∿0.60 V as identified in Figure 13). The observed current density for this reaction, however, increases distinctly with rising potential up to 1.2 V, and then decreases gradually with reducing potential. No oxidation peak is detected in either the anodic or the cathodic i-V curve. The experimental results show that the growth of oxide films on the Pd anode does not inhibit the electrochemical oxidation of SO_2. More precisely, an oxide-covered Pd electrode exhibits great electrocatalytic activity for SO_2 oxidation.

The effect of the oxidation state of palladium oxides on the kinetics of the SO_2 oxidation reaction was investigated by increasing the upper limit potential up to 1.50 V. Figure 14 shows the cyclic i-V curves on freshly prepared Pd electrodes in SO_2-saturated sulfuric acid solutions (50 w/o) within the following potential ranges: 0.30 - 1.20 V, 0.30 - 1.25 V, 0.30 - 1.30 V, 0.30 - 1.35 V, 0.30 - 1.40 V and 0.30 - 1.50 V. Prior to the determination of voltammetric curves, each test electrode was maintained at 0.30 V for 5 minutes. During the experiment, only the first and tenth traces of cyclic i-V curves were recorded. In spite of the upper limit potential, no anodic peak is found in the first traces of cyclic i-V curves (see Figure 14). As the upper limiting potential is increased from 1.20 V to 1.25 V, however, there is a strong tendency to form an anodic peak on the subsequent i-V curves. As demonstrated in Figure 14, the anodic peaks at ∿0.9 V become distinctive in the tenth traces of cyclic i-V curves if the upper limit potential is increased to 1.30 V or higher.

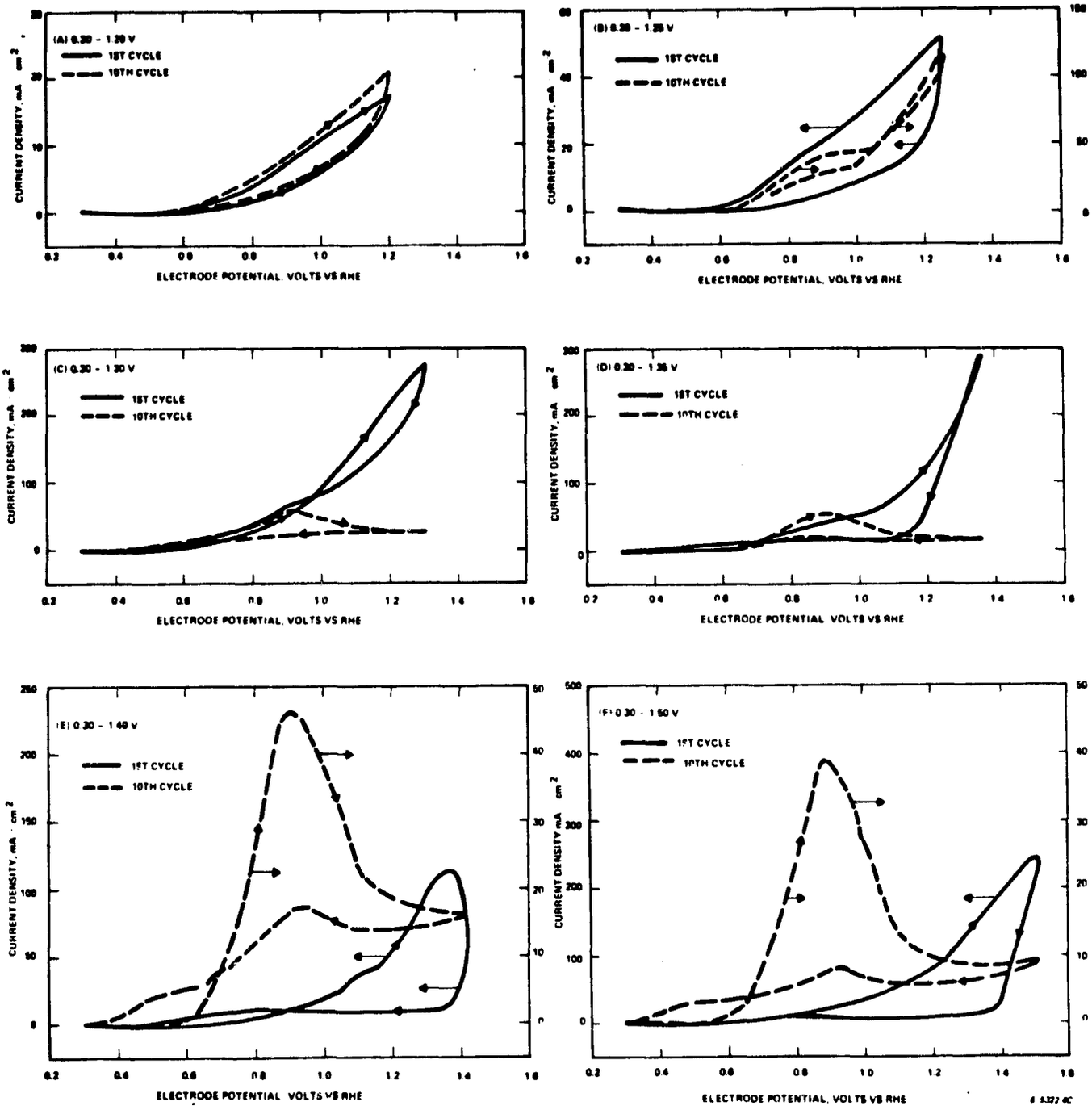

Figure 14. Cyclic Voltammograms on Freshly Prepared Palladium Electrodes in SO_2-Saturated Sulfuric Acid Solutions (50 w/o, 25°C), within Various Potential Ranges as Indicated (Scanning Rate: 100 mV/sec).

It has been pointed out[18] that $Pd(OH)_2$ can be further oxidized to $Pd(OH)_4$, namely:

$$Pd(OH)_2 + 2\ H_2O \rightarrow Pd(OH)_4 + 2\ H^+ + 2\ e^- \qquad (22)$$

The thermodynamic reversible potential for this reaction is 1.283 V vs. RHE at 25°C. As discussed previously, the formation of anodic peaks takes place on the susbsequent cyclic i-V curves only if the upper limit potential for cyclic voltammograms is at or over 1.30 V. These observations indicate that the appearance of anodic peaks on Pd electrodes is associated with the formation and reduction of the species $Pd(OH)_4$ which is a hydrated form of PdO_2. In other words, the SO_2 oxidation reaction is inhibited by the chemical transformation taking place on the reduced species of $Pd(OH)_4$. It is thus concluded that the further oxidation of $Pd(OH)_2$ seems to create a passivated surface layer for SO_2 oxidation.

Figure 15 shows the cyclic i-V curves on the freshly prepared electrodes of Ru, Ir and Rh in SO_2-saturated sulfuric acid solutions. Like the Pt anode, broad anodic peaks are normally observed on these electrodes. At the potential sweep rate 100 mV/sec, the peak-maximum potentials on Ru, Ir and Rh electrodes are approximately 1.12, 1.08 and 0.88 V, respectively, in the anodic i-V curves. As observed on the Pt anode, the conversion of chemisorbed oxygen-containing species to metal oxides on these electrodes also creates passivated surface layers which inhibit the SO_2 oxidation reaction.

2.1.5 Evaluation of Alternate Catalysts

As mentioned previously, the oxide-covered palladium electrode is superior to the Pt electrode in the anodic oxidation of SO_2. A number of oxides and mixed oxides have attracted considerable attention for use as electrocatalysts. Ruthanium oxide (RuO_x) on a titanium, for instance, is highly active for the anodic evolution of chlorine, and has found wide application as an electrocatalyst in the chlor-alkali industry[34-36]. This DSA-type electrode also shows low anodic overpotentials for oxygen evolution from acid[37] and alkaline[38] media. In addition to metal electrodes, the present work has been

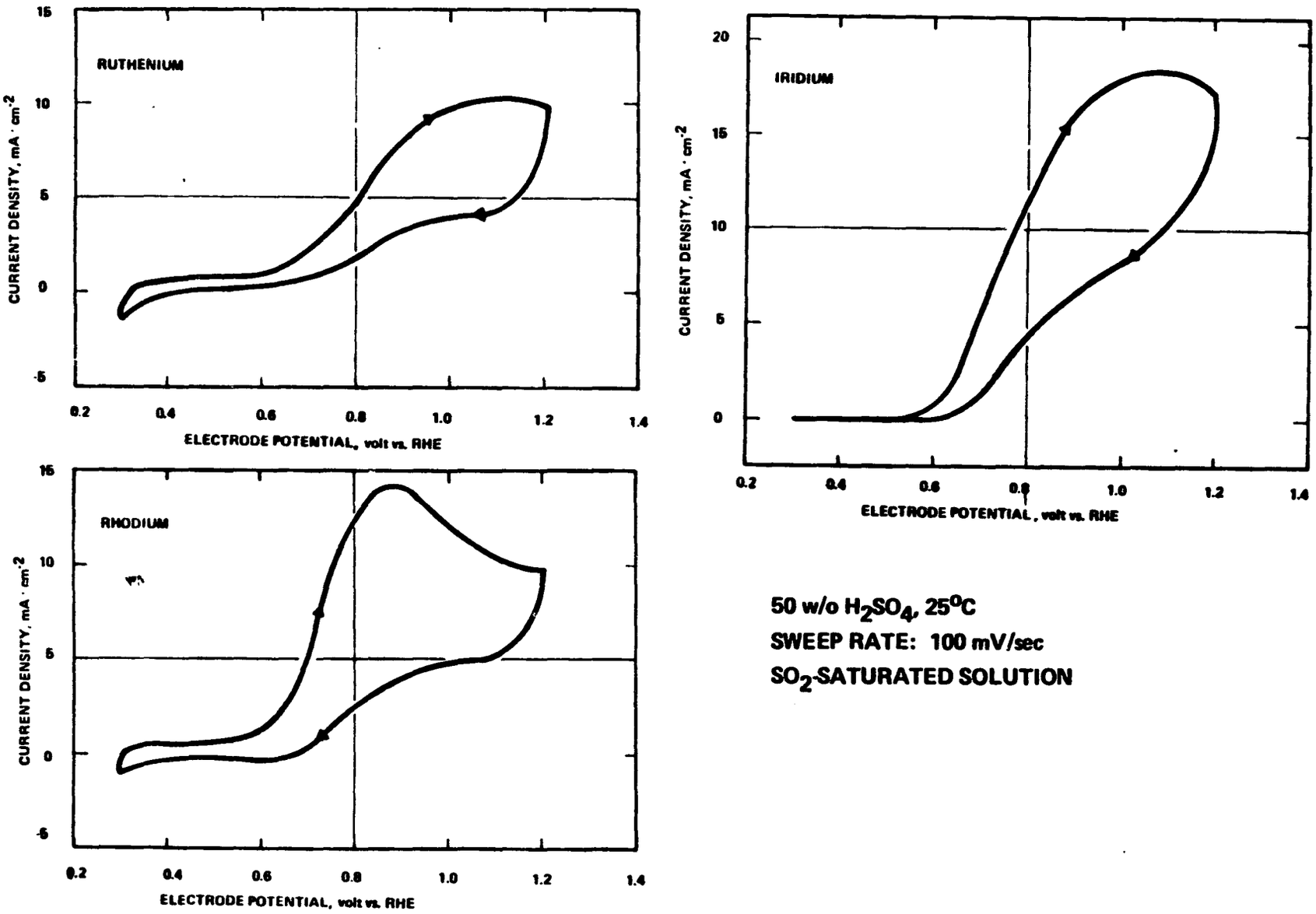

Figure 15. Cyclic Voltammograms on Various Candidate Electrodes in SO_2-Saturated Sulfuric Acid Solutions (50 w/o, 25°C; Scanning Rate: 100 mV/sec).

extended to investigate oxides and mixed oxides as electrocatalysts for SO_2 oxidation. The anode in an SO_2-depolarized electrolyzer is normally operated at potentials below 0.7 V vs. RHE[2]. Apparently, a majority of noble metal oxides or mixed oxides are electrochemically stable under this operating condition.

The PdO_x/C electrode was fabricated by applying a uniform PdO_x layer on a porous pure carbon substrate using a proprietary manufacturing process. The potential-current density relationships for SO_2 oxidation on pure carbon, PdO_x/C and Pt-black/C electrodes are given in Figure 16. The carbon substrate itself is extremely inactive for the anodic oxidation of SO_2. The PdO_x/C electrode exhibits higher limiting current density and lower polarization potentials as compared to the Pt-black/C electrode. At 1 mA/cm^2, for example, the anodic overpotential on the former is approximately 50 mV less than on the latter.

The PdO_x-TiO_2/Ti electrode was prepared by a thermal decomposition method as described elsewhere[39]. The resulting electrode was examined using scanning electron microscopy. The microstructure of the electrode surface is shown in Figure 17. The distribution of catalyst particles is uniform with a maximum particle size of $\sim$3μm. Figure 18 illustrates electrochemical properties of the mixed oxide electrodes in SO_2-saturated sulfuric acid solutions. The PdO_x-TiO_2/Ti electrode exhibits an electrocatalytic activity quite comparable to the Pt-black/Ti electrode for the SO_2 oxidation reaction. An anodic overpotential of $\sim$0.31 V was measured on this electrode at 10 mA/cm^2. Ruthenium oxide and iridium oxide on titanium substrates are excellent electrocatalysts for the anodic evolution of chlorine[34-36] and oxygen[37,38]. As seen from Figure 18, however, both RuO_x-TiO_2/Ti and IrO_x-TiO_2/Ti electrodes are very ineffective for the anodic oxidation of SO_2 in acid media.

2.2 DEVELOPMENT OF ELECTRODE FABRICATION TECHNIQUES

During earlier work[40], a standard process was developed for fabricating briquetted carbon electrodes from a mixture of catalyst and carbon powder. The appearance of a briquetted carbon electrode is shown in Figure 19. As has been noted[40], the briquetted electrodes provide very limited porosity and

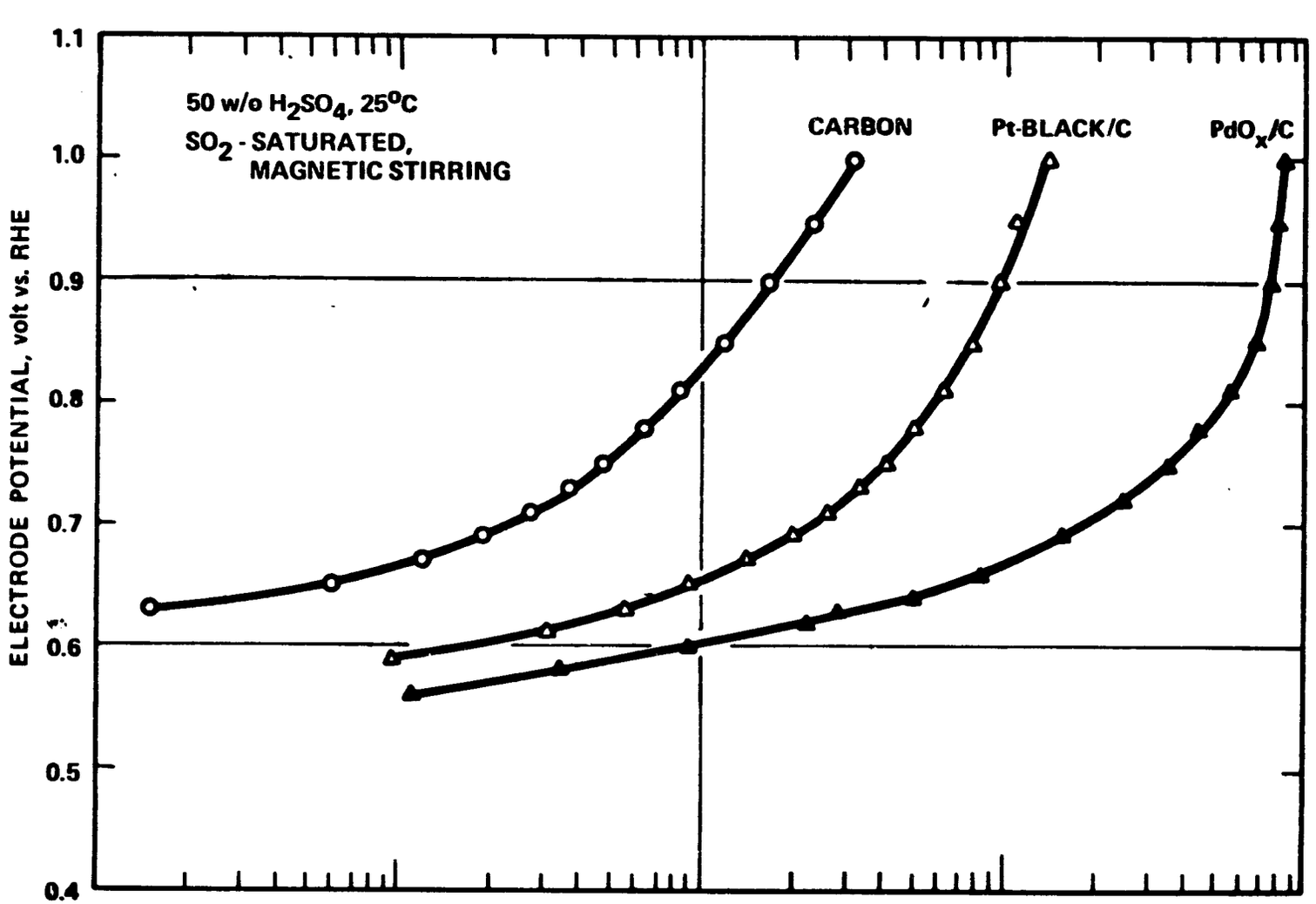

Figure 16. Current Density - Potential Relationships for SO_2 Oxidation on Pure Carbon, PdO_x/C and Pt-black/C Electrodes in SO_2-Saturated Sulfuric Acid Solutions (50 w/o, 25°C).

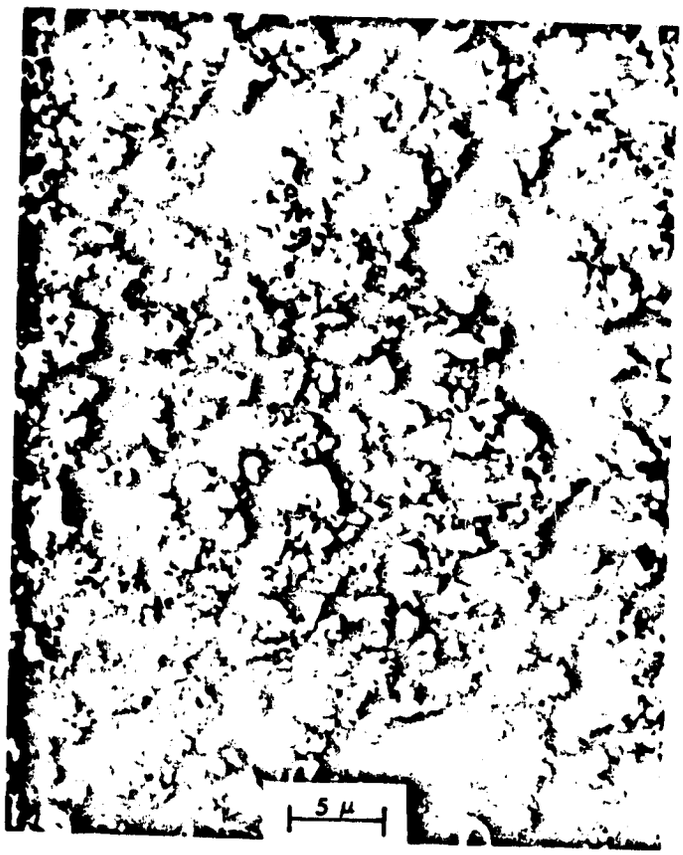

Figure 17. Scanning Electron Micrographs of a PdO_x-TiO_2/Ti Electrode.

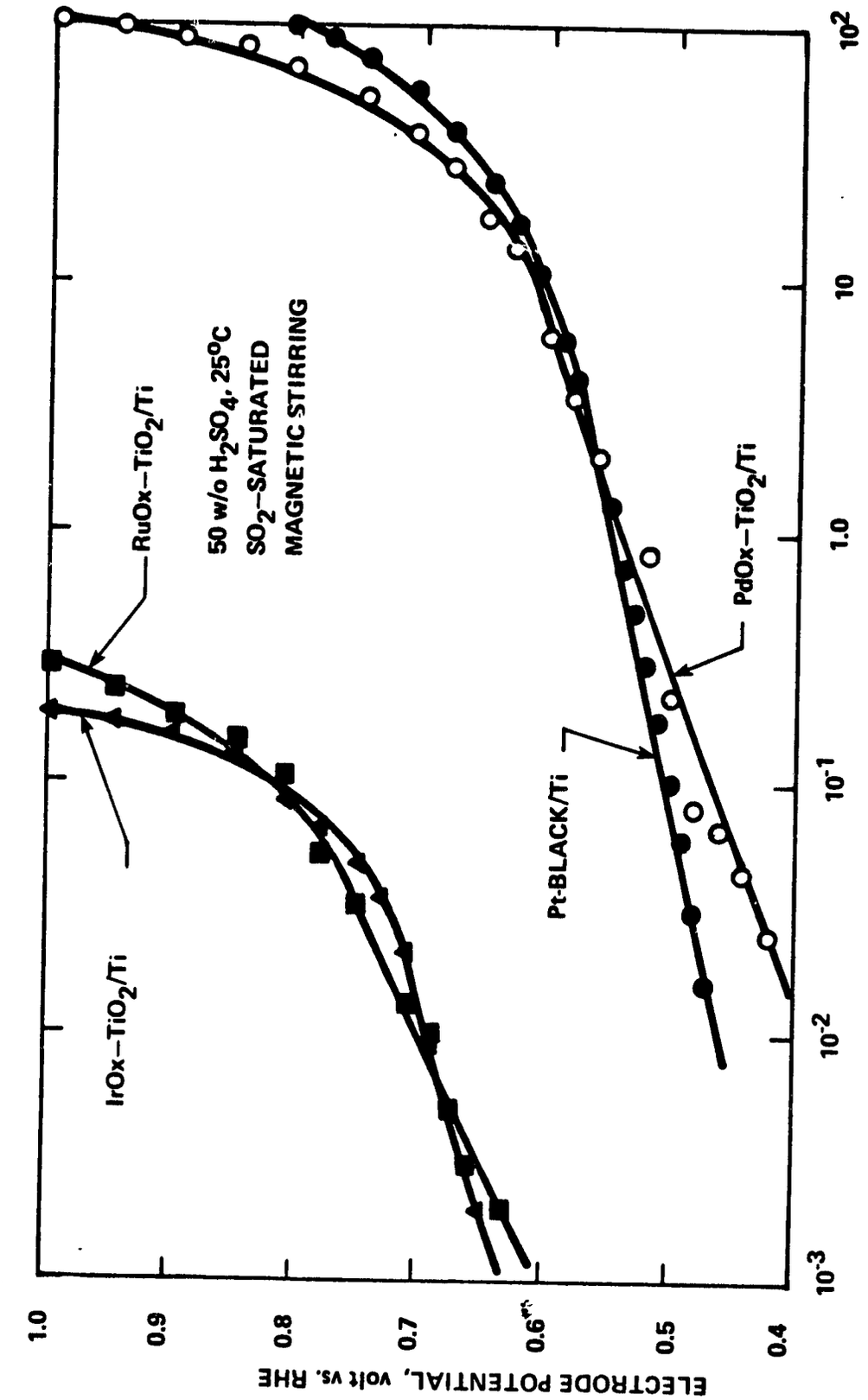

Figure 18. Current Density - Potential Relationships for SO_2 Oxidation on Various Mixed Oxide Electrodes in SO_2-Saturated Sulfuric Acid Solutions (50 w/o, 25°C).

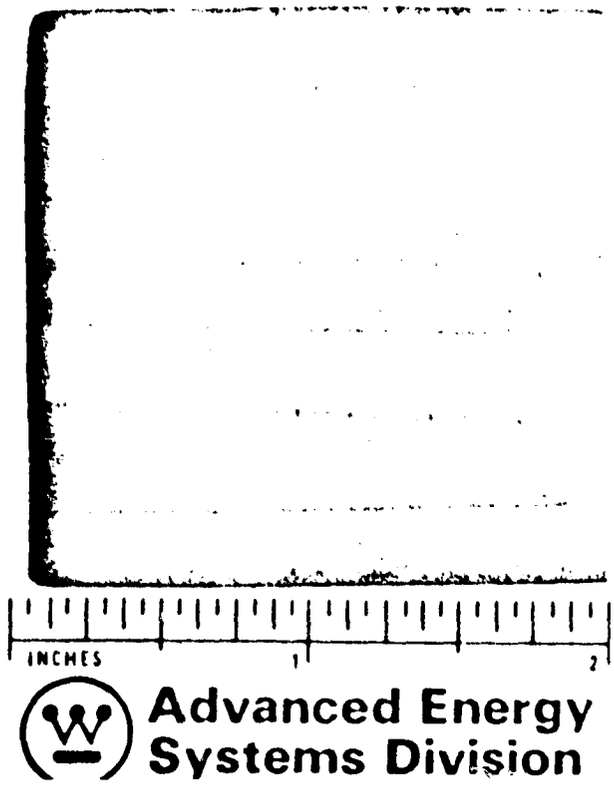

Figure 19. The Appearance of a Briquetted Carbon Electrode.

mechanical strength. They also exhibit low electrocatalytic activity and high performance degradation when evaluated as anodes for the electrochemical oxidation of sulfur dioxide. With a view of optimizing porosity, electric conductivity, mechanical strength and electrocatalytic activity, experimental efforts have been made to develop alternate processes for the electrode fabrication.

A number of commercially available porous carbon plates were investigated for use as substrates. Impregnation[41] and ion-exchanging[42,43] methods were used to catalyze the porous carbon substrates. As described in the previous report[40], an aqueous solution of noble metal compounds such as dihydrogen hexachloroplatinate or palladium acetate was applied onto the surface of a carbon plate by painting. The resulting carbon plate was then evaporated in a furnace or on a hot plate. During the evaporation process, the pressure of water vapor in the pores started to build up and gradually repelled the remaining solution out of the pores. Before the electrode was dried completely, the aqueous solution on the surface of the carbon plate also migrated toward the low temperature regions. As a result, catalyst compound was deposited on the edges only. Very little or no catalyst was found in the center of the electrode.

In the period of this report, efforts were made to develop manufacturing processes for preparing a uniformly distributed and well-bonded catalyst layer on a porous carbon plate. A carbon cloth also was evaluated for use as a substrate to back a Teflon-bonded catalyst layer. The catalyst particle distribution and chemical compositions of freshly prepared and tested electrodes were investigated by SEM (scanning electron microscopy), EDA (energy dispersive analysis) and ESCA (electron spectroscopy for chemical analysis) techniques. An improved test electrolyzer was designed, constructed and used for the evaluation of cell components.

The performance characteristics of test electrodes were determined at 50°C and atmospheric pressure, using 50 w/o sulfuric acid solution. In addition, a successful week-long endurance test was conducted in which stable cell performance was measured.

2.2.1 Preparation of Catalyzed Carbon Plate Electrodes

Methods to expedite electrochemical reactions in a sulfur dioxide depolarized electrolyzer include the use of appropriate electrocatalysts having preferred reaction sites and the maximization of active surface areas of the electrodes. For the preparation of high-surface-area electrodes, catalysts are generally supported on porous substrates which are electrically conductive and chemically stable to the electrolyte environment. Porous carbon plates that have many attractive properties, such as electrical conductivity, chemical stability, mechanical strength, high specific surface area and low cost, are the most promising materials for use as substrates. Various kinds of porous carbon plates, supplied by Pure Carbon Company, have been evaluated. It was found that porous carbon plates, designated P7620 and FC-13 exhibit the desired characteristics, and thus are ideal for use as catalyst supports. Note that the latter has a much higher specific surface area than the former (being $\sim$1 and $\sim$450 M^2/gm respectively).

As a first approach, two grooved carbon plates (P7620) were delivered to a vendor for the impregnation of Pt and Pd catalysts, respectively. Figure 20 illustrates the appearance of a resulting electrode in which the loading of Pt catalyst is $\sim$10 mg/cm^2. Apparently, the catalyst distribution is not uniform on the surface of the Pt-catalyzed carbon electrode. By use of briquetted carbon cathodes, these two types of catalyzed carbon plate electrodes were incorporated and evaluated in a test electrolyzer using lead cell frames. Electrochemical measurements were made in 50 w/o sulfuric acid solution at 50°C and atmospheric pressure.

Figure 21 shows the initial performance of the electrolyzers in which the vendor-prepared anodes were tested. The carbon plate anodes, impregnated with Pt and Pd, were incorporated in the electrolyzers OC-2 and OC-3, respectively. It should be noted that the reference cell OC-1 used a Pt-catalyzed carbon plate anode (10 mg/cm^2 in loading), prepared by a proprietary fabrication process as described in Section 2.2.2. As illustrated in Figure 21, the cell voltages of OC-2 and OC-3 are approximately 190 and 280 mV, respectively, higher than that of the reference cell OC-1 at 100 mA/cm^2. Obviously, the vendor-prepared anodes were inferior in performance.

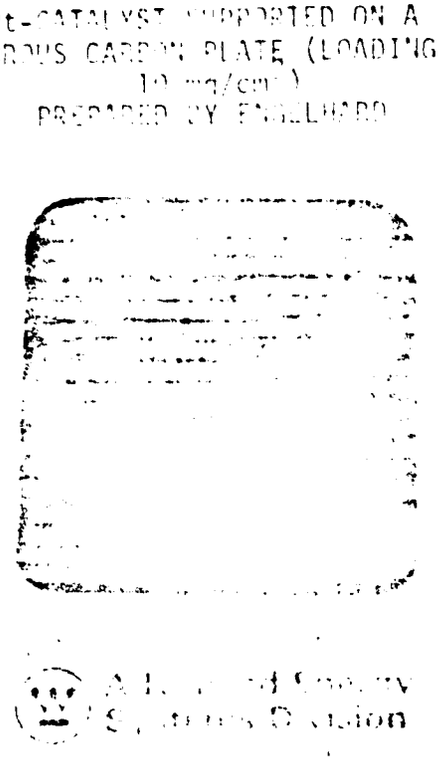

Figure 20. The Appearance of a Commercially Available Pt-Catalyzed Carbon Plate Electrode.

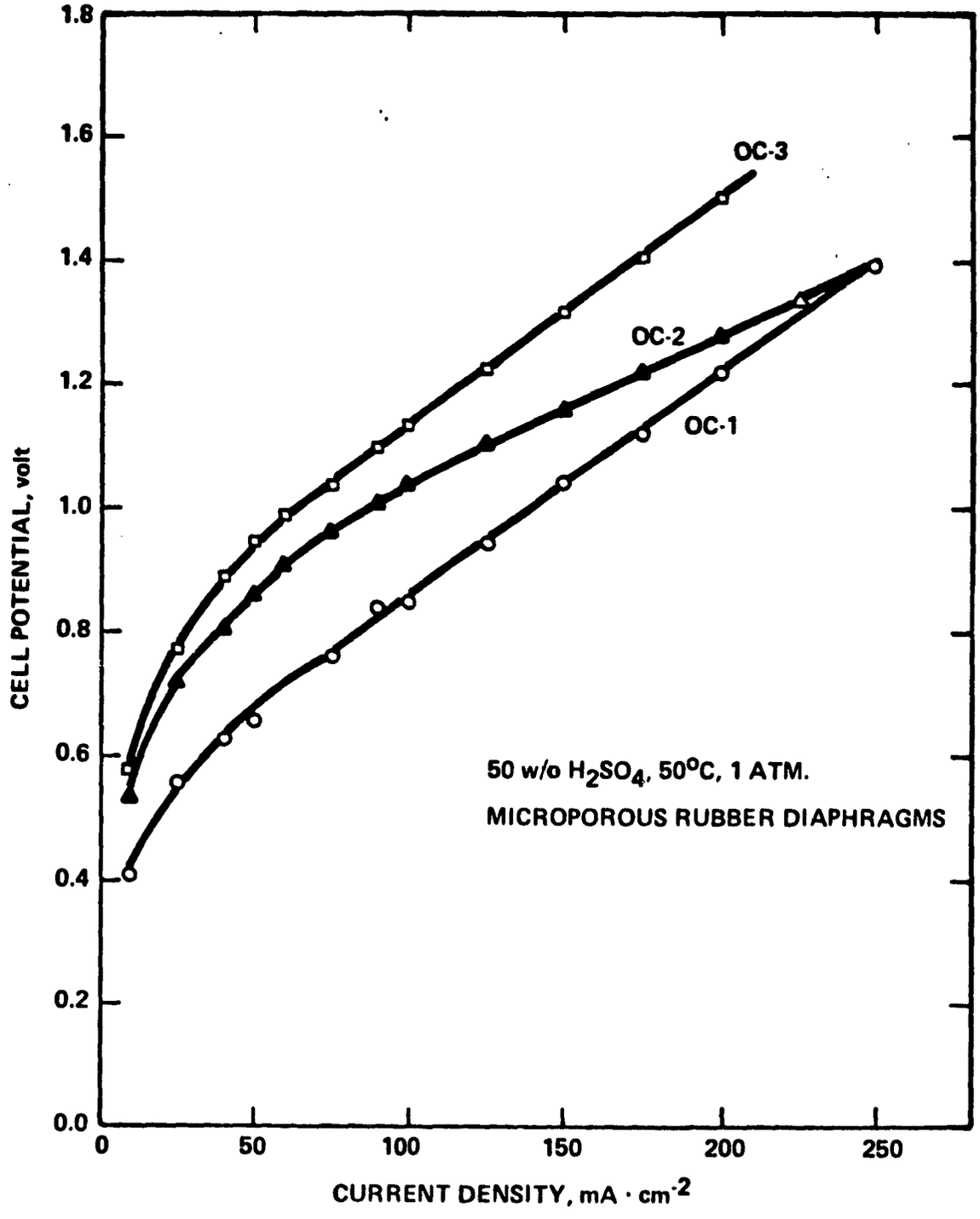

Figure 21. Performance of Electrolyzers OC-1, OC-2, and OC-3 Using Lead Cell Frames.

Prior to the procurement of catalyzed carbon plate anodes from the vendor, a novel manufacturing process was devised for preparing a uniformly distributed and well-bonded catalyst layer on porous carbon substrates. Figure 22 gives an example to demonstrate the detailed procedures for fabricating a PdO_x-catalyzed carbon electrode. A grooved porous carbon plate (P7620) was activated by oxidizing in a hot concentrated nitric acid (13.5 N at 80°C) for 4 hours. Due to the formation of soluble mellitic acid, $C_6(COOH)_6$, the oxidation process increased the volume of pores and roughened the wall of each macropore as described in the previous report[40]. An appropriate amount of aqueous solution of palladium acetate was applied to the surface of a carbon plate by a vacuum filtration method and an in-situ heat treatment (at ∿40°C) using an infrared lamp. The carbon plate coated with a uniform layer of palladium acetate was then thermally decomposed in a nitrogen atmosphere at 600°C. This process resulted in the formation of a thin layer of Pd-containing species on the surface. The resulting electrode was further treated at ∿450°C in a stream of helium gas containing 5% oxygen. After the oxidation process, the electrode surface turned greenish black, which is a typical color of palladium monoxide (PdO). When a metal-catalyzed carbon electrode was to be fabricated, the thermal decomposition process was conducted in a hydrogen atmosphere and the oxidation process was eliminated.

Figure 23A shows the microstructure of a pretreated porous carbon plate. The mean pore diameter of this substrate is ∿9 μm prior to the pretreatment. Nevertheless, a maximum pore diameter of about 60 μm was measured in the SEM micrograph. The distribution of catalyst particles on the PdO_x-catalyzed carbon plate electrode is illustrated in Figure 23B. Obviously, the density of catalyst particles on the resulting electrode is high and the particle distribution is uniform.

In the early work, the thermal decomposition and the oxidation processes in the electrode fabrication were performed in a small furnace, constructed of refractory bricks.

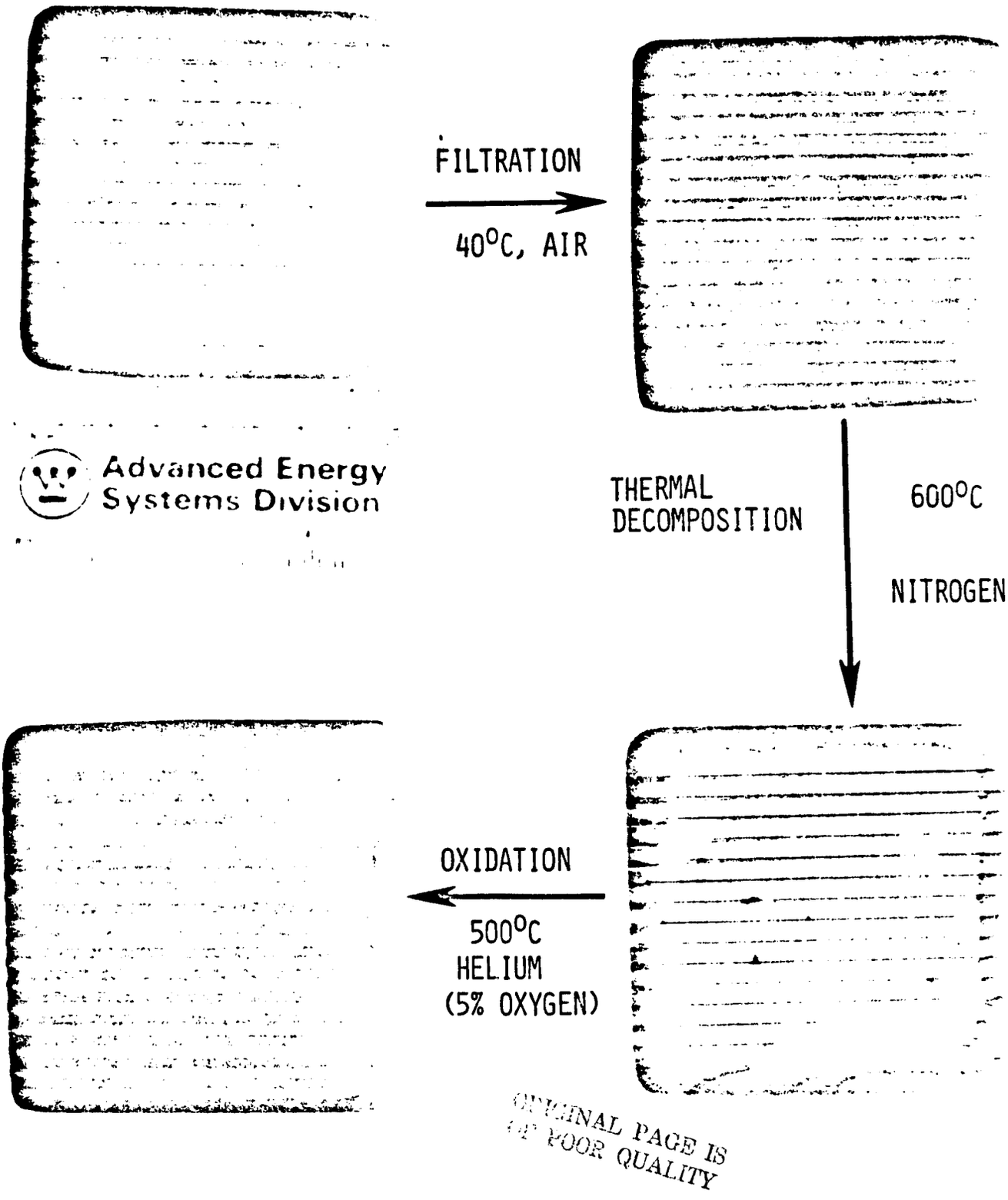

Figure 22. A Novel Process for the Fabrication of a PdO_x-Catalyzed Carbon Electrode.

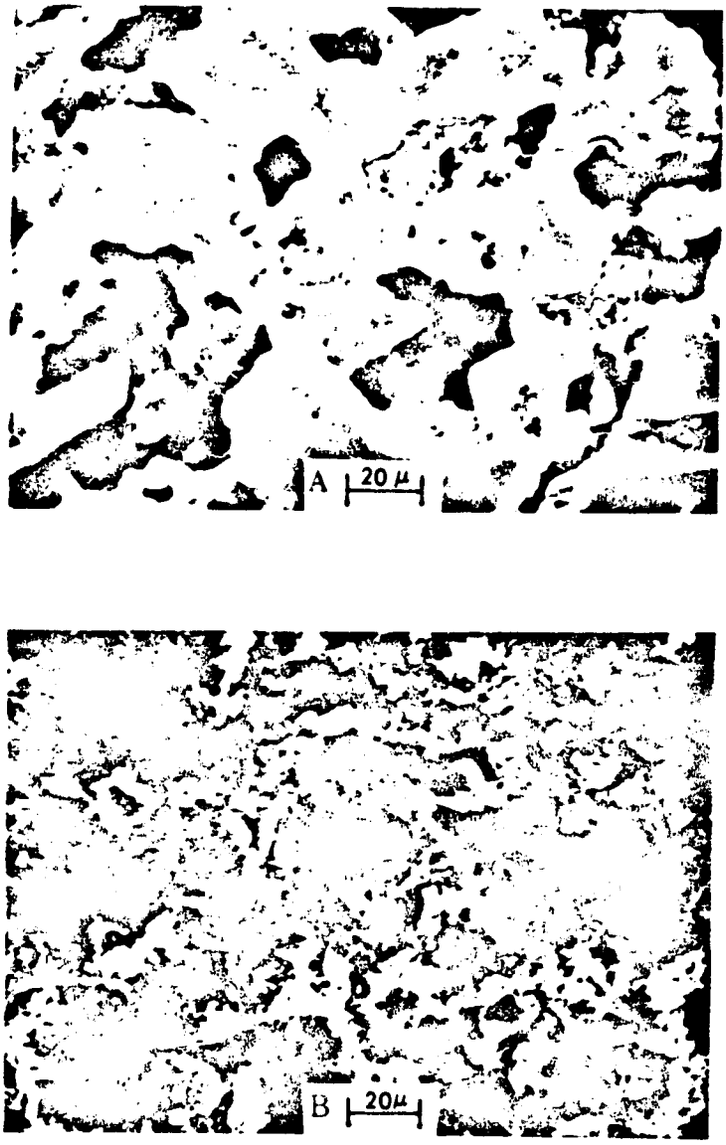

Figure 23. Scanning Electron Micrographs of (A) a Polished Carbon Plate after Pretreatment, and (B) a PdO_x-Catalyzed Carbon Plate Electrode. (Loading: 10 mg-PdO_x/cm^2).

The resulting electrodes were then examined by energy dispersive analysis (EDA). As seen from Figure 24, significant amounts of impurities such as Fe, Cr and Ni were found on the electrode surfaces. To eliminate the contamination problem, a quartz-tube furnace was designed and constructed for use in the fabrication of test electrodes. Along with the power supplier and temperature controller, the appearance of a quartz tube furnace is shown in Figure 25. The thermocouple was inserted in the interior of the sample support so that the measure temperature was not affected by the radiation heat from heating elements. The temperature distribution in the furnace was well calibrated. The influence of the flow rates of processing gases on the surface temperature of the sample support was also investigated.

By use of the quartz-tube furnace, the processing temperature for the electrode fabrication can be controlled more accurately. Figure 26 shows EDA results on a Pt-catalyzed carbon electrode prepared in this furnace. Apparently, there is no detectable impurity on the electrode surface. This furnace is currently employed in the preparation of test electrodes, including catalyzed carbon (plate) electrode, carbon cloth backed electrodes and mixed oxide anodes.

2.2.2 Preparation of Carbon Cloth Backed Electrodes

By use of a carbon cloth as a support for the catalyst layer, an alternate fabrication process has been developed for preparing high-surface-area electrodes. Figure 27A is the appearance of a carbon cloth (SWB-8), supplied by Stackpole Fibre Company. The carbon cloth has a thickness $\sim$0.08 cm and flexural strength $\sim$330 MPa.

In the preparation of a test electrode, a carbon cloth of desired dimension was degreased using acetone and then cleaned ultrasonically in distilled water. An appropriate amount of catalyzed carbon powder and PTFE (30B, DuPont) was suspended in distilled water by gently stirring the solution. The resulting suspension was deposited on the pretreated carbon cloth using a vacuum filtration technique. After being dried, the catalyst/cloth assembly was pressed in a stainless steel compression die at pressures ranging from 15 to 30 MPa. The resulting electrode was finally sintered in a hydrogen or nitrogen atmosphere

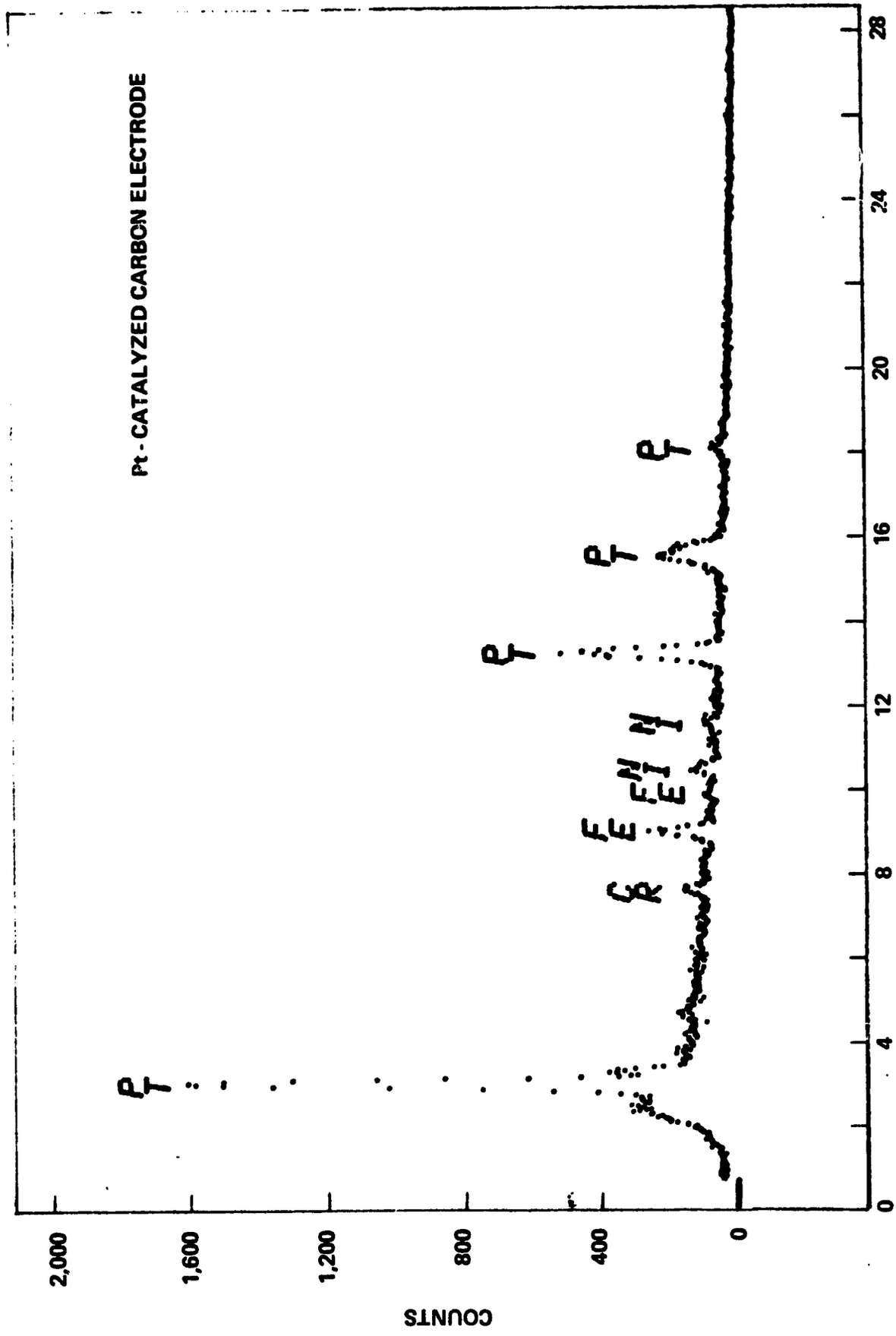

Figure 24. X-Ray Spectrum on a Freshly Prepared Pt-Catalyzed Carbon Electrode.

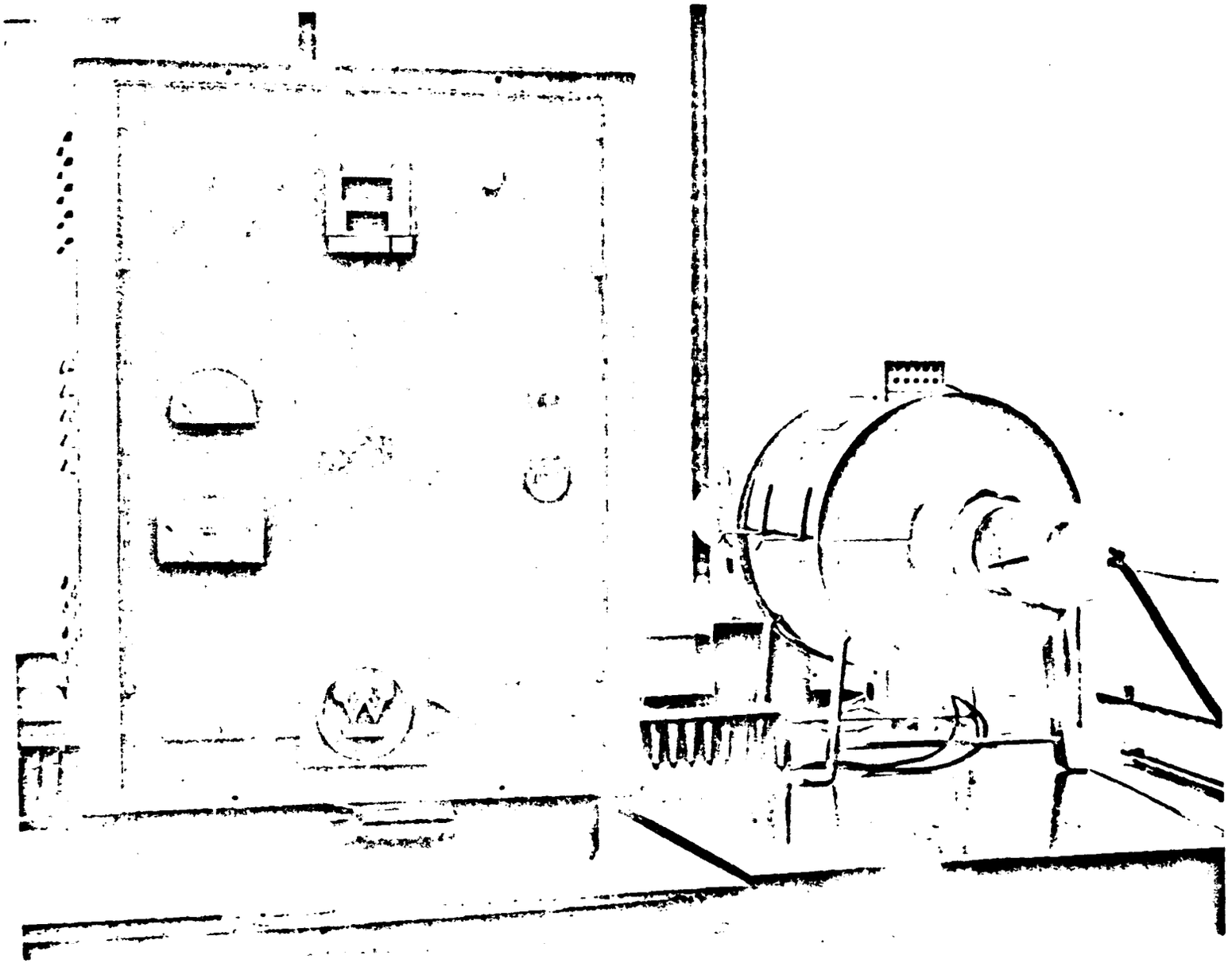

Figure 25. A Quartz-Tube Furnace Used in the Fabrication of Test Electrodes.

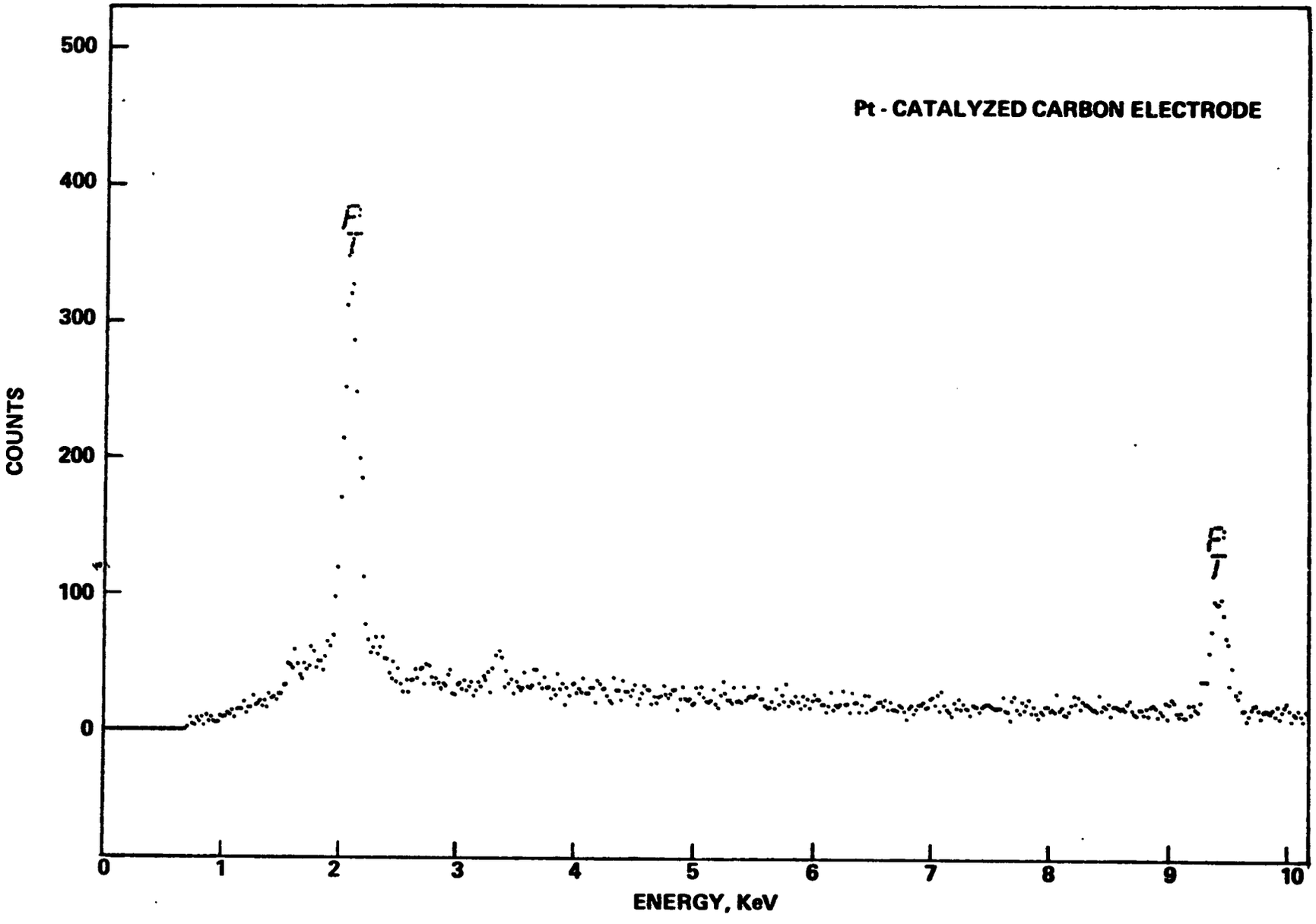

Figure 26. X-Ray Spectrum on a Pt-Catalyzed Carbon Electrode Prepared in the Quartz-Tube Furnace.

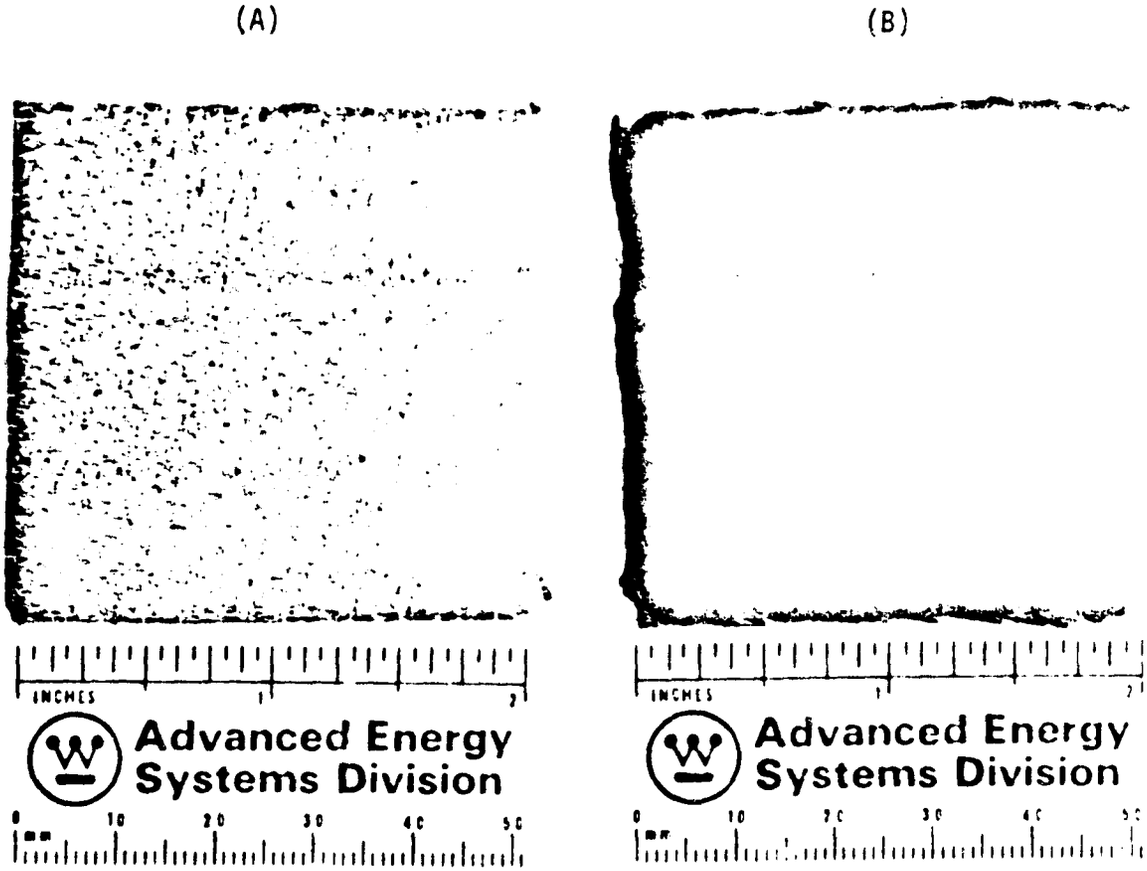

Figure 27. The Appearances of (A) a Carbon Cloth (SWB-8) and (B) a Carbon Cloth Backed Electrode.

at 360°C. The appearance of a carbon cloth backed electrode is shown in Figure 27B. In general, the thickness of the catalyst layer on the cloth is 0.03-0.05 cm. The catalyst layer contains 20-23 w/o PTFE. The catalyst loading in the electrode is normally ~2 mg/cm^2.

Scanning electron microscopy (SEM) and energy dispersive analysis (EDA) techniques were applied to examine the microstructure and chemical identity of the catalyst layer on a freshly prepared electrode. Figure 28 shows the results of SEM and EDA studies on a carbon cloth backed anode in which a Pt/C catalyst (EC-9885), supplied by Engelhard Minerals and Chemicals Corporation, was applied. The catalyst distribution is uniform with no detectable impurities. Note the x-ray spectra for the spots 1, 2 and 3. The intensity of characteristic peaks for Pt is highest on the bright spot 1. With the dark spot 3, trace amounts of Pt are identified by short x-ray counts.

In addition to the Pt/C catalyst, palladium oxide (PdO_x) was evaluated for use in the fabrication of carbon cloth backed anodes. The microstructure of palladium oxide obtained from Ventron Corporation, is illustrated in Figure 29. For preparing a PdO_x/C (powder) mixture, a palladium oxide sample was pulverized using a mortar and pestle, and then oxidized in a helium stream containing 5% oxygen for at least six hours. It is noted that the oxidation states of Pd in an oxidized and an unoxidized palladium oxide sample were examined using ESCA (electron spectroscopy for chemical analysis) technique and the results will be presented in Section 2.2.7. After the oxidation process, the sample was mixed with a desired amount of activated carbon powder using a ball mill technique. The resulting mixture contained approximately 10 w/o PdO_x.

The carbon cloth backed anode of loading 2 mg-PdO_x/cm^2 was prepared by the standard fabrication process as described previously. Figure 30 shows the microstructure and chemical identities of the catalyst layer of a freshly prepared anode. The catalyst distribution in the PdO_x/C mixture is less uniform as compared to the Pt/C catalyst. Agglomerations as large as 100 μm were observed in the PdO_x/C catalyst. As evidence in the fluorescence spectrum, no detectable impurity is present near the PdO_x particle (that is, the spot 1). However, considerable amounts of Al, Fe, S and Si are observed at

(A)

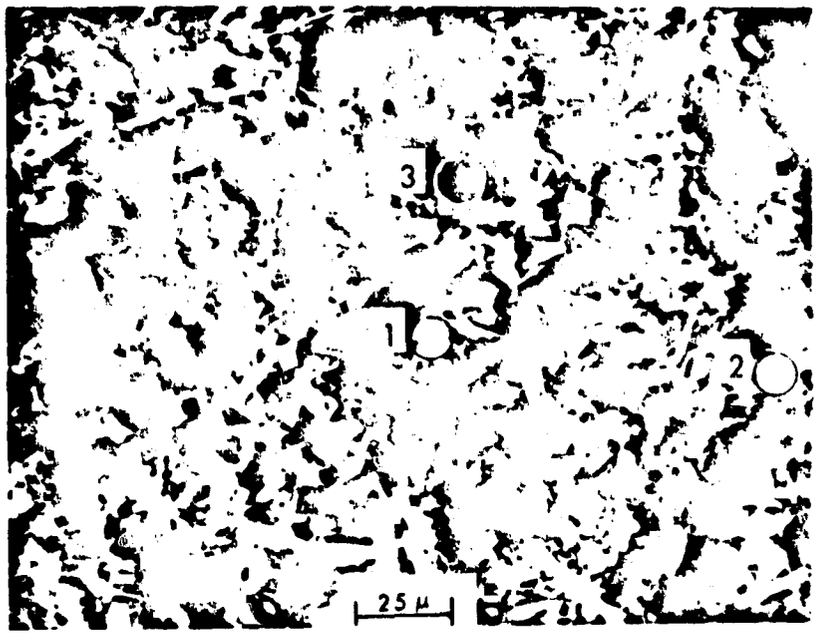

(B)

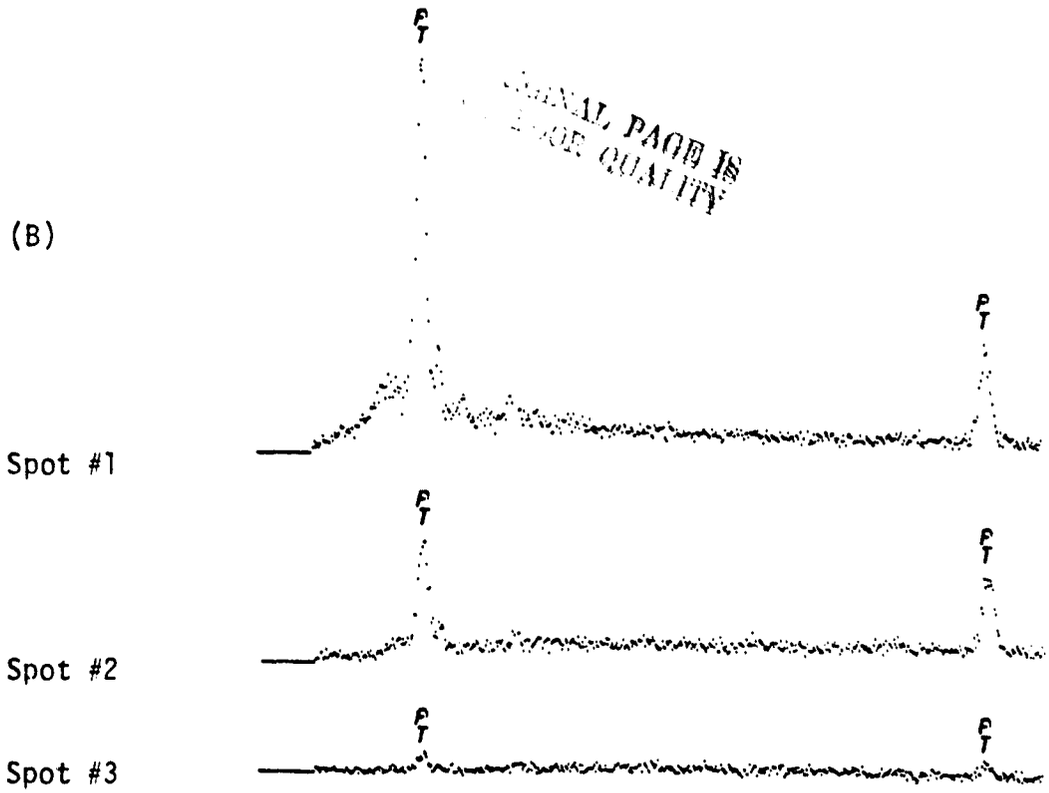

Figure 28. (A) Scanning Electron Micrograph of the Pt/C Catalyst (EC-9885) on a Carbon Cloth Backed Electrode; (b) X-Ray Spectra on the Spots #1, #2 and #3 as indicated.

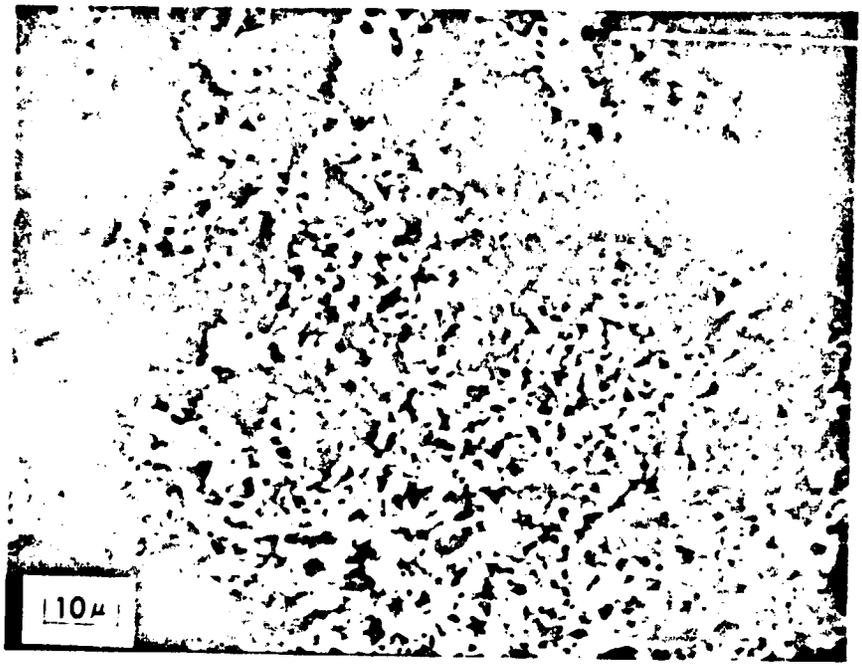

Figure 29. Scanning Electron Micrograph of an Unsupported Palladium Oxide Catalyst.

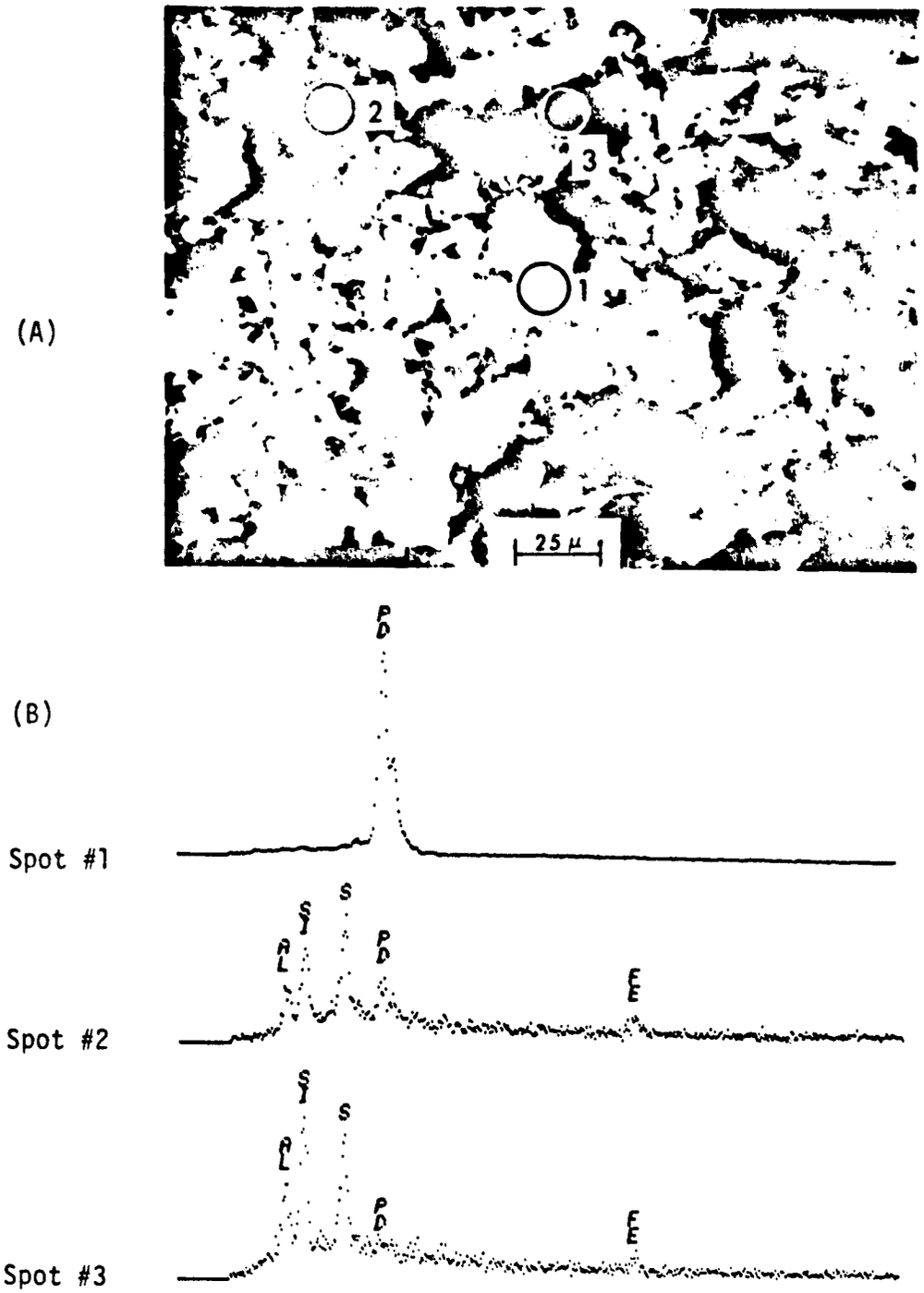

Figure 30. (A) Scanning Electron Micrograph of the PdO_x/C Catalyst on a Carbon Cloth Backed Electrode; (b) X-Ray Spectra on the Spots #1, #2 and #3 as indicated.

the spots 2 and 3. The impurities were apparently the result of the process of mixing PdO_x catalyst with carbon powder. Therefore, it is concluded that the ball mill technique is not suitable for use in the preparation of catalyst-carbon mixtures.

More recently, a new Pt-containing catalyst (MBI-303-8) has been procured from Matthey Bishop, Inc. The microstructure of this catalyst is shown in Figure 31. Fine Pt particles are deposited on carbon black pearls. The mean particle size of Pt catalyst is approximately 100 Å. The catalyst MBI-303-8 is currently used to substitute for EC-9885 in the fabrication of carbon cloth backed anodes.

2.2.3 Alternate Substrates for Porous Electrodes

Apart from carbon, attempts were made to investigate different types of porous substrates for use in the electrode fabrication. As mentioned previously, the candidate materials should exhibit promising chemical stability, electric conductivity, mechanical strength and high specific surface area. It was proposed that the technique used for preparing Raney-type catalysts[44] would be explored to fabricate porous titanium substrates. During the course of this work, however, a sintered titanium substrate was identified to have the desired properties for use in the electrode fabrication. Figure 32 shows the optical micrographs of a sintered titanium plate, obtained from Gould, Inc. The mean pore size of this porous substrate is ~10 μm. As seen from Figure 32B, large pores are observed in the metal/air interface and in the bulk of the sintered plate. In the near future, experimental efforts will be made to evaluate the sintered titanium substrate in the fabrication of mixed oxide electrodes.

2.2.4 An Improved Cell Configuration

In the early work[40], test electrodes were mounted on lead frames using silver-conducting epoxy as demonstrated in Figure 33. In the old cell configuration, lead frames served as current collectors. The ESCA studies on tested membranes indicated[40] that there was a serious contamination problem on test electrodes arising from the presence of Pb- and Ag-containing species in the electrolyte. Apparently, silver epoxy and lead frames were not chemically stable under the operating conditions. More recently, an improved test cell has been constructed

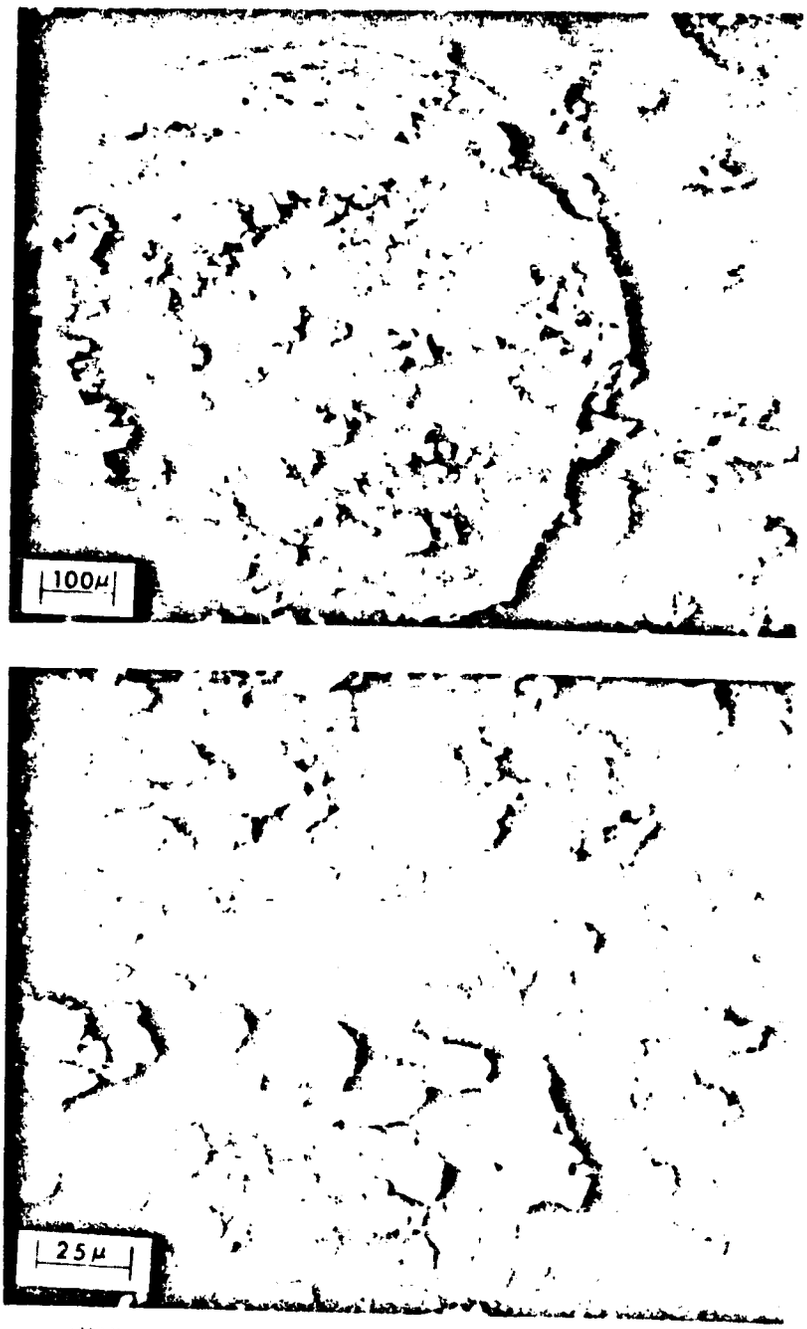

Figure 31. Scanning Electron Micrographs of a Pt/C Catalyst (MBI-303-8).

(A)

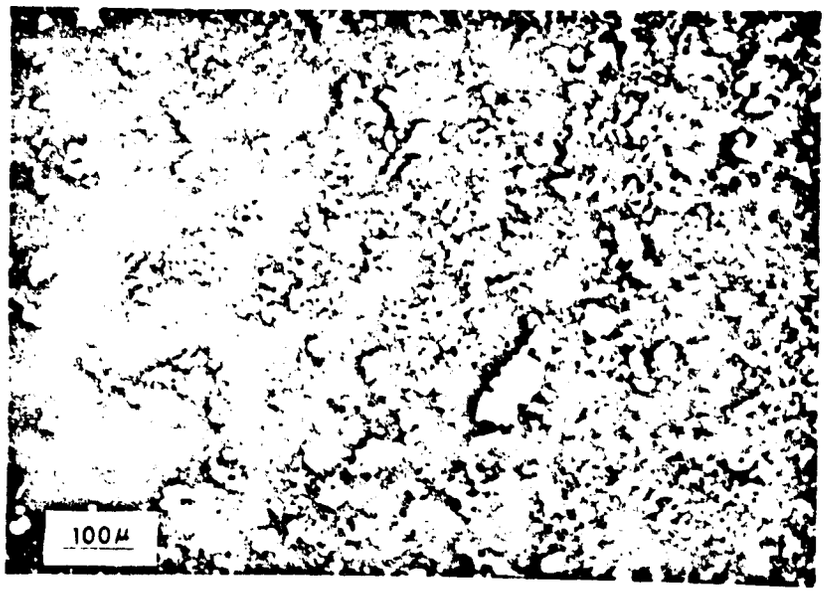

(B)

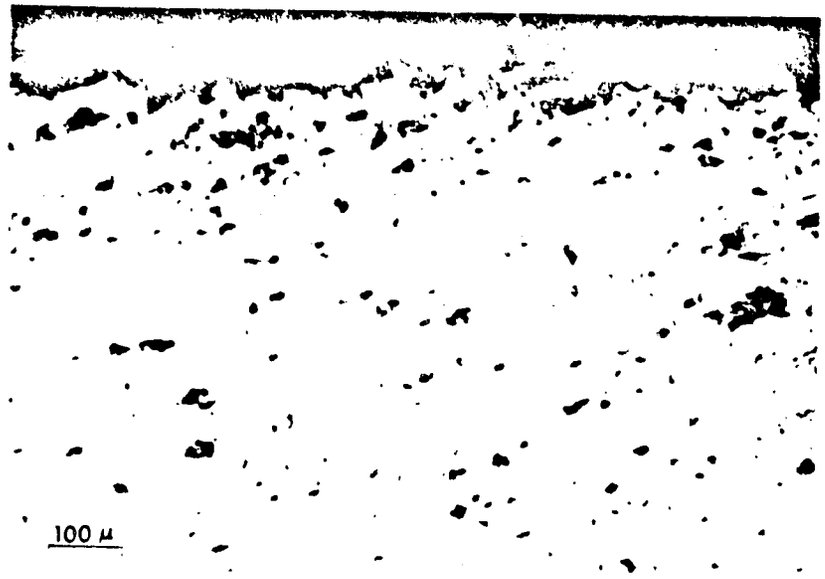

Figure 32. Optical Micrographs of (A) the Surface and (B) the Cross-Section a Sintered Titanium Plate.

(A)

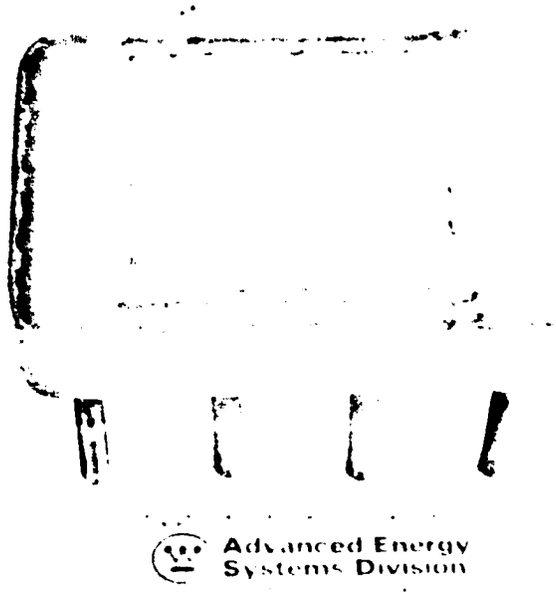

(B)

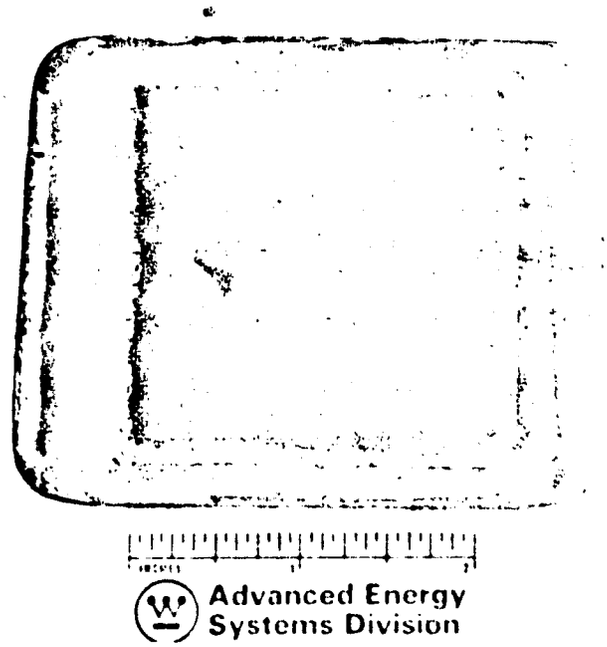

Figure 33. The Appearance of (A) a Briquetted Carbon Electrode and (B) a Platinized Pt-Screen Electrode Mounted on Lead Frames.

using Lucite as the cell frame. This Lucite cell is currently employed for the evaluation of cell components. It is noted that the use of Lucite as the structural material significantly reduces impurities in the electrolyte.

Figure 34 shows the details of the lucite cell. The electrolyzer used O-ring seals. A microporous rubber diaphragm was applied as the separator. The active electrode area was approximately 20 cm^2. A spacer (i.e., a perforated platinum foil of thickness 0.012 cm) was incorporated between the separator and a test electrode to obtain sufficient electrolyte flowing over the electrode surface. On the back of each (platinum screen) current collector, a pressure pad was placed to assure good electrical contact in the electrode/collector interface and to reduce the inter-electrode spacing.

The electrolysis test system is illustrated in Figure 35. During an experiment, both anolyte and catholyte were circulated. A hydraulic overpressure was maintained between the cathodic and anodic compartments of the electrolyzer to prevent the migration of SO_2-containing species through the separator. The anolyte was presaturated with SO_2 before it flowed into the cell. In each compartment, a Hg/Hg_2SO_4 reference electrode was connected to study the electrochemical behavior of the anode and cathode, respectively.

2.2.5 Electrochemical Evaluation of Porous Electrodes

Electrochemical measurements were made at 50°C and atmospheric pressure, using 50 w/o sulfuric acid solutions. Microporous rubber diaphragms were used as separators in the test cells. In an electrolysis experiment, the flow rates of anolyte and catholyte were ∿700 ml/min, respectively. Table 5 summarizes the cell components and performance characteristics of test cell configurations. The potential-current relationships in these cells are shown in Figure 36.

In the old cell configuration (OC-1) using lead frames, a Pt-catalyzed carbon anode and a briquetted carbon cathode were incorporated. The platinum loadings in these electrodes were ∿10 mg/cm^2. As seen from Table 5, the measured cell

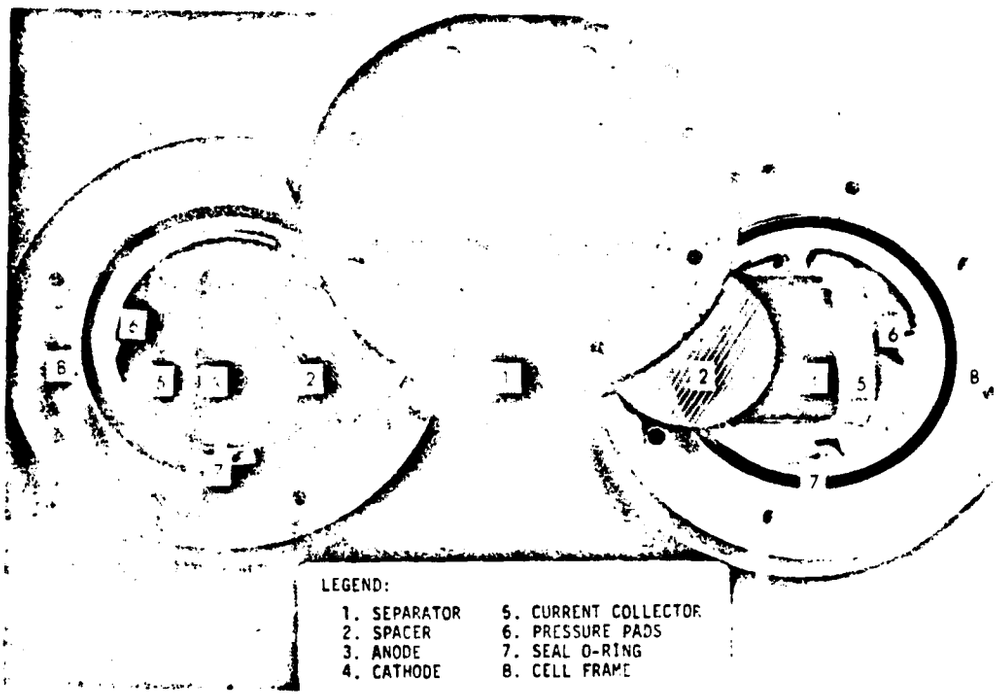

Figure 34. The Details of a Lucite Cell.

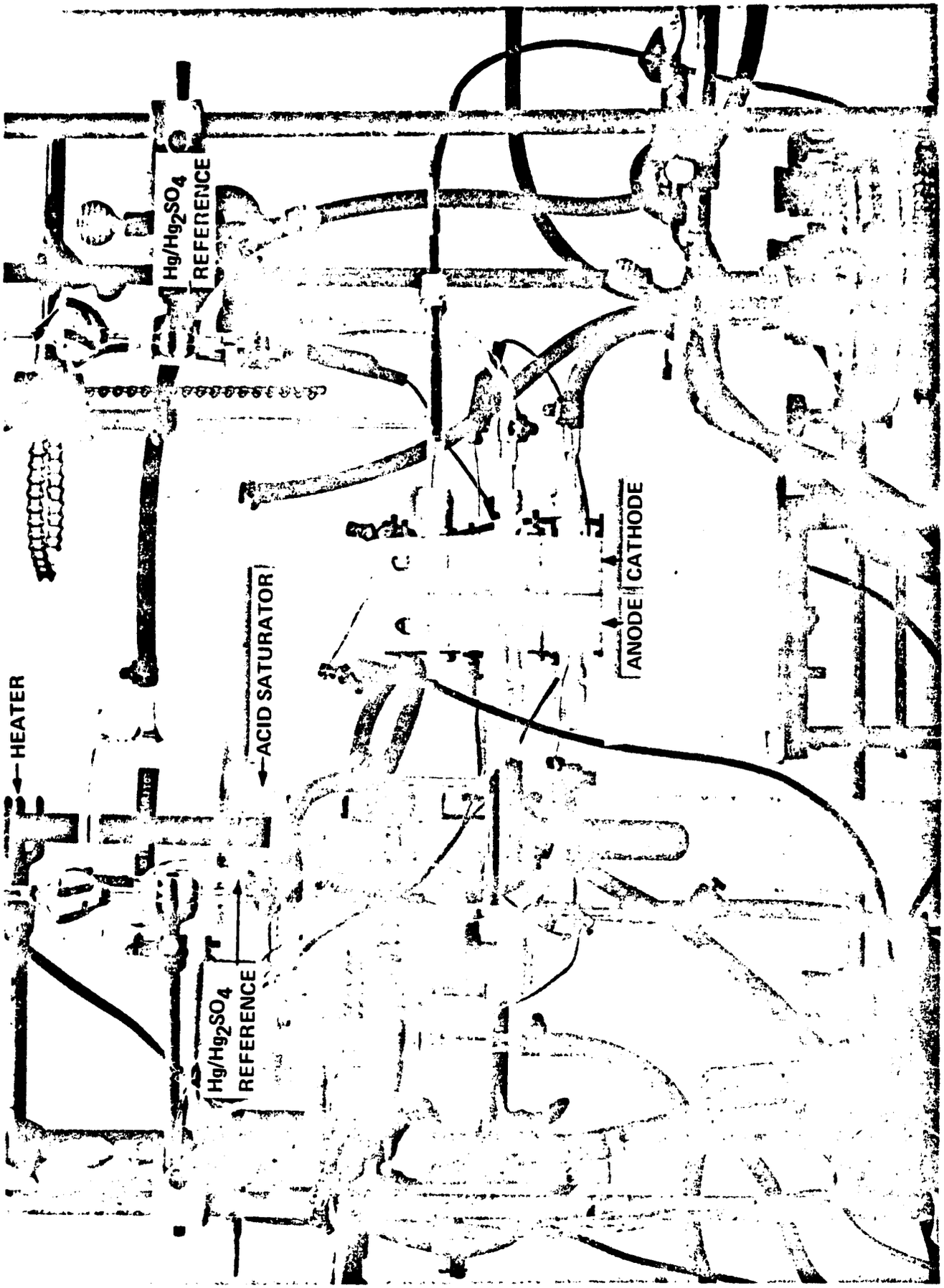

Figure 35. The Electrolysis Test System.

TABLE 5

CELL COMPONENTS AND PERFORMANCE CHARACTERISTICS OF MAJOR ELECTROLYZERS[1]

ELECTROLYZER	ANODE	CATHODE	E_{cell} at 200 mA/cm^2 (mV)	IMPROVEMENT[2] (mV)	$\frac{dE_{cell}}{dt}$[3] (mV/hr)
OC-1	Pt/C-plate (P7620) 10 mg/cm^2	B.C.E.[4] 10 mg/cm^2	1,220	-	16
LC-1	Pt/C-plate (P7620) 10 mg/cm^2	B.C.E. 10 mg/cm^2	1,150	70	4
LC-2	Pt/C-plate (FC13) 10 mg/cm^2	B.C.E. 10 mg/cm^2	930	220	4
LC-3	Pt/C-plate (FC13) 10 mg/cm	Pt/C-plate (FC13) 10 mg/cm^2	930	220	5
LC-5	Pt/C-plate (FC13) C.C.E. (EC-9885)[5] 12 mg/cm^2	Pt/C-plate (FC13) 10 mg/cm^2	840	90	<1
LC-8	Pt/C-plate (FC13) C.C.E. (EC-9885) 7 mg/cm^2	Pt/C-plate (FC13) 10 mg/cm^2	830	10	<1
LC-12	Pt/C-plate (FC13) C.C.E. (MBI-303-8) 7 mg/cm^2	Pt/C-plate (FC13) 10 mg/cm^2	770	60	<< 1

(1) Testing Conditions: 50 w/o H_2SO_4 at 50°C and atmospheric pressure, anolyte flow rate 700 ml/min., microporous rubber diaphragm used as a separator.

(2) Achievable improvement in cell voltage in comparison with the previous electrolyzer.

(3) Performance degradation rate after operating at a constant current density 100 mA/cm^2 for 2 hours.

(4) B.C.E. = Briquetted carbon electrode.

(5) C.C.E. = Carbon cloth supported electrode.

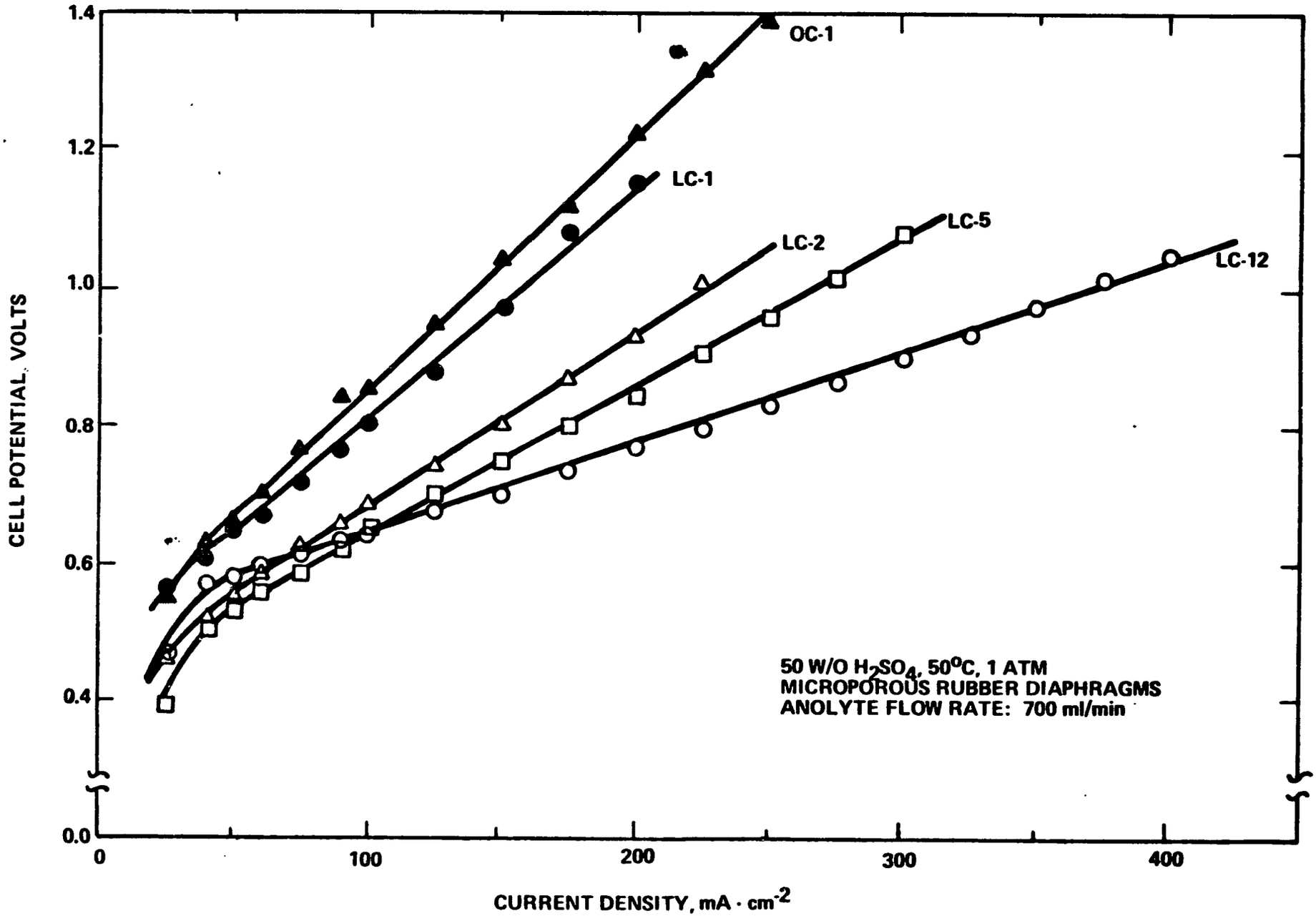

Figure 36. Performance of Major Electrolyzers OC-1, LC-1, LC-2, LC-5 and LC-12.

potential at 200 mA/cm^2 was as high as 1.22 V in cell OC-1, including the ohmic loss. This electrolyzer also exhibited a considerable performance degradation (being ∿16 mV/hr at 100 mA/cm^2). The cell components tested in the lucite cell LC-1 were quite similar to those in cell OC-1. The use of new cell configuration, however, resulted in a significant improvement in the performance stability, reducing the degradation rate from 16 to 4 mV/hr. In comparison with OC-1, a decrease of ∿70 mV in the overall cell potential was also achieved at the current density 200 mA/cm^2.

In the electrolyzer LC-2, the low-surface-area carbon plate, P7620, was replaced by a high-surface-area substrate FC-13 in the fabrication of the anode. A briquetted carbon cathode of laoding 10 mg/cm^2 was used. The cell LC-2 exhibited performance stability similar to cell LC-1 (the degradation rate being ∿4 mV/hr at 100 mA/cm^2). As shown in Table 5, an improvement of ∿220 mV in the cell potential was obtained in cell LC-2, essentially arising from the use of high-surface-area carbon plate as the catalyst support.

Starting with cell LC-5, a carbon cloth backed anode of loading 2 mg/cm^2 was added between the spacer and the diaphragm. The catalyst applied on the carbon cloth was a Pt/C (Powder) mixture (EC-9885). As seen from Table 5, this modified cell configuration exhibited an additional improvement of ∿90 mV in its cell potential at 200 mA/cm^2. The performance stability of cell LC-5 is shown in Figure 37. While applying a constant current density 100 mA/cm^2 through the electrolyzer, the cell voltage was measured as a function of time. After 2 hours of equilibration, the observed performance degradation rate in cell LC-5 was less than 1 mV/hr. As seen from Table 5, cell LC-3 shown in Figure 37 used the same cell components as LC-5 except for the carbon cloth backed anode that was incorporated in LC-5 only. The measured degradation rate in LC-3 was approximately 5 mV/hr. It is obvious that the incorporation of carbon cloth backed anode in the electrolyzer results in significant improvements in the cell performance and its stability.

Attempts were made to reduce the noble metal content in test electrodes. At the anode of cell LC-8, an intentional reduction of Pt loading from 12 to 7 mg/cm^2

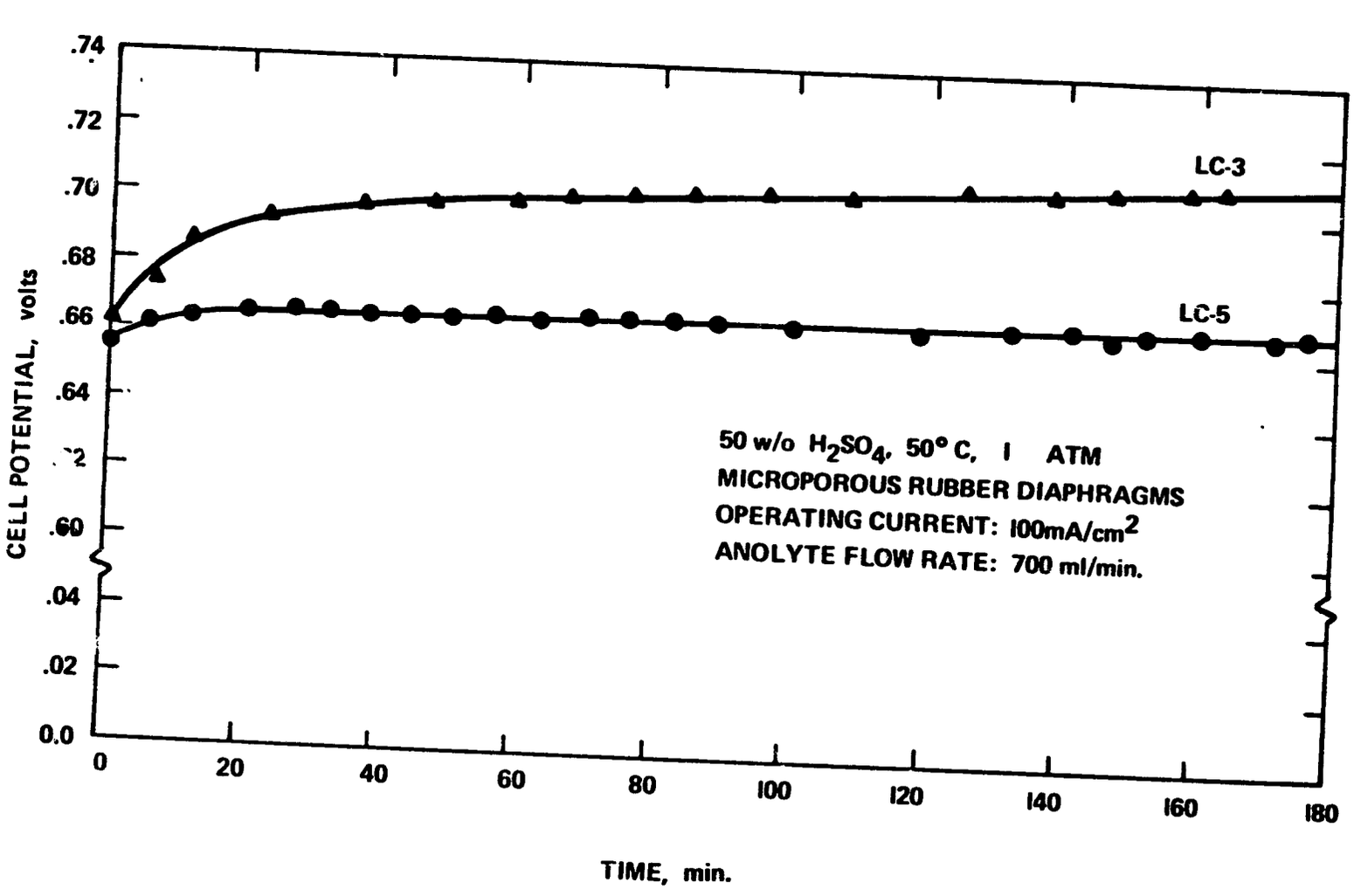

Figure 37. Variations of Cell Voltages in Electrolyzers LC-3 and LC-5 with Time.

caused a small improvement in the cell potential and performance stability as compared to cell LC-5 (see Table 5). As discussed in Section 2.2.2, a new Pt-containing catalyst (MBI-303-8) was obtained to replace EC-9885 for preparing carbon cloth backed anodes. The use of MBI-303-8 in cell LC-12 provided a further reduction of ~60 mV in the cell potential. After operating at 100 mA/cm^2 for 2 hours, the cell performance of LC-12 was stable with undetectable degradation.

As evidenced in Table 5, the recent progress in the electrolysis technology development has resulted in substantial improvements in both voltage efficiency and performance stability of an electrolyzer. At 200 mA/cm^2, for example, the observed cell potential has been reduced from 1.22 V in OC-1 to 0.77 V in LC-12. With LC-12, stable cell potentials of 0.64, 0.77, 0.90, and 1.05 V have been attained at current densities 100, 200, 300 and 400 mA/cm^2, respectively, including ohmic losses in the electrolyzer.

In addition, the electrochemical characterization was carried out on an electrolyzer LC-10 in which the Pt/C catalyst, EC-9885, at the anode was completely substituted by the PdO_x/C mixture (loading ~7 mg/cm^2). The cell LC-10 used the same separator and cathode as earlier cells, LC-5 and LC-8. In comparison with cell LC-5, the performance characteristics of the electrolyzer LC-10 is shown in Figure 38. The observed cell potentials in LC-10 are 0.72, 0.89 and 1.06 V at 100, 200 and 300 mA/cm^2, respectively. In the low current density region, the slightly poor performance of LC-10, as compared to LC-5, is due to the less uniform distribution and larger size of catalyst particles in PdO_x/C mixture than in Pt/C catalyst (see Figures 28 and 30). Further effort will be made to evaluate a new PdO_x/C catalyst, prepared by Matthey Bishop, Inc.

2.2.6 Cell Endurance Test

Aiming at finding an optimum temperature for the endurance test, the dependence of cell performance on the oeprating temperature was studied in cell LC-8 using 50 w/o sulfuric acid solution at atmospheric pressure. At temperatures of 24, 37, 50 and 60°C, the cell voltage of LC-8 at a constant current 100 mA/cm^2

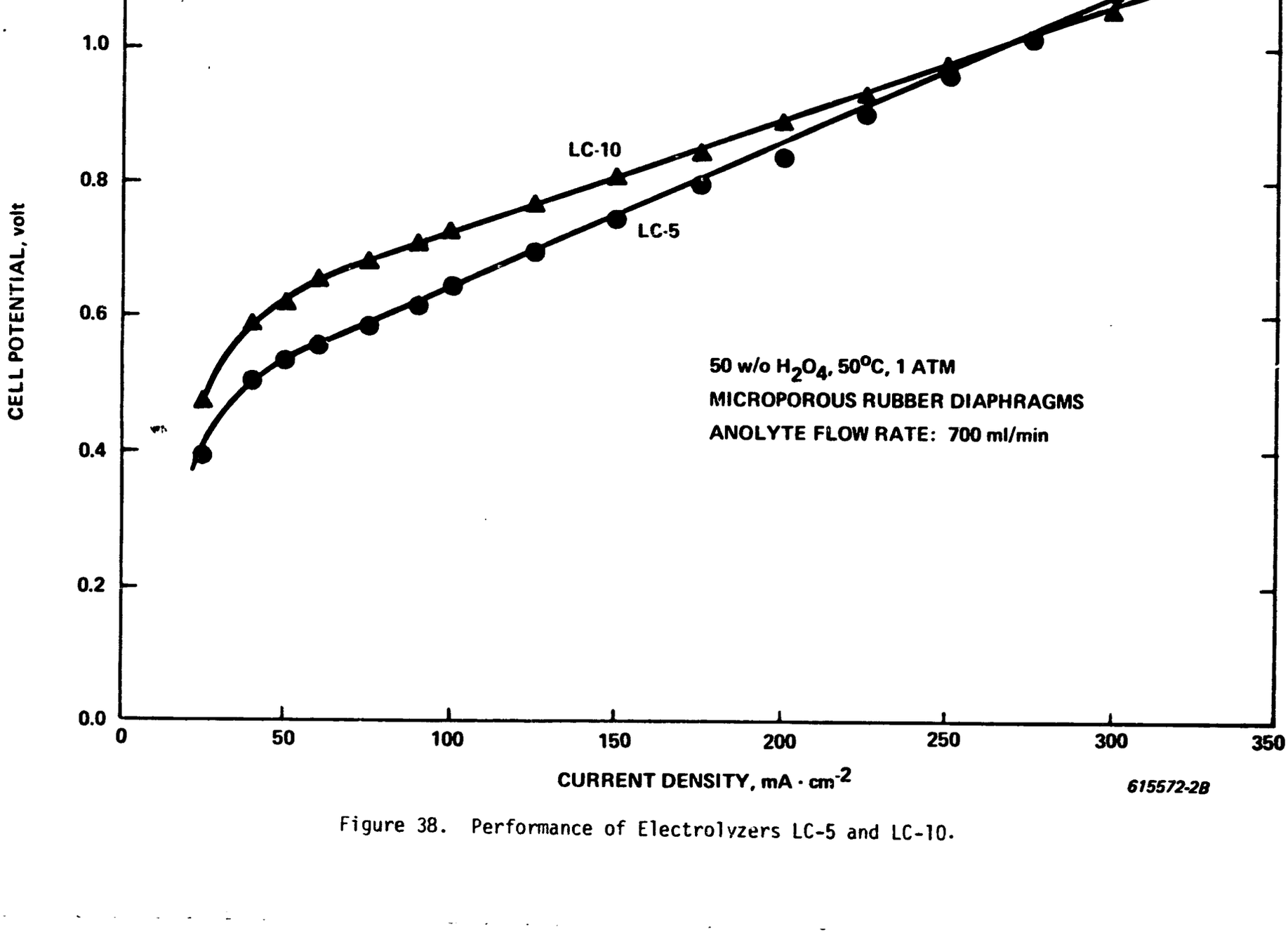

Figure 38. Performance of Electrolyzers LC-5 and LC-10.

was measured as a function of time. As shown in Figure 39, the electrolyzer LC-8 exhibited cell voltages of approximately 0.76, 0.70, 0.65, and 0.69 V at 24, 37, 50, and 60°C, respectively, after operating for 2 hours. It is obvious that, with increasing temperature, a significant improvement in the cell performance can be attained. Above 50°C, however, the improvement in the electrode kinetics probably is offset by the decrease of SO_2-solubility in the anolyte. It is thus believed that, without pressurizing an electrolyzer, the performance improvement of an SO_2-depolarized cell, arising simply from the temperature increase, is limited.

To evaluate the long-term stability of an SO_2-depolarized electrolyzer, cell LC-8 was operating continuously at a constant current density 100 mA/cm^2, using 50 w/o sulfuric acid at 50°C. Simultaneously, the cell voltage, anodic overpotential, cathodic overpotential and ohmic loss were monitored as a function of time. During the test, a gradual increase of acid concentration in the anolyte resulted in a detectable effect on the cell voltage. Therefore, makeup water was introduced into the anolyte at an appropriate rate to maintain a constant concentration. Because of a double pump failure, the endurance test on cell LC-8 was terminated after ∿173 hours of operation. The planned operating time had been 200 hours. Figure 40 depicts variations of the observed cell potential and anodic overpotential with time.

During the first three days, the cell voltage increased from an initial value 644 mV to ∿675 mV, showing an average degradation of 10 mV/day. As evidenced in Figure 40, the gradual increase of cell voltage is essentially due to performance degradation at the anode. After 80 hours of continuous operation, the cell performance became practically invariant with time. The stabilized cell potential and anodic overpotential were ∿675 and ∿265 mV, respectively. The observed cathodic overpotential and ohmic loss (being ∿50 and ∿60 mV, respectively) remained nearly constant throughout the course of the endurance test. The resulting gas from the cathodic compartment of LC-8 was collected and then analyzed by mass spectroscopy. The purity of hydrogen gas evolved in the electrolyzer was as high as 98.7 v/o. The detectable impurities included H_2S and SO_2.

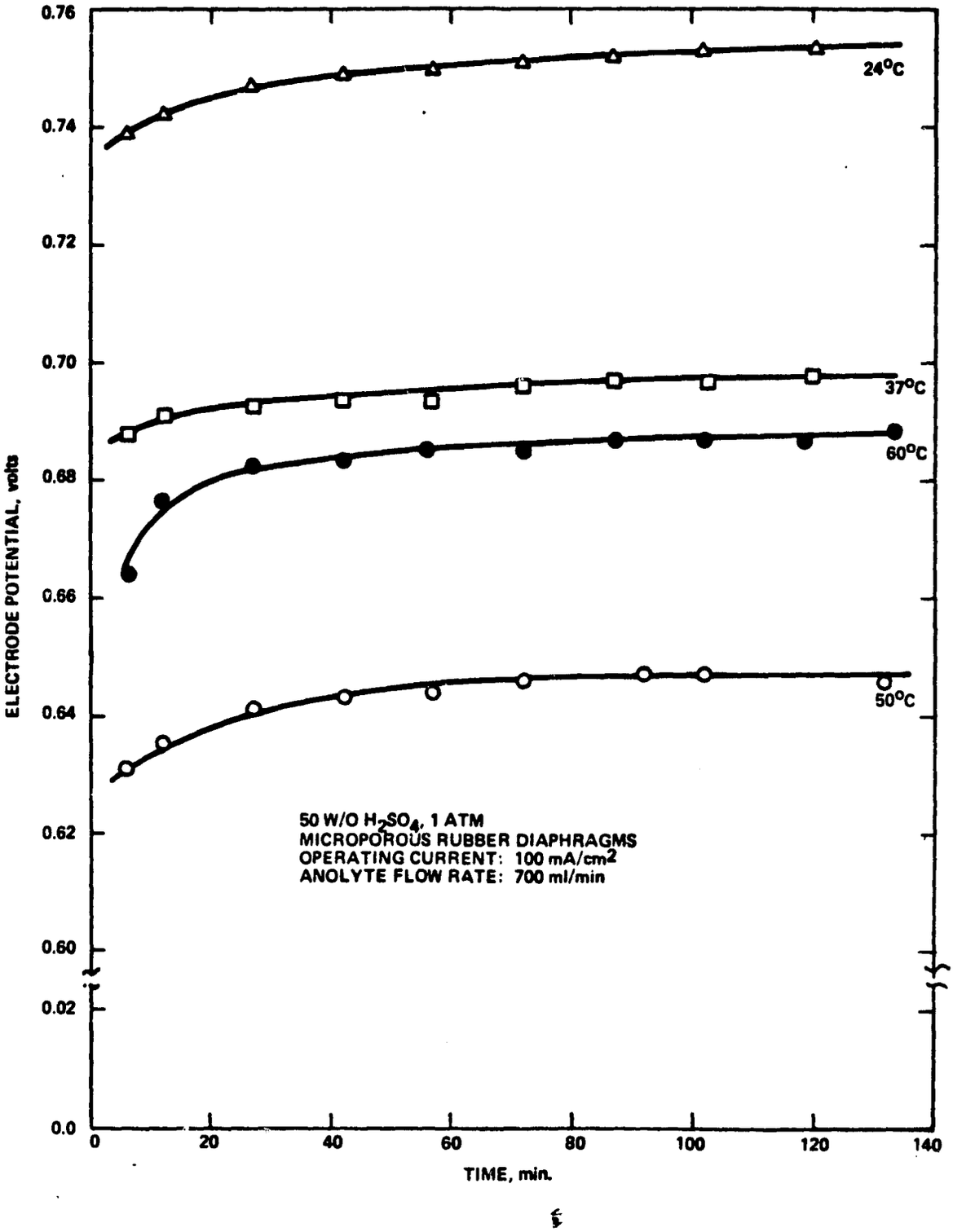

Figure 39. The Time Dependence of Cell Voltage of Electrolyzer LC-8 as a Function of Temperature.

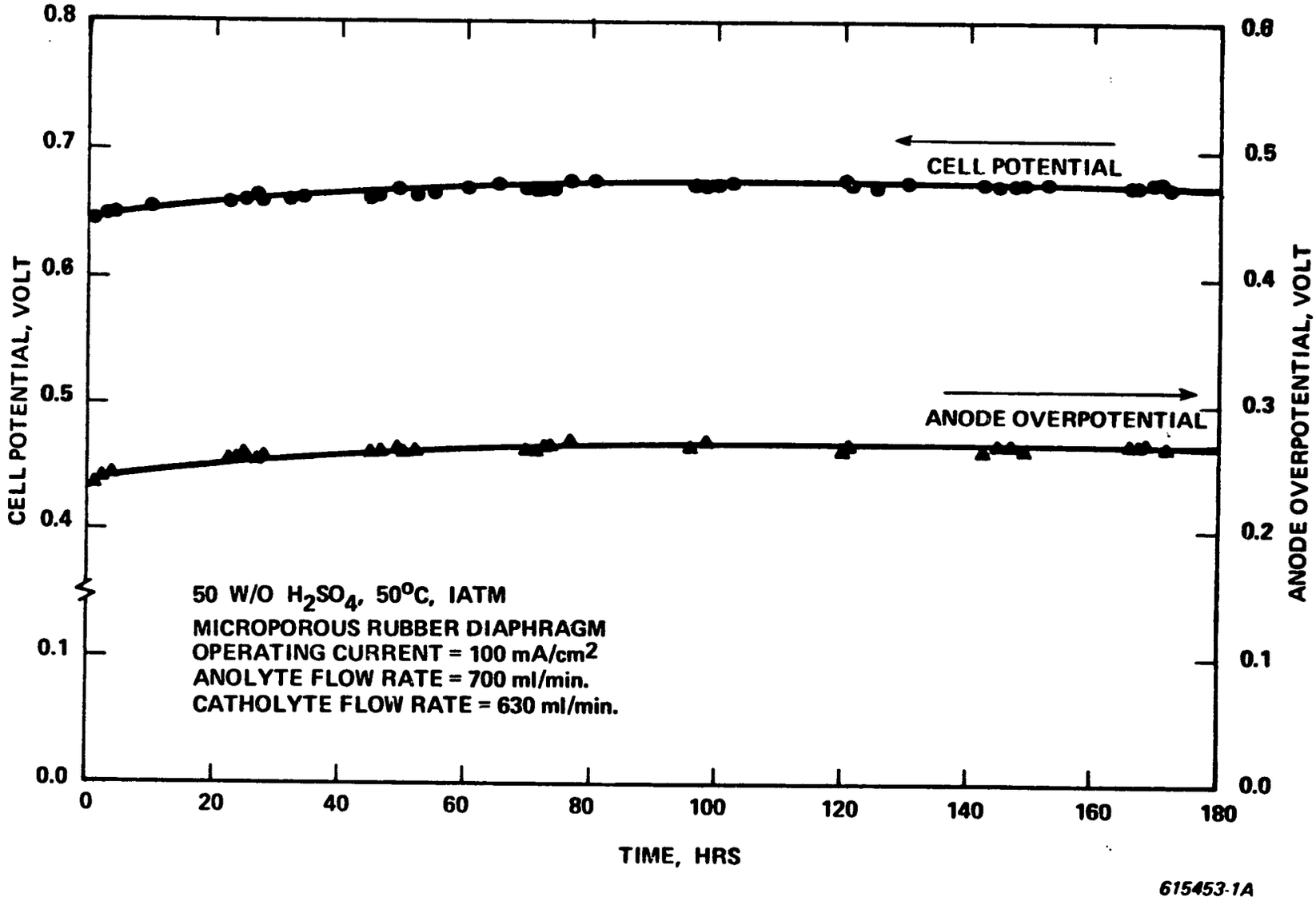

Figure 40. The Time Dependence of Cell Voltage and Anodic Overpotential of Electrolyzer LC-8 Operating at a Constant Current Density 100 mA/cm^2.

2.2.7 ESCA Studies

Electron Spectroscopy for Chemical Analysis (ESCA) is a powerful analytical tool for studying surfaces of solids[45,46]. This technique yields information on the chemical compositions and the oxidation states of a solid sample. In the present work, ESCA studies were conducted to identify the oxidation state of an unoxidized and an oxidized palladium oxide sample (referring to Section 2.2.2). The chemical compositions of a tested Pt-catalyzed carbon plate cathode were determined using this technique. Quantitative analyses of Pd-containing and S-containing species were also performed on a tested carbon cloth backed anode catalyzed with palladium oxide.

Identification of Palladium Oxide Catalyst. Experimental efforts were made to determine the chemical compositions of palladium oxide catalyst, obtained from Ventron Corporation. This catalyst was treated at 600°C in a helium stream containing 5% oxygen to ensure a complete oxidation. ESCA studies were conducted on a treated and an "as received" samples. The results are shown in Figure 41. The X-ray photoelectron spectra of Pd $3d_{3/2,5/2}$ and O 1S levels are approximately identical for both samples. The binding energy of the Pd $3d_{5/2}$ electrons was determined to be 336.8 eV. The full width at half maximum (FWHM) for this peak was ~1.4 eV. Apparently, the measured binding energy for the Pd $3d_{5/2}$ peak in both samples is between the values for PdO (336.3 eV) and PdO_2 (337.9 eV) as reported in the literature[47]. The lack of agreement may be attributed to slight variations in the published binding energies, arising from incorrect compensation of the charging effect that were not observed in this work. On the basis of the Pd/O ratios, both samples were identified as PdO. No metal palladium was detected in either of the two catalyst samples. It is thus concluded that, in the "as received" condition, the palladium oxide catalyst is substantially composed of PdO without the presence of Pd° or PdO_2.

Characterization of a Tested Carbon Cloth Backed Anode. After evaluation in the electrolyzer LC-10 (referring to section 2.2.5), the carbon cloth backed anode was rinsed thoroughly in distilled water and then delivered to the Institute for Mining and Minerals Research, University of Kentucky, for ESCA

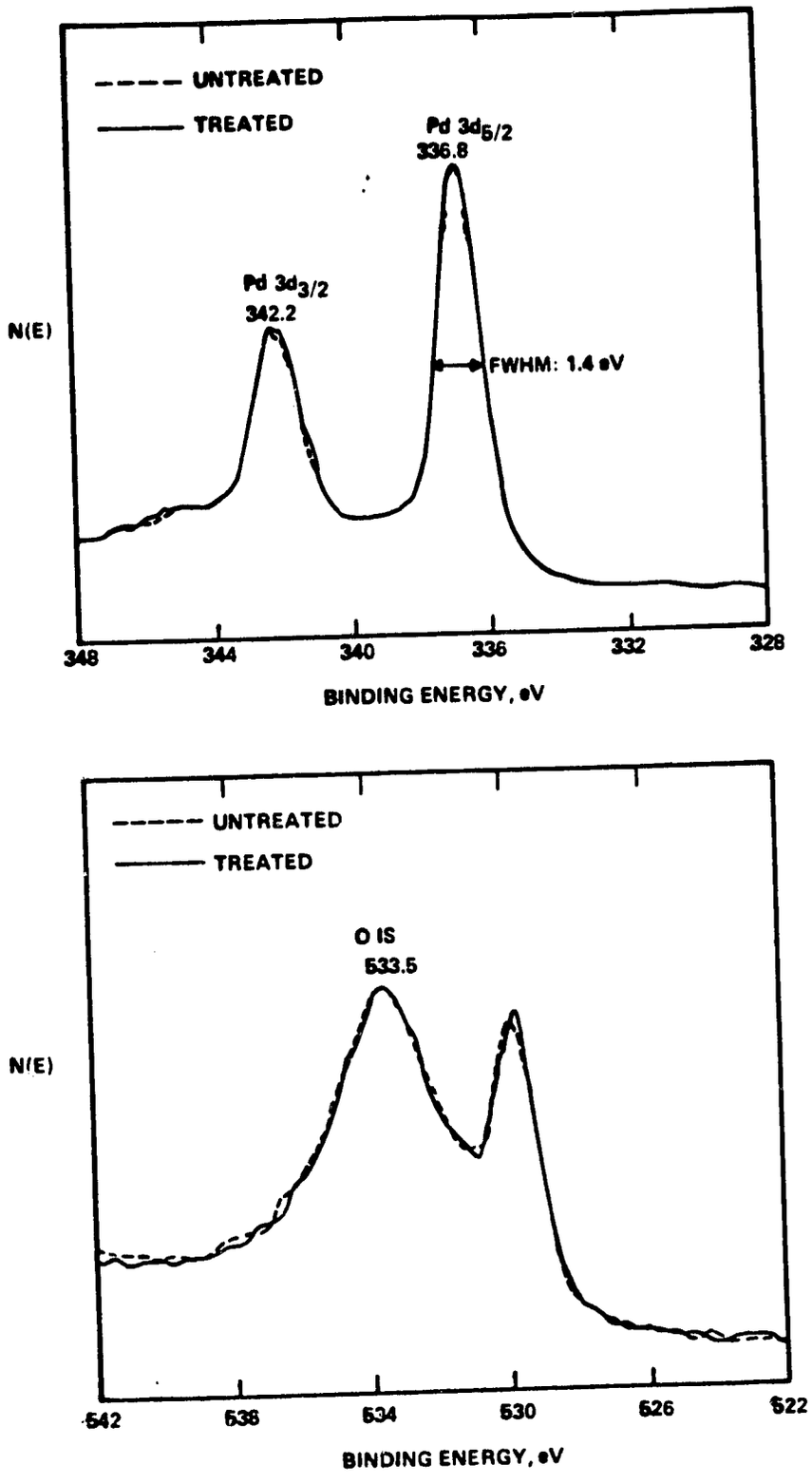

Figure 41. ESCA Spectra for an Untreated and a Treated Palladium Oxide Catalyst.

studies. The sample surface was etched by argon ion bombardment (at 1 KeV) for 5 and 15 minutes. The elements C, Pd, S, O, F, Si and Fe were detected in the ESCA spectra. The binding energy and chemical composition data for various detectable species are summarized in Table 6.

Two distinguishable peaks were observed in the carbon spectrum: a large one with binding energy ∿284.5 eV due to graphite and a second, smaller one (only ∿10% of the total C signal) at 291.5 eV which is attributed to fluorinated carbon (C-F). The F 1S peak had a binding energy in good agreement with that expected for C-F bonds. It is noted that polytetrafluoroethylene (PTFE) was incorporated as a binder in the catalyst layer on the carbon cloth. As seen from Table 6.B, both the C-F carbon 1S peak and the F 1S peak decrease in intensity with argon ion etching. It is obvious that more PTFE-binder was present on the surface of the catalyst layer than in the layer itself. Further investigation on the relative intensities of the C-F C 1S peak and the F 1S peak revealed that C-F bonds are in a CF_2 form.

Prior to the argon ion bombardment, the Pd $3d_{3/2}$ peak at 341.5 eV appears to be due to PdO. A decrease of ∿0.5 eV in the binding energy was observed on the etched sample. As has been noted in the literature[47], the Pd^{+2} ions were apparently reduced to Pd° during the etching process. The S spectrium exhibits a doublet structure of $S^{=}$ and $SO_4^{=}$. The S 2P peak for the $SO_4^{=}$ species (being at ∿168.6 eV) is favored on the outer surface of the catalyst layer. As shown in Table 6.B, however, the atomic concentration of $S^{=}$ species becomes the higher of the two inside the catalyst layer although there is still a significant amount of sulfate ions. It should be noted that the overall atomic concentration of S-containing species is reasonably constant, indicating a deep penetration of these species into the catalyst layer on the carbon cloth backed anode.

The concentration of Si-containing species is small (∿1.5 a/o) and may be due to SiO_2 or other silicates. The O 1S peak is probably caused from SiO_2 and $SO_4^{=}$. As seen from Table 6.A, the full width at half-maximum (FWHM) for this peak is as high as ∿4.0 eV, indicating that a weak O 1S signal for PdO species is present. The Fe signal is very weak and may be ascribed to Fe_2O_3, Fe_3O_4 or Fe-containing hydroxide.

TABLE 6

BINDING ENERGIES AND ATOMIC CONCENTRATION OF VARIOUS SPECIES ON A TESTED CARBON CLOTH BACKED ANODE

(A) Binding Energies (in eV)

SPECIES	ELECTRON LEVEL	ETCHING TIME* 0	5 MIN.	15 MIN.
C (graphite)	1S	284.2 (1.9)‡	284.6 (2.1)	284.5 (2.2)
C (in C-F)	1S	291.5 (-)	291.5 (-)	291.5 (-)
Pd (in PdO)	$3d_{3/2}$	341.5 (3.9)	341.0 (3.4)	341.0 (3.4)
S (in $S^{=}$)	2P	163.0 (2.9)	163.4 (3.0)	163.6 (3.6)
S (in $SO_4^{=}$)	2P	168.6 (2.9)	168.4 (3.2)	168.8 (3.3)
O (in $SO_4^{=}$, PdO, SiO_2)	1S	532.1 (3.4)	532.4 (4.0)	532.5 (4.1)
F (in C-F)	1S	688.8 (3.0)	688.7 (3.1)	688.0 (2.8)
Si (in SiO_2)	$2P_{3/2}$	-	711 (-)	-

*Argon Ion Bombardment at 1 KeV

‡The values in ( ) representing the full width at half maximum.

(B) Atomic Composition (in percentage)

SPECIES	ETCHING TIME 0	5	15 MIN
C (graphite)	57.1	63.4	66.5
C (in C-F)	8.5	7.1	7.3
Pd (in PdO)	1.4	1.7	1.6
S (in $S^{=}$)	1.0	2.3	2.8
S (in $SO_4^{=}$)	3.0	2.4	1.8
O (in $SO_4^{=}$, PdO, SiO_2)	13.1	10.6	11.1
F (in C-F)	14.4	10.8	6.8
Si (in SiO_2)	1.3	1.5	1.7
Fe	0.2	0.3	0.3

The atomic compositions of the lightly etched surface (5 minutes, 1 KeV Ar ions) is probably the most accurate representation for the catalyst layer of a tested anode. The chemical compositions of the tested catalyst layer are summarized as follows:

C: graphite and a small amount (10%) in CF_2

Pd: PdO

S: $SO_4^=$ and $S^=$ at about equal concentrations

O: SiO_2 and $SO_4^=$ with a small amount in PdO

F: fluorinated carbon

Si: SiO_2 or silicate

Fe: FeO_x or hydroxide

Characterization of a Tested Carbon Plate Cathode. ESCA studies were also carried out on a catalyzed carbon plate cathode that was incorporated in the electrolyzer LC-8 for the endurance test. The binding energies and atomic concentrations for various species on the unetched and etched samples are listed in Table 7. The carbon 1S peak at ~284.3 eV is typically for graphite which is the major component to form the porous carbon substrate. The observed binding energy of the Pt $4f_{7/2}$ electrons (72.1 eV) is about 1 eV higher than it is in the Pt metal (71.1 ev). Note that the Pt $4f_{7/2}$ peak for PtO has been reported to be at 73.8 eV[47]. Thus, the Pt catalyst on the cathode is probably in the form of Pt°. In this work, small Pt particles is imbedded in a highly porous carbon substrate. Obviously, there is a slight binding force between Pt-particles and the carbon substrate. As a result, a small binding energy shift is observed in the Pt $4f_{7/2}$ peak for Pt° although there is no chemical shift (say, from Pt° to PtO). Referring to Table 7.B, the binding energy for the Pt $4f_{7/2}$ electrons remains approximately constant during the argon etching. As mentioned previously, the reduction of oxides to metals does occur after exposing the sample to argon ion bombardment[47]. Therefore, the stability of the observed Pt spectrum during the argon etching strongly supports the identification of the Pt chemical state as Pt°.

TABLE 7

BINDING ENERGIES AND ATOMIC CONCENTRATION OF VARIOUS SPECIES ON A TESTED CARBON PLATE CATHODE

(A) Binding Energy (in eV)

SPECIES	ELECTRON LEVEL	ETCHING TIME* 0	5 MIN.	15 MIN.
C (graphite)	1S	284.3 (1.9)‡	284.2 (2.1)	284.3 (2.2)
Pt (metal)	$4f_{7/2}$	72.1 (∿3)	71.9 (∿3)	71.9 (∿3)
S (in $SO_4^=$)	2P	168.7 (3.7)	168.8 (2.8)	168.8 (2.8)
S (in $S^=$)	2P	163.3 (2.4)	163.3 (2.9)	163.5 (2.9)
O (in $SO_4^=$, SiO_2)	1S	532.2 (2.7)	532.3 (2.7)	532.2 (2.8)
Si (in SiO_2)	2P	103.0 (2.4)	103.4 (2.4)	103.2 (2.6)
Na	Auger**	264.0 (3.0)	264.3 (2.8)	264.3 (2.9)

*Argon ion bombardment at 1 KeV

‡The value in ( ) representing the full width at half maximum.

**Data were taken from the Auger electron peak.

(B) Atomic Composition (in percentage)

SPECIES	ETCHING TIME 0	5 MIN.	15 MIN.
C (graphite)	60.0	58.8	54.5
Pt (metal)	0.64	0.95	1.07
S (in $SO_4^=$)	6.79	5.29	6.40
S (in $S^=$)	1.29	2.73	3.60
O (in $SO_4^=$, SiO_2)	25.1	26.1	27.1
Si	4.55	5.60	6.42
Na	0.70	0.58	0.73

Two distinctive peaks for the S 2P electrons are found: one for $S^{=}$ (at ~163.3 eV) and the other for $SO_4^{=}$ (at ~168.8 eV). On the lightly etched sample, the ratio of $SO_4^{=}$ to $S^{=}$ is about 2:1. As seen from Table 7.B, the atomic concentation of Si-containing species increases distinctly during the argon ion etching, indicating that this species is present in the porous carbon substrate rather than in the catholyte. The trace quantity of Na-containing species is probably due to the slight attack of glassware by the strong acidic catholyte (50 w/o sulfuric acid) during the endurance test.

In summary, ESCA results incidate that the palladium oxide and Pt-black catalysts, impregnated in the carbon cloth backed anodes and catalyzed carbon plate cathodes, are in the chemical states of PdO and Pt°, respectively. After an electrolysis experiment, sulfide ions are present on the tested electrodes, presumably due to the reduction of SO_2-containing species by hydrogen gas or the electroreduction of SO_2-containing species at the cathode. However, no sulfur or SO_2-containing species are observed on the tested electrodes. The porous carbon substrate contains a small quantity of SiO_2.

2.3 INVESTIGATION OF SEPARATOR MATERIALS

In an SO_2-depolarized electrolyzer, SO_2-containing species dissolved in the anolyte tends to migrate from the anode to the cathode with a subsequent electroreduction to form sulfides. The chemisorption or deposition of these impurity by-products on the cathode may cause poisoning or blocking effect on the electron catalytic activity for hydrogen evolution. A separator is thus needed to incorporate between the anodic and cathodic compartments of a cell. Microporous rubber diaphragms are currently used in electrolysis experiments. As has been pointed out[11,40], the migration of SO_2-containing species through a separator resulted in the formation of inclusions inside a tested membrane. Furthermore, ESCA studies on tested membranes revealed that the inclusions are essentially composed of sulfide, presumably formed through the reduction of penetrating SO_2-containing species by hydrogen gas.

A number of membranes and diaphragms, developed by DuPont, RAI Research Corporation and Ionics, Inc., have been experimentally evaluated as gas separators in the SO_2-depolarized electrolyzers. The criteria for the selection

of reliable separator materials include (a) great chemical stability to the electrolyte environment, (b) good mechanical strength under operating conditions, (c) low permeation rate for SO_2-containing species, (c) low permeation rate for SO_2-containing species, (d) high electric conductivity for H_3O^+ ions and (e) prolonged lifetime. The present work has focused on the investigation of diffusion coefficient of SO_2-containing species and ionic (H_3O^+) resistivity in the candidate materials. The dependence of diffusion coefficient on temperature was also studied on a microporous rubber diaphragm, a Nafion® 120 membrane and a RAI P-4010 membrane.

2.3.1 Investigation on Diffusion Coefficient of SO_2-Containing Species

The permeation rate of SO_2-containing species through a separator material was monitored by an electrochemical technique[48,49]. The permeation cell for studying the diffusion coefficient of SO_2-containing species is illustrated schematically in Figure 42.A. By use of Teflon as the structural material, the appearance of this cell is shown in Figure 42.B. The permeation cell consisted of two compartments which were separated by a test membrane or diaphragm. The left compartment was used for introducing the diffusant (i.e., SO_2-containing species) in the separator and the other compartment for the electrochemcial measurements of the permeation rate. A platinized Pt-screen working electrode was fixed adjacent to the surface of the test membrane. During each experiment, purified nitrogen gas was bubbled into the right compartment to eliminate impurity traces such as O_2 and CO_2 in the electrolyte. A reversible hydrogen electrode (RHE) was used as the reference. By potentiostating the working electrode at 0.65 V versus RHE, the permeation rate of SO_2-containing species was monitored by electrochemically oxidizing SO_2 as it diffused through the separator. The measuring solution was presaturated with SO_2 and then introduced instantaneously into the left compartment of the permeation cell. The anodic current at the working electrode was recorded as a function of time.

By referring to Figure 43.A, the flux J of SO_2-containing species through a test membrane (or diaphragm) of thickness L is given by the Fick's first law of diffusion, namely

$$J = -D\left[\frac{\partial C(x,t)}{\partial x}\right]_{x = L} \qquad (23)$$

(A)

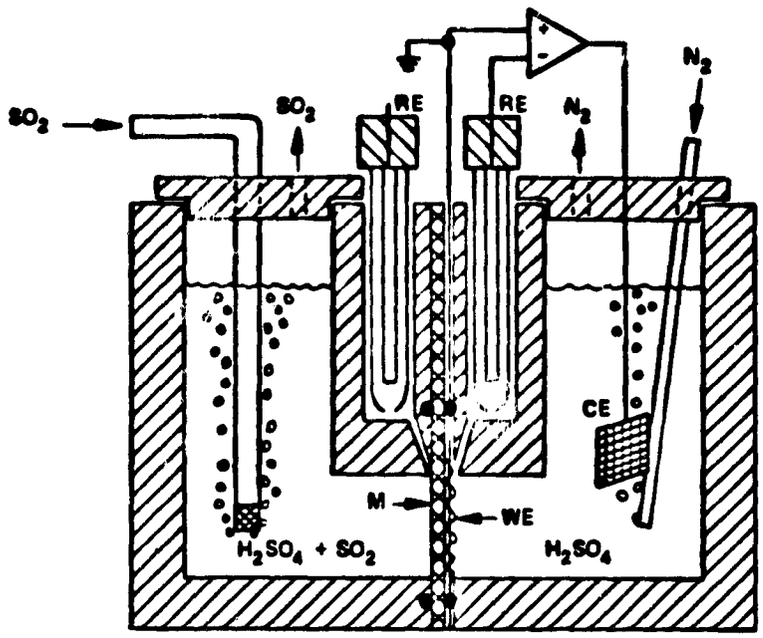

(B)

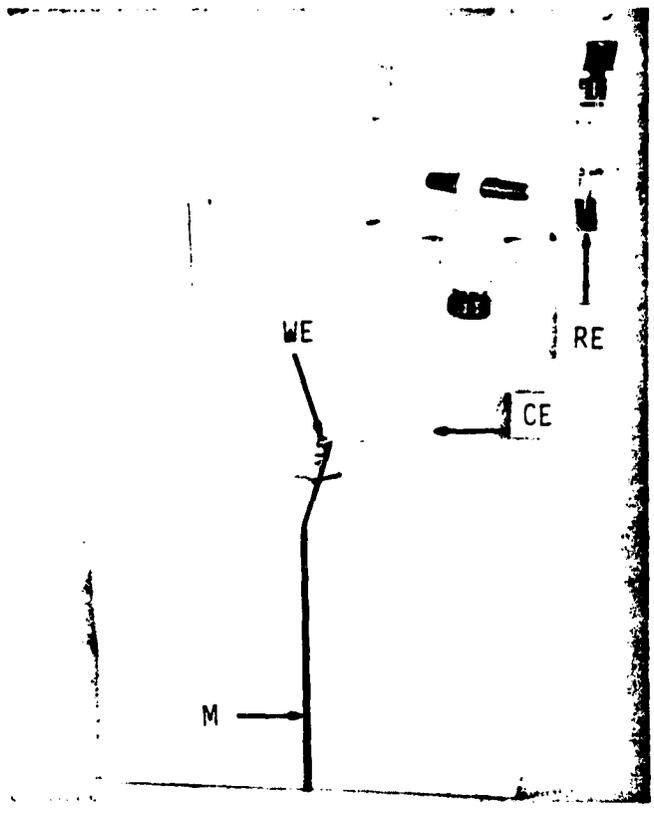

WE – WORKING ELECTRODE
RE – REFERENCE ELECTRODE
CE – COUNTER ELECTRODE
M – MEMBRANE

Figure 42. (A) Schematic Diagram and (B) Photo of a Permeation Cell.

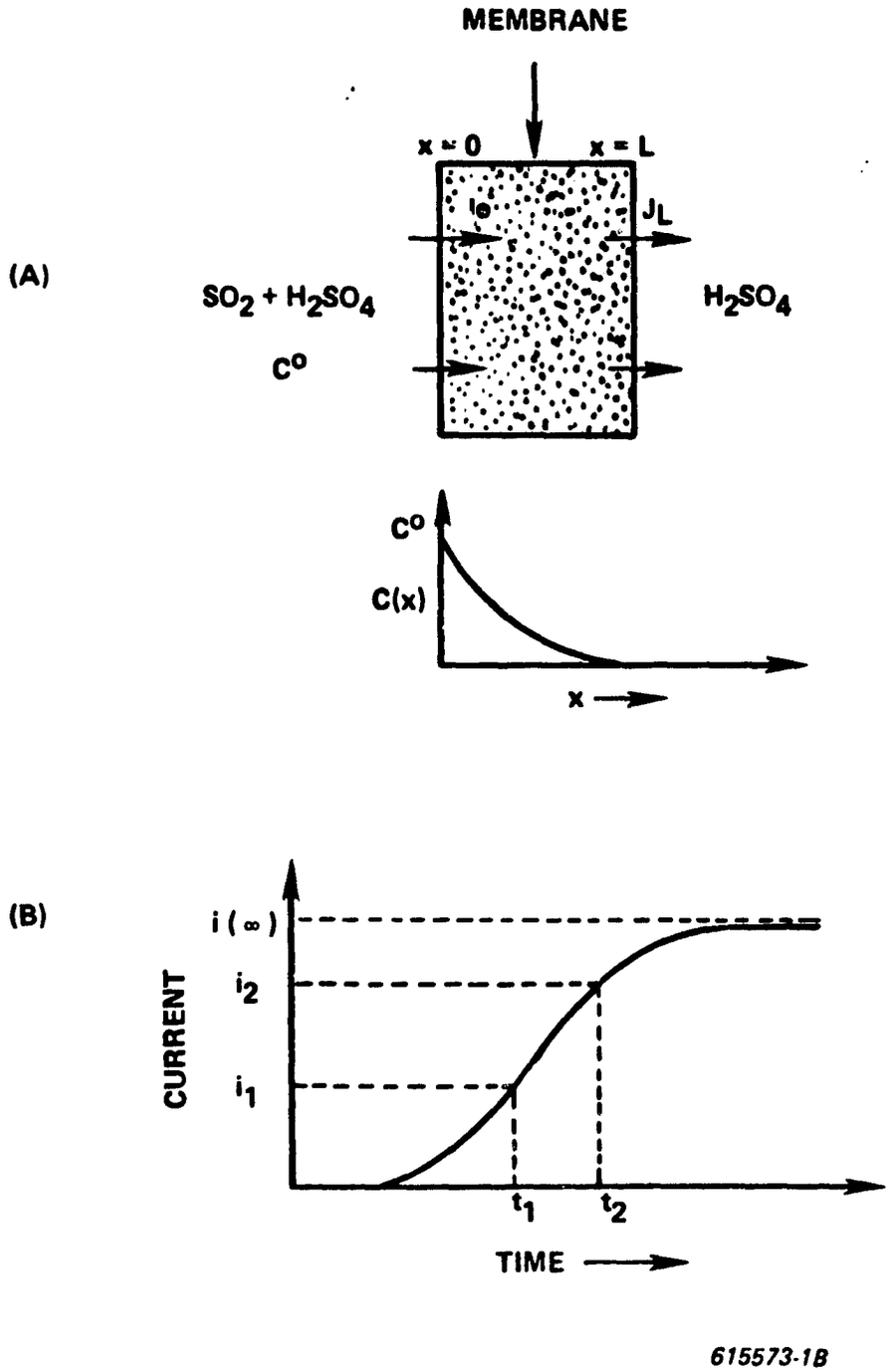

Figure 43. (A) The Concentration Gradient of SO_2-Containing Species in a Test Membrane, (B) A Permeation-Current Transient Typically Observed during the Experiments.

where D is the diffusion coefficient and C(x,t) is the concentration of diffusant at a point x within the membrane and at a time t. If the SO_2-containing species diffused through the separator is completely oxidized on the working electrode, the resulting anodic current, i(t), at a time t is expressed by the equation

$$i(t) = 2FJ = -2DF \left[\frac{\partial C(x,t)}{\partial x}\right]_{x = L} \tag{24}$$

where F is the Faraday constant. As derived in Appendix A, the measured current during the permeation transient is given by the expression

$$i(t) = \frac{2L \cdot i(\infty)}{\sqrt{\pi Dt}} \exp\left(-\frac{L^2}{4Dt}\right) \tag{25}$$

where $i(\infty)$ is the measured current at the steady state. Experimentally, a permeation current transient that reflects the buildup of the concentration gradient of diffusant within a membrane is shown in Figure 43.B. The diffusion coefficient D can be calculated from the initial part of this transient curve. If i_1 and i_2 represent the currents at time t_1 and t_2 , respectively, Equation 25 can be rewritten as

$$\frac{i_2}{i_1} = \left(\frac{t_1}{t_2}\right)^{\frac{1}{2}} \exp\left[\frac{L^2}{4D}\left(\frac{1}{t_1} - \frac{1}{t_2}\right)\right] \tag{26}$$

By choosing a fixed value 2 for the ratio of i_2/i_1, we obtain

$$\log\left(\frac{t_2}{t_1}\right) = \frac{L^2}{4.606D}\left(\frac{1}{t_1} - \frac{1}{t_2}\right) - 0.602 \tag{27}$$

Thus, the diffusion coefficient D can be calculated from the slope of the plot of log (t_2/t_1) versus $[(1/t_1) - (1/t_2)]$. In this study, measurements of diffusion coefficients of SO_2-containing species within candidate materials were made in 50 w/o sulfuric acid at atmospheric pressure. Typical plots of log (t_2/t_1) versus $[(1/t_1) - (1/t_2)]$ for a microporous rubber diaphragm are shown in Figure 44. As expected, straight lines are generally observed.

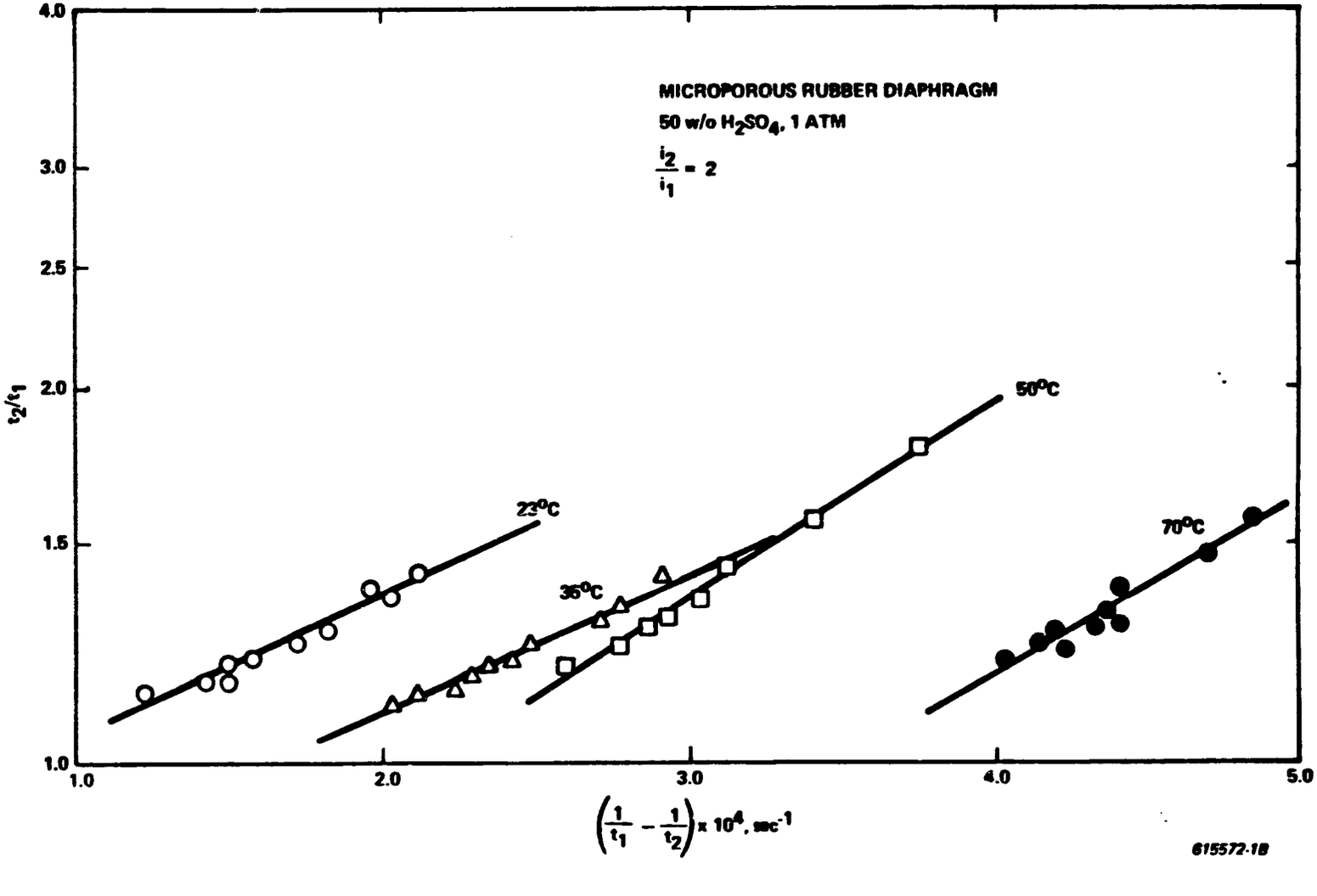

Figure 44. The t_2/t_1 Versus $(\frac{1}{t_1} - \frac{1}{t_2})$ Plots for the Diffusion of SO_2-Containing Species in a Microporous Rubber Diaphragm at Temperatures of 23, 35, 50 and 70°C.

In certain cases, when the steady-state permeation current $i(\infty)$ is low (e.g., in the RAI P-4010 membrane), or when relatively thin membranes are to be evaluated, it is convenient to measure D values from $i(\infty)$. By referring to Figure 43, the concentration gradient of SO_2-containing species in a test membrane can be expressed, under steady-state conditions, by the equation

$$-\left[\frac{\partial C(x,t)}{\partial x}\right]_{x=L} = \frac{C_o}{L} \qquad (28)$$

where C_o is the concentration of diffusant in the measuring solution in the left compartment. The combination of Equations 24 and 28 gives

$$i(\infty) = \frac{2FDC_o}{L} \qquad (29)$$

Thus, the value of D can be calculated from the measured current $i(\infty)$ at the steady state.

The measured diffusion coefficients for SO_2-containing species in various candidate materials at 23°C are summarized in Table 8. The measured diffusion coefficients in Nafion ® 120 and RAI P-5025 are $\sim 3.8 \times 10^{-7}$ and $\sim 1.6 \times 10^{-7}$ cm^2/sec. A relatively high D is found in microporous rubber diaphragm ($\sim 2.2 \times 10^{-6}$ cm^2/sec). Of all the candidate materials, RAI P-4010 is most promising for use as a separator in the SO_2-depolarized electrolyzer. As illustrated in Table 8, the measured diffusion coefficient in P-4010 is lower than that in a microporous rubber diaphragm by more than two orders of magnitude.

The permeability, $\bar{P}$, of a separator material to SO_2-containing species is defined as the ratio of $J/(\Delta P/L)$, where ΔP is the partial pressure difference of the diffusant across the separator. Assuming that the diffusion of SO_2-containing species through the membrane follows the Fick's law with a constant D, one has

TABLE 8

COMPARISON OF DIFFUSION COEFFICIENTS AND IONIC RESISTIVITIES IN CANDIDATE MATERIALS FOR USE AS SEPARATORS*

MATERIALS	THICKNESS, cm	D, cm^2/sec	P, cm^3 (STP)/ sec·cm·cm-Hg	IONIC RESISTIVITY IN SO_2-FREE SOLUTION (Ω-cm)	IONIC RESISTIVITY IN SO_2-SATURATED SOLUTION (Ω-cm)
Microporous Rubber Diaphragm	0.114	2.2×10^{-6}	7.8×10^{-7}	1.75	2.02
Nafion 110	0.028	8.0×10^{-7}	2.8×10^{-7}	10.4	10.4
Nafion 120	0.028	3.8×10^{-7}	1.3×10^{-8}	13.6	15.0
Nafion 315	0.040	2.4×10^{-6}	8.5×10^{-7}	19.2	19.2
Nafion 390	0.040	2.4×10^{-6}	8.5×10^{-7}	8.5	9.0
P-4010	0.013	4.7×10^{-9}	1.7×10^{-9}	20.2	20.8
P-5025	0.025	1.6×10^{-7}	5.7×10^{-8}	8.0	8.4
Yumicron	0.020	1.9×10^{-7}	6.7×10^{-8}	9.0	9.5

*In 50 w/o sulfuric acid solutions at 23°C and atmospheric pressure.

$$\bar{P} = D\,\bar{S} \qquad (30)$$

Where $\bar{S}$ is the solubility of SO_2-containing species in the electrolyte. At 23°C, the measured $\bar{S}$ in 50 w/o sulfuric acid solution is 0.354 cm^3 (STP)/cm^3. cm-Hg. On the basis of Equation (30), the $\bar{P}$ values for various candidate materials, calculated via the observed D values, are listed in Table 6.

The temperature dependence of diffusion coefficients D in microporous rubber diaphragm, Nafion (R) 120 and RAI P-4010 membranes was studied over the range of 23-70°C. Empirically it has been found that D can be described by the equation

$$D = D_0 \exp\left(-\frac{Q}{RT}\right) \qquad (31)$$

where D_0 is a constant and Q is the activation energy for diffusion. It is noted that D_0 and Q may vary with the concentration of diffusant but are independent of temperature. Experimentally, D_0 and Q are obtained by plotting log D vs 1/T. The slope of this plot gives

$$\frac{d \log D}{d(1/T)} = -\frac{Q}{2.303\,R} \qquad (32)$$

The measured D values in these candidate materials at various temperatures are shown in Table 9. In microporous rubber diaphragm, the diffusion coefficient is approximately independent of temperature. Within the temperature range of 23-70°C, the observed D values in this material are $(2.2 \pm 0.5) \times 10^{-6}$ cm^2/sec. In Nafion (R) 120 and RAI P-4010 membranes, however, the measured D values increase slightly with increasing temperature. Figure 45 gives the plots of log D versus 1/T for the two membranes. For the diffusion of SO_2-containing species through Nafion 120 (R) and P-4010 membranes, the apparent energies of activiation, obtained from the approximately straight semilogarithmic plots, are 2.04 and 5.48 Kcal/mole, respectively. Further analyses of the experimental results indicate that the temperature dependence of diffusion coefficients in these membranes is given by the equations

$$D_{Nafion} = 1.4 \times 10^{-5} \exp(-1027/T)\ cm^2/sec \qquad (33)$$

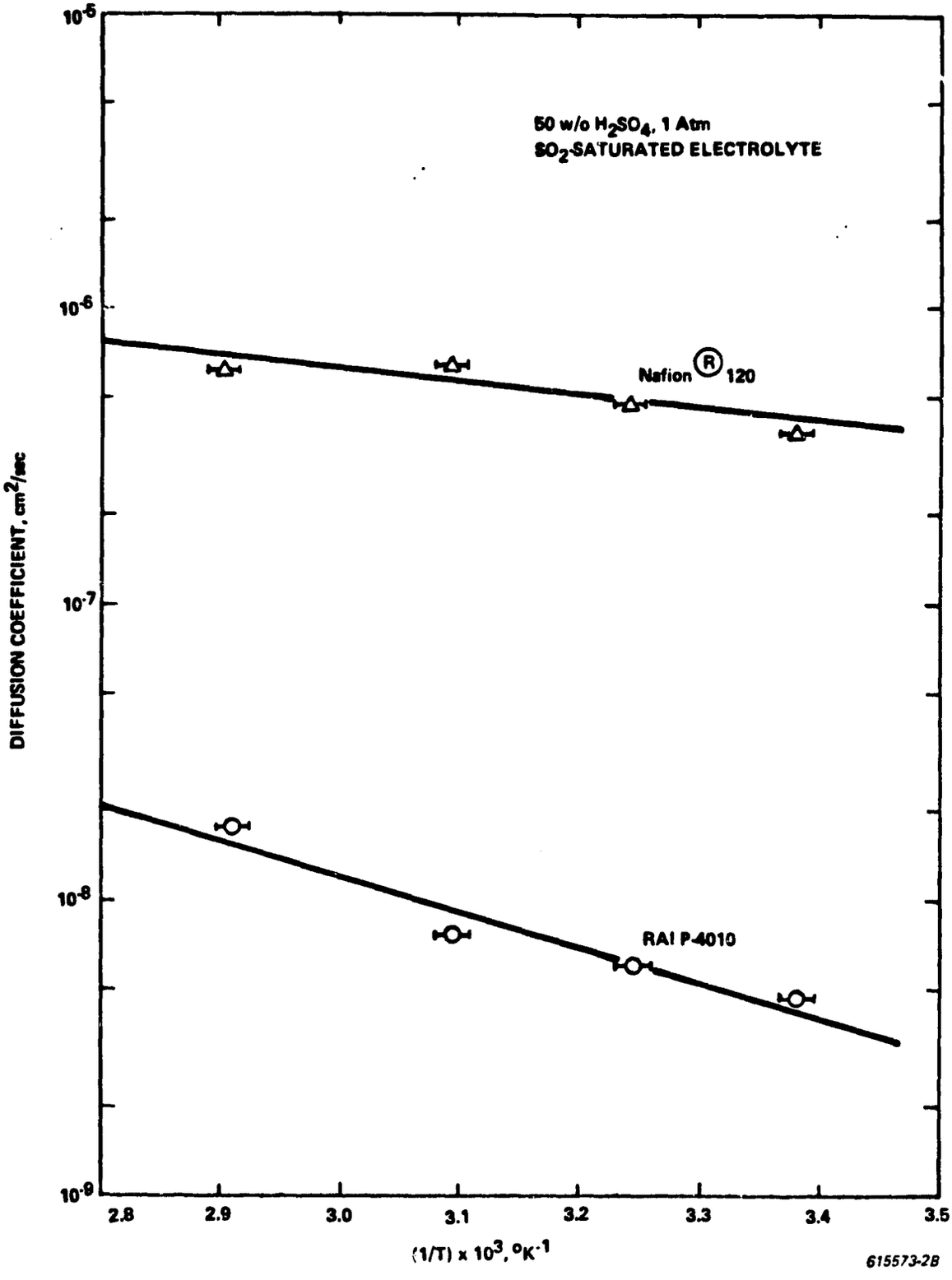

Figure 45. Arrhenius Plots for the Diffusion of SO_2-Containing Species in a Nafion (R) 120 and an RAI P-4010 Membrane.

TABLE 9

DIFFUSION COEFFICIENTS OF SO_2-CONTAINING SPECIES IN SELECTED SEPARATOR MATERIALS

TEMPERATURE, °C	SO_2 CONCENTRATION, M	DIFFUSION COEFFICIENT, cm^2/s		
		MICROPOROUS RUBBER DIAPHRAGM	NAFION (R) 120	RAI P 4010
23	1.20	2.2×10^{-6}	3.8×10^{-7}	4.7×10^{-9}
35	0.74*	2.6×10^{-6}	4.8×10^{-7}	6.1×10^{-9}
50	0.48*	1.8×10^{-6}	6.7×10^{-7}	7.8×10^{-9}
70	0.29*	2.0×10^{-6}	6.1×10^{-7}	1.8×10^{-8}

*Estimated values[20]

and

$$D_{P\text{-}4010} = 4.7 \times 10^{-5} \exp(-2758/T) \text{ cm}^2/\text{sec} \quad (34)$$

From the viewpoint of measured diffusion coefficients, the RAI P-4010 is better than Nafion (R) 120 membrane and microporous rubber diaphragm for use as a gas separator in an SO_2-depolarized electrolyzer.

2.3.2 Measurements of Hydronium Ionic Resistivity

The ionic (H_3O^+) resistance across a candidate material was measured by use of an interruptor technique[50]. Referring to Figure 42, the Pt-screen working electrode on the membrane surface was moved to the left compartment of the permeation cell, where an additional reference electrode was also connected. In this study, two saturated calomel electrodes (SCE) were used as the references. With each candidate material, experiments were conducted in SO_2-free and SO_2-saturated sulfuric acid solutions. The potential difference between two reference electrodes were measured as a function of current. The typical curves, appearing on an oscilloscope, for the decay of potentials between two reference electrodes are shown in Figure 46. The abrupt potential drops, ΔV, arising from the ionic resistance across the separator material, are about 7.2 and 27.5 mV at the currents 200 and 800 mA, respectively. The ionic resistivities through various candidate materials, determined from the plots of ΔV versus current, are given in Table 8.

Of all the separator materials investigated, the microporous rubber diaphragm exhibits the lowest ionic resistivity. In SO_2-free and SO_2-saturated sulfuric acid solutions at 23°C, the measured ionic resistivities in this diaphragm are ∿1.75 and ∿2.02 Ω-cm, respectively. It is noted[50] that the ionic resistivity in 50 w/o sulfuric acid is ∿1.8 Ω-cm at 23°C. Apparently, the presence of microporous rubber diaphragm in the permeation cell does not cause an increase in the ionic resistance. The RAI P-4010 exhibits ionic resistivities over 20 Ω-cm, being higher than those in the microporous rubber diaphragm by a factor of at least 10.

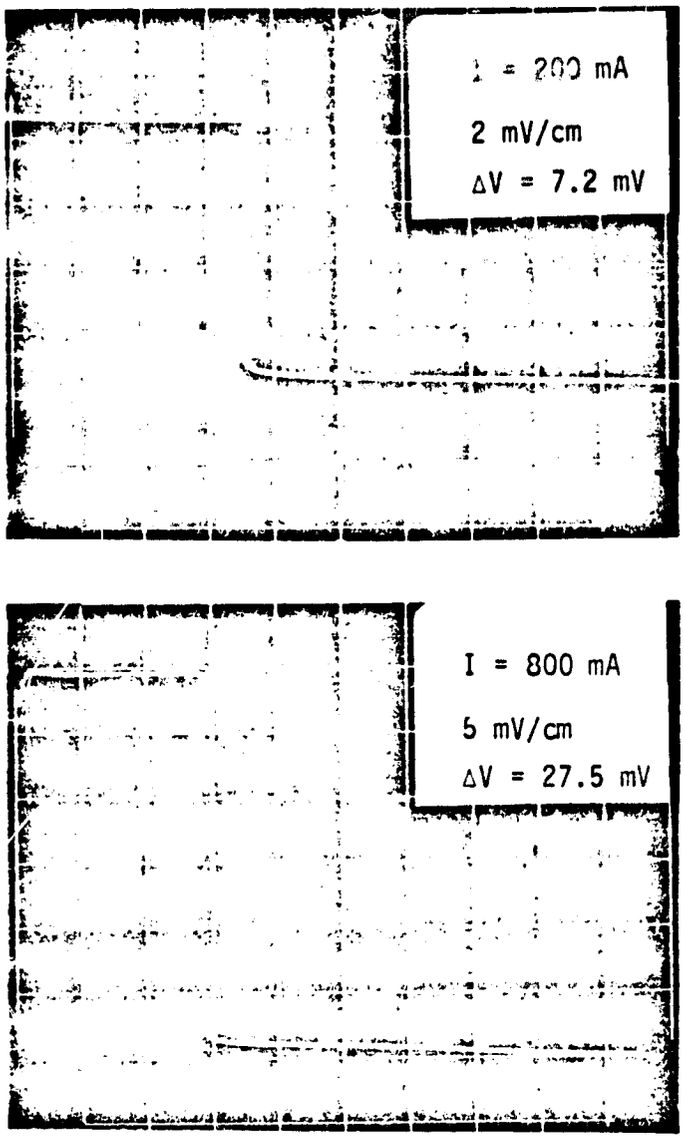

Figure 46. Typical Curves for the Decay of Potentials Between Two Reference Electrodes, Recording on an Oscilloscope.

For most candidate materials, the ionic resistivities in SO_2-saturated solutions are, in general, slightly higher than in SO_2-free solutions. In Nafion (R) 120 membrane, the measured ionic resistivities (being ∿13.6 and ∿15.0 Ω-cm, respectively) are in good agreement with the value reported in the literature[12]. After equilibrating at 100°C in pure water, the ionic resistivity of a Nafion (R) 120 membrane has been identified to be ∿15.3 Ω-cm at 25°C[12].

2.4 LABORATORY MODEL OPERATIONS

The closed cycle Laboratory Model of the Sulfur Cycle that had been built by Westinghouse in 1978 was used periodically during the year to support the electrolyzer work. The Model also was operated, including the high temperature subsystems, for demonstration purposes to visitors and dignitaries. The Model is shown in Figure 47 and a schematic diagram is illustrated in Figure 48. When operating as a closed cycle, sulfuric acid is fed into a vaporizer where it is evaporated at temperatures above 400°C. The acid vapor (now a steam-sulfur trioxide mixture) then flows to a catalyst-containing reduction reactor, where, at temperatures near 870°C, the sulfur trioxide is reduced to sulfur dioxide and oxygen. Thermal energy is supplied to both the vaporizer and the reduction reactor with multi-zone electric furnaces.

The product stream —— a mixture of sulfur dioxide, oxygen, and unreacted sulfuric acid —— leaves the reduction reactor and enters a water-cooled condenser, where the unreacted sulfuric acid is condensed. The non-condensables, sulfur dioxide and oxygen, flow to a cryogenic separation system where residual moisture is removed and the two gases are separated. The oxygen is a process co-product, while the sulfur dioxide is returned to the cycle.

The recycled sulfur dioxide is piped to the anode reservoir of the electrolyzer subsystem. In the electrolyzer, the sulfur dioxide, dissolved in a dilute sulfuric acid solution to form sulfurous acid, is oxidized at the anode to form additional sulfuric acid. Hydrogen is produced at the cathode. The sulfuric acid produced at the anode is recycled back to the vaporizer; makeup water is added at the anode reservoir.

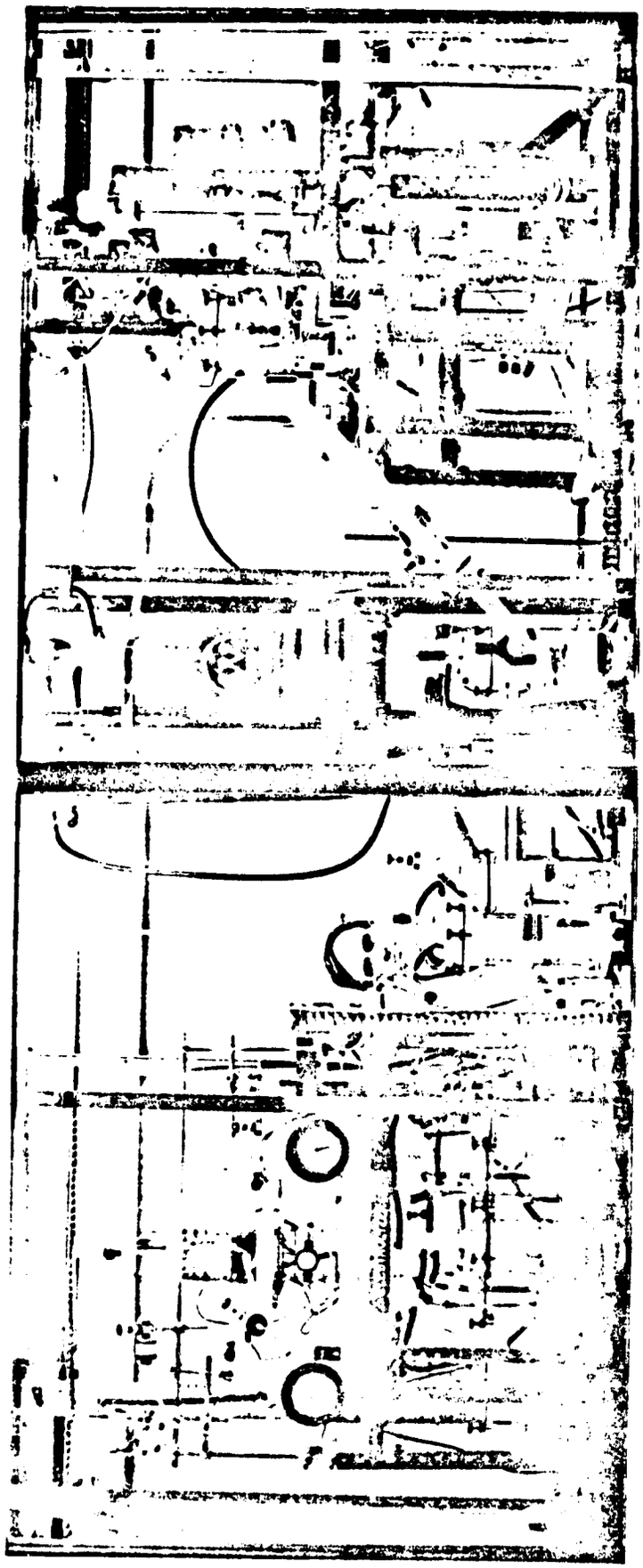

Figure 47. Photo of Westinghouse Sulfur Cycle Laboratory Model.

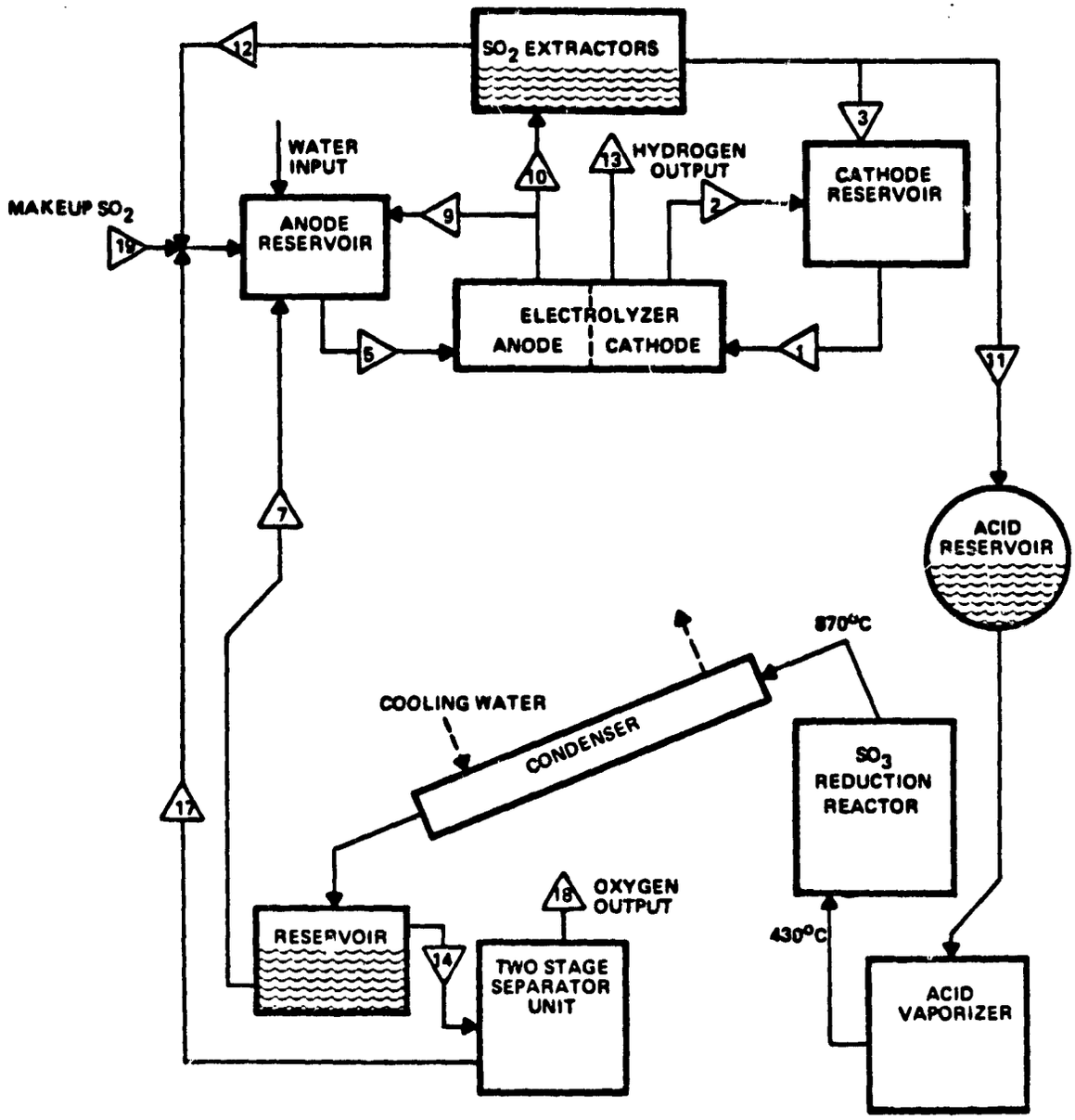

Figure 48. Schematic of the Hydrogen Laboratory Model.

Early in the year, the Model's electrolyzer substem was used to evaluate a small cell with platinum screen electrodes while the electrolyzer test facility was being refurbished. Later, the Model was used to evaluate the performance of an experimental bi-polar packed bed multicell that had been devised and built at the Westinghouse Research and Development Center.

3.0 CONCLUSIONS

A novel manufacturing process has been devised for preparing a uniformly distributed and well-bonded catalyst layer on porous carbon plates without altering the structure of the carbon substrate. Another fabrication process to prepare carbon cloth supported electrode was also developed. By use of Pt/C catalysts, the recent progress in the electrolysis technology development has resulted in substantial improvement in both voltage efficiency and performance stability of an SO_2-depolarized electrolyzer. In 50 w/o sulfuric acid solution (at 50°C and atmospheric pressure), the electrolyzer LC-12 exhibited stable cell voltages of 0.77 and 1.05 V (including ohmic losses) at current densities 200 and 400 mA/cm^2, respectively. After operating at a constant current 100 mA/cm^2 for 2 hours, the cell performance was stablized with approximately undetectable degradation.

According to experimental data from the endurance test, the cell voltage of an SO_2-depolarized electrolyzer became practically invariant with time (with little or no detectable performance degradation) after 80 hours of continuous operation. At 100 mA/cm^2, the stabilized cell voltage was ~675 mV. The purity of hydrogen gas evolved in the electrolyzer was approximately 98.7 v/o as verified in the mass spectroscopic analysis. Under the atmospheric conditions, the effect of temperature on the performance characteristics of LC-8 was also studied. Experimental results indicated that, without a pressurized cell, the achievable improvement in the performance of an SO_2-depolarized electrolyzer is limited by decreasing SO_2 solubility with increasing temperature.

For the anodic oxidation of SO_2, there are indications that palladium and palladium oxide are better electrocatalysts than platinum. In concentrated acid media, the formation of adsorbed oxygen species on an active site M (that is, $MOH \rightarrow MO_{ads} + H^+ + e^-$) is rate determining in the SO_2 oxidation reaction. Increasing temperature results in improvements in the exchange current density and anodic overpotential. The reaction mechanism is, however,

independent of temperature. The measured activation energy for SO_2 oxidation is as high as ∿25 Kcal/mole, indicating that this reaction is highly irreversible. In the anodic sweep, SO_2 oxidation reaction commences at potentials where the growth of chemisorbed oxygen-containing layer is initiated. On most metal electrodes, the chemical transformation of the chemisorbed species to metal oxides (at potentials above 0.88 V) creates passivated surface layers which strongly inhibit the SO_2 oxidation reaction. However, the oxide-covered Pd electrode exhibits high electrocatalytic activity for SO_2 oxidation.

ESCA studies revealed that the Pt-black and palladium oxide catalysts, impregnated in the carbon plate cathodes and carbon cloth backed anodes, are in the chemical states of Pt° and PdO, respectively. The measured concentrations of $S^{=}$ containing species at the surfaces of a tested carbon cloth backed anode and a tested carbon plate cathode are ∿2.3 and ∿2.7 a/o, respectively. Other detectable impurities on the tested electrodes include Si, Fe and Na. Surprisingly, the presence of these small amounts of impurities on the anode and cathode does not significantly influence their electrocatalytic activities as evidence from the results of the endurance test.

Of all the separator materials evaluated, RAI P-4010 membrane is most promising for use as a separator in the SO_2-depolarized electrolyzer. The measured diffusion coefficient for SO_2-containing species in P-4010 membrane (being $\sim 4.7 \times 10^{-9}$ cm^2/sec) is lower than in the microporous rubber diaphragm that is currently used in the electrolysis experiments, by more than two orders of magnitude. However, the former also exhibits a high ionic resistivity, approximately 10 times greater than that of the latter.

Continuing work on the electrolysis technology development will focus on (a) reduction of noble metal contents on electrodes, (b) optimization of cell configuration, and (c) fabrication and evaluation of Pd- to PdO_x-catalyzed carbon electrodes. Further improvements in the performance of an SO_2-depolarized electrolyzer are anticipated from the use of Pd or PdO_x catalysts and the enhancement of SO_2 solubility in the anolyte by increasing the operating pressure.

4.0 NEW TECHNOLOGY

The work performed under this contract (No. JPL 955380) has resulted in the invention of two novel processes for the fabrication of catalyzed porous carbon electrodes. Two separate invention disclosures were submitted to the Patent Department of Westinghouse Electric Corporation. The electrode fabrication processes are briefly described as follows:

A New Process of Electrode Fabrication for Uniformly Distributing a Catalyst Layer Upon a Porous Carbon Substrate - A new process has been developed for preparing a uniformly distributed and well-bonded catalyst layer on a porous carbon electrode without altering the structure of the carbon substrate. Referring to Figure 22, an appropriate amount of metal compounds is first applied onto a grooved surface of a pre-oxidized carbon electrode by a filtration technique and in situ heat treatment using an infrared lamp. After thermally decomposed at 600°C under a nitrogen or hydrogen atmosphere, the electrode surface is coated with a uniform layer of metal catalyst as evidenced in the SEM micrographs. If a carbon-supported-metal-oxide electrode is fabricated, the metal-covered carbon electrode is further treated at a temperature or 450 - 500°C in a stream of helium gas containing 5% oxygen.

Carbon Cloth Supported Electrodes for Sulfur Dioxide Oxidation - This invention deals with a new fabrication process and the potential use of carbon cloth supported electrodes in electrochemical devices, particularly in sulfur dioxide depolarized electrolyzers. A mixture of noble-metal or noble-metal-oxide catalyzed carbon powder and polytetrafluoroethylene (PTFE) binder is suspended in an appropriate amount of distilled water. The content of PTFE in the mixture is 20-23 w/o. The suspension is deposited on a pretreated carbon cloth by a vacuum filtration method and dried in situ at ∿40°C using an infrared lamp. The resulting catalyst layer on the cloth is then pressed in a stainless steel compression die, followed by a sintering process at ∿360°C in a hydrogen or nitrogen atmosphere. The carbon cloth supported electrodes display great

flexibility and electric conductivity for use in electrochemical devices. Experimental results revealed that these electrodes exhibit high catalylic activity and excellent performance stability for the anodic oxidation of sulfur dioxide in acidic media.

5.0 REFERENCES

1. S. S. Lin, Private Communication.

2. P. W. T. Lu and R. L. Ammon, in "Proceedings of 3rd World Hydrogen Energy Conference," Tokyo, Japan, June 23-26, 1980.

3. K. I. Rozanthal and V. I. Veselovskii, Zh. Fiz. Khim., 27 1163 (1953).

4. G. A. Rogdanoskii and A. I. Shlygin, ibid., 32, 418 (1958).

5. E. T. Seo and D. T. Sawyer, Electrochim. Acta, 10, 239 (1965).

6. M. Comtat and J. Mahenc, Bull. Soc. Chim., Fr., 3862 (1969).

7. A. J. Appleby and B. Pichon, J. Electroanal. Chem., 95, 59 (1979).

8. K. Wiesener, Electrochim. Acta, 18, 185 (1973).

9. Z. Samec and J. Weber, ibid, 20, pp. 403-412 and pp. 413-419, (1975).

10. I. P. Voroshilov, N. N. Nechiporenko and E. P. Voroshilova, Elektrokhim., 10 , 1378 (1974).

11. P. W. T. Lu and R. L. Ammon, Abstract No. 653, Extended Abstracts of the 156th Meeting of the Electrochemical Society, Los Angeles, CA., October 14-19, 1979.

12. B. V. Tilak, P. W. T. Lu, J. E. Colman and S. Srinivasan in "Comprehensive Treatise of Electrochemistry," Vol. 10, J. O'M. Bockris, B. E. Conway and E. Yeager, Editors, Plenum Press, New York (in press).

13. W. Böld and M. Breiter, Electrochim. Acta, 5, 145 (1961).

14. A. N. K. Reddy, M. A. Genshaw and J. O'M. Bockris, J. Chem. Phy., 48, 671 (1968).

15. G. H. Farbman and L. E. Brecher, in "Proceedings of the 10th Intersociety Energy Conversion Energy Conference," pp. 1199-1204, Newark, Delaware, August 1975.

16. G. H. Farbman and G. H. Parker, paper presented in "ACS Symposium Series, ACS/CSJ Chemical Congress," Honolulu, Hawaii, April 1-6, 1979.

REFERENCES (Continued)

17. J. P. Hoare, J. Electrochem. Soc., 111, 611 (1964).

18. J. F. Llopis and F. Colom, in "Encyclopedia of Electrochemistry of Elements," A. J. Bard, Editor, Vol. 6, pp. 253-275, Mercel Dekker, New York (1976).

19. C. A. Hampel, "The Encyclopedia of the Chemical Elements," Renold, New York (1968).

20. A. J. Appleby and B. Pichon,in "Proceedings of the 2nd World Hydrogen Energy Conference," Vol. 2, pp. 687-707, Zürich, Switzerland, August 21-24, 1978.

21. F. D. Miles and J. Fenton, J. Chem. Soc., 117, 59 (1920).

22. F. D. Miles and T. Carson, ibid., 786 (1946).

23. M. H. Miles, G. Kissel, P. W. T. Lu and S. Svinivasan, J. Electrochem. Soc., 123, 332 (1976).

24. B. D. Struck, R. Junginger, D. Bolterdorf and J. Gehrmann, paper presented at First I.E.A. Thermochemical Hydrogen Workshop, Ispra, Italy, August 28-31, 1978.

25. E. B. Robertson and H. B. Dunford, J. Am. Chem. Soc., 86, 5080 (1964).

26. International Critical Tables, Vol. 7, 237, McGraw-Hill, New York (1930).

27. E. T. Seo and D. T. Sawyer, J. Electroanal. Chem., 7, 184 (1964).

28. A. W. Contractor and H. Lal, ibid., 93, 99 (1978).

29. G. L. Klyanina and A. I. Shlygin, Zh. Fiz. Khim., 36, 1849 (1962).

30. A. H. Lanyon and B. M. W. Trapnell, Proc. Roy. Soc., A227, 387 (1955).

31. H. B. Wroblowa, B. J. Piersma and J. O'M Bockris, J. Electroanal. Chem., 6, 401 (1963).

32. W. Hauffe and J. Heitbaum, Electrochim. Acta, 23, 299 (1978).

33. R. N. Goldberg and L. G. Hepler, Chem. Rev., 68, 229 (1968).

34. R. R. Buker and R. G. Milner, J. Electrochem. Soc., 117, 9C (1970).

35. A. T. Kuhn and C. J. Mortime, ibid., 120, 231 (1973).

36. S. Puschaver, Chem. and Ind., 236 (1975).

37. S. Trasatti and G. Buzzanca, J. Electroanal. Chem., 29, App. 1 (1971).

REFERENCES (Continued)

38. W. O'Grady, C. Iwakura, J. Huang and E. Yeager, in "Proceedings of the Symposium on Electrocatalysis," M. W. Breiter, Ed., pp. 286-297, The Electrochemical Society, Princeton, NJ. (1974).

39. H. B. Beer, South Africa Patent No. 680,834 (1968).

40. Westinghouse Advanced Energy Systems Division, "Sulfur Cycle Hydrogen Production Process," Annual Technical Progress Report, Contract No. EG-77-C-02-4378, G. H. Parker, Ed., Pittsburgh, PA, 1978.

41. J. H. Sinfelt, J. Catal., 29, 308 (1973).

42. I. Furnoya and T. Shirasaki, J. Chem. Soc., Japan, Ind. Chem. Section, 72, 1223 (1969).

43. I. Furnoya, T. Yanagihara and T. Shirasaki, ibid., 72, 1436 (1969).

44. R. Sassoulas and Y. Trambouze, Bull. Soc. Chim., Fr., 5, 985 (1964).

45. S. B. M. Hagstrom and C. S. Fadley, in "X-Ray Spectroscopy," L. V. Azaroff, Ed., Chap. 8, McGraw-Hill, New York (1974).

46. S. H. Hercules and D. M. Hercules, in "Characterization of Solid Surfaces," P. F. Kane and G. B. Larrebee, Eds., Chap. 13, Plenum Press, New York (1974).

47. K. S. Kim, C. D. Sell and N. Winograd, in "Proceedings of the Symposium on Electrocatalysts," M. W. Breiter, Ed., pp. 242-264.

48. S. Schuldinger and J. P. Hoare, J. Electrochem. Soc., 103, 178 (1956).

49. M. A. V. Devanathan and Z. Stachursky, Proc. Roy. Soc., 270 A, 90 (1962).

50. K. R. Williams, "Introduction to Fuel Cells," pp. 57-63, Elsevier, New York, 1968.

51. G. W. Vinal, "Storage Batteries," p. 77, Joh Wiley, New York (1930).

APPENDIX A

THE PERMEATION CURRENT THROUGH A SEPARATOR MATERIAL

Let $c(x,t)$ represent the concentration of diffusant at a point x within a separator material and at a time t (see Figure 43). The variation of diffusant concentration with time at that point can be expressed by the Fick's second law of diffusion

$$\frac{\partial c(x,t)}{\partial t} = D \frac{\partial^2 c(x,t)}{\partial x^2} \tag{1}$$

where D is the difficient coefficient in the separator material. Initially, the concentration of diffusant within the separator is equal to zero. Thus, we have

$$c(x,o) = 0 \tag{2}$$

Assuming the SO_2-containing species diffusing through a separator material of thickness L is completely oxidized, the boundary conditions are

$$c(o,t) = C_o \tag{3}$$

and

$$c(L,t) = 0 \tag{4}$$

where C_o is the concentration of SO_2-containing species in the solution in the left compartment of the permation cell (see Figure 44).

The flux of diffusant through the separator material is

$$J = -D \left[\frac{\partial C(x,t)}{\partial x}\right]_{x = L} \tag{5}$$

Thus, the anodic current detected at the working electrode is expressed as

$$i(t) = 2FJ = -2DF \left[\frac{\partial C(x,t)}{\partial x}\right]_{x = L} \qquad (6)$$

where F is the Faraday constant.

With the initial and boundary conditions given by Equations (2) to (4), the solution of Equation (2) obtained by use of the Laplace transformation, is a series. In the transient current region, a good approximation representing the series solution is given by its first term, namely,

$$i(t) = \frac{2Li(\infty)}{\sqrt{\pi Dt}} \exp\left(-\frac{L^2}{4Dt}\right) \qquad (7)$$

where $i(\infty)$ is the permeation current at the steady state.